Development of polymer composite membranes with functionalized nanoparticles for fuel cell application

Vom Promotionsausschuss der
Technischen Universität Hamburg-Harburg
zur Erlangung des akademischen Grades
Doktor der Naturwissenschaften (Dr. rer. nat.)
genehmigte Dissertation.

von
Yaowapa Treekamol

aus
Khon Kean, Thailand

2013

Gutachter: Prof. Dr.-Ing. Karl Schulte
(Technische Universität Hamburg-Harburg)
Prof. Dr. Suzana P. Nunes
(King Abdullah University of Science and Technology)
Prof. Dr.-Ing. Thomas Klassen
(Helmut-Schmidt-Universität)

Vorsitzender des Prüfungsausschusses:
Prof. Dr.-Ing. Jörg Müller
(Technische Universität Hamburg-Harburg)

Tag der mündlichen Prüfung: 19.08.2013

Acknowledgements

I gratefully acknowledge the funding provided by the cooperation project between the National Research Council (NRC) of Canada and the Helmholtz Association of Germany, on development of membrane electrode assemblies for high temperature and low humidity PEMFC.

I would like to express my sincere gratitude to my supervisor, Professor Karl Schulte, for his precious suggestions, constructive criticism, constant encouragement and vital help throughout this research work. I likewise wish to thank Professor Thomas Klassen for giving me full support and the opportunity to realize my research work in the Materials Research Institute at Helmholtz-Zentrum Geesthacht. I am deeply indebted to my advisors, Professor Suzana Nunes and Dr. Mauricio Schieda for their valuable discussions, suggestions, and help with the research work and publications.

I would also like to thank Dr. Lucie Robitaille, Dr. Sean MacKinnon, Dr. Asmae Mokrini and Dr. Anna Sui for their advice on polymer synthesis and processing during the whole project and especially during 6 months of work at NRC Industrial Materials Institute, and Dr. Ken Shi and Dr. Zhong Xie for their advice and experience on fuel cell testing during the entire project and especially during 6 months of work at NRC Institute for Fuel Cell Innovation.

I am thankful to Silvio Neumann, Regina Just and Dr. Thomas. Emmler at Helmholtz-Zentrum Geesthacht for their contributions to the NMR, SEM, and thermal characterizations; F. Vachon, N. Raymond at NRC Industrial Materials Institute for their contribution to membrane processing; Dave Edwards and P. Le Marquand at NRC Institute for Fuel Cell Innovation for MEA processing; Dr. Louis Prado and Alejandra de la Vega at Technische Universität Hamburg-Harburg (TUHH) for their help with DMA measurements; Dr. Hans Wittich for his advice on curriculum at TUHH. I would also like to thank the staff at the Institut für Werkstofftechnik at Helmut-Schmidt-Universität for helpfully providing the facilities for SEM characterization.

Zusammenfassung

In der vorliegenden Arbeit wird die Präparation von Komposit-Polymermembranen mit Siliziumdioxid-Partikeln, die teilweise mit fluoriertem Polyoxadiazol Oligomer (ODF) funktionalisiert wurden, vorgestellt. Die dabei verwendeten Polymere reichen vom quasi-Industriestandard Nafion® über Poly(arylenether 1,3,4-oxadiazol) zu fluoriertem Polyoxadiazole Random Copolymer. Die Herstellung von Polymermembranen mit Oxadiazol-Matrix erfolgte ausschließlich mittels Solvent Casting; Polymermembranen mit Nafion®-Matrix wurden mittels Solvent Casting und Schmelzextrusion hergestellt. In den vorgenommenen Untersuchungen wurden wichtige Parameter zu Ionenaustauschkapazität (IEC), Leitfähigkeit, Wasserrückhaltung, Quellung, thermischer Stabilität und Morphologie näher ermittelt.

Für Membranen auf Polyoxadiazol Basis zeigte sich, dass die Einbettung funktionalisierter Siliziumdioxid-Patikel eine Verbesserung der mechanischen Stabilität bei unveränderter IEC bzw. Protonenleitfähigkeit bewirkt. Nichtsdestotrotz ist die Protonenleitfähigkeit der Membranen für eine Anwendung in PEM-Brennstoffzellen zu gering.

Bei Nafion®-basierten Membranen erwies sich der Einbau von (ODF-) funnktionalisierten Nanopartikeln als günstig, was vor Allem auf ein mögliches „physikalisches“ Crosslinking und Wasserrückhaltung – im Vergleich mit unfunktionalisierten Silika-Partikeln – zurückzuführen ist. Bei gleicher Konzentration an Füllstoffen wurde in Nafion® basierten Membranen aus Solvent Casting eine bessere Dispergierung der Füllstoffe erreicht, was zu einer Erhöhung der Protonenleitfähigkeit führt. Nafion®-Kompositmembranen zeigen exzellente thermische Stabilität, was sie für den Einsatz in Hochtemperatur-PEM Brennstoffzellen empfiehlt. Die optimale Leistung der Brennstoffzellen wird bei einer Konzentration von 10 wt.% ODF-funktionalisierter Silika-Partikel bei Membranen aus Solvent Casting und bei 5

wt.% für extrudierte Membranen erreicht. Im Gegensatz dazu steht der Befund, dass der Durchtritt von Wasserstoff durch die Kompositmembranen im Vergleich gegen eine reine Nafion®-Membranen durch den Einbau der Füllstoffe erleichtert wird, was wahrscheinlich auf die höhere Porosität der Silika-Partikel im Vergleich zur dichten Nafion®-Matrix zurückzuführen ist. Die Kompositmembranen zeigten beim Einsatz in der Brennstoffzelle mit abnehmender Feuchte den zu erwartenden Leistungsabfall, jedoch wurden bei 34% relativer Feuchte und 95°C immer noch gute Leistungsdaten erhalten.

Abstract

A series of composite membranes were prepared by dispersing fluorinated polyoxadiazole oligomer (ODF)–functionalized silica nanoparticles in Nafion®, poly(arylene ether 1,3,4-oxadiazole) and fluorinated polyoxadiazole random copolymers. For membrane preparation, solvent casting was used for oxadiazole-matrix composites, while both melt extrusion and solvent casting processes were explored for Nafion® composites. Ion exchange capacity, conductivity, water uptake and thickness expansion, thermal stability and morphology were characterized.

For polyoxadiazole-matrix membranes, the inclusion of functionalized silica was shown to improve the mechanical stability of the membranes without significantly losing IEC or proton conductivity. Nevertheless, the proton conductivity values were too low for use in practical fuel cells.

For Nafion®-matrix membrnes, the inclusion of functionalized nanoparticles proved advantageous, mainly due to a physical crosslinking effect and better water retention, with functionalized nanoparticles performing better than the pristine silica particles. For the same filler loading, better nanoparticle dispersion was achieved for solvent-cast Nafion® membranes, resulting in higher proton conductivity. The Nafion® composite membranes showed excellent thermal stability, allowing for operation in high temperature PEM fuel cells. The best fuel cell performance was obtained for membranes loaded with 10 wt.% ODF-functionalized silica for solvent-cast membranes, while the optimal loading was 5 wt.% for the extruded composites. The composite membranes allowed for operation in high temperature PEM fuel cells. Hydrogen crossover, however, was higher for the composites than for pure Nafion® membranes, probably due to the replacement of the dense fluorinated matrix with porous silica phase. Even though the fuel cell performance of the composite membranes decreased with decreasing the relative humidity, good performance values were still obtained at 34% RH and 95°C

Table of Contents

Introduction

Fuel cells are electrochemical devices in which a chemical reaction produces electrical energy from a chemical fuel. The conversion of the fuel takes place via an electrochemical process, which is quiet and highly efficient, and without emission [1] of contaminant gases. Fuel cells are highly versatile energy converters, but it is their relevance to automobiles in particular that has gathered massive interest, especially after the advances made by companies like Ballard in the early 1980s. Since proton exchange membrane fuel cells (PEMFCs) are the best suited for transport applications, an ever increasing number of research efforts have been directed towards the development of materials for this type of cell. Together with the catalysts, the polymer electrolyte membranes [2–6] present a large number of challenges to commercialization, mainly due to their cost, durability, and limited operating condition range.Several advantages are ascribed to the operation of PEMFCs at medium to high temperatures (>100°C), including improved electrochemical kinetics, simpler water management and cooling, and waste heat recovery [7]. Furthermore, cost reduction requires the elimination of humidifier systems, which implies fuel cell operation at low relative humidity (RH). While perfluorosulfonic acid (PFSA) polymers such as Nafion® are still the standard solid electrolyte employed in commercial PEMFCs, their performance decreases rapidly at high temperatures and low RH, as the membrane dehydrates [8–11]. Hence the development of new membrane materials with properties suited to high temperature and low humidity operation remains one of the pressing issues towards wide commercialization of PEMFCs.

The two main research approaches are the development of new polymers, with structures designed in a bottom-up fashion, or the modification of previously known polymers, by functionalization, blending or composite manufacture. The group of S. Nunes investigated the preparation of proton conducting polyoxadiazole membranes, both by concurrent sulfonation and synthesis of polymers containing sulfonatable aromatic ether moieties [12,13], and by preparation of composites with sulfonated inclusions [14,15].

A number of reviews have been published recently on the preparation of hybrid inorganic-organic composite membranes for fuel cell applications [16–24]. Widely explored strategies consist of introducing clay [25,26], layered metal phosphates and phosphonates [27], or hydrophilic oxides [28–30] (MO_2, with M= Si, Ti, Zr, Sn) in a conducting polymer matrix, either by simple dispersion or by in-situ generation via sol-gel process. In all cases the aim is to reduce the dehydration and the reactant permeability of the polymer electrolyte matrix.

Several groups have investigated the preparation of polyelectrolyte composite membranes containing sol-gel in-situ generated SiO_2 [31–34]. However, because of its wide availability and low cost, the simplest approach is still the dispersion of silica particles as filler in a conducting polymer matrix. Previous studies have demonstrated the advantage of employing functionalized silica over neat silica [35,36], and of nanoparticles over larger particles [37].

Processing technology is also a significant factor for the commercial availability and environmental impact of proton exchange membranes (PEM). A number of manufacturing methods have been reported, the simplest, conventional process being solvent casting [38–40]. It is suitable for polymers with high or no melting temperatures. More efficient processes such as melt extrusion [41] and electrospining [42,43] have also been increasingly studied in the past decade.

In this study we report the preparation of Nafion®, poly (arylene ether 1,3,4-oxadiazole) and fluorinated polyoxadiazole random copolymer composite membranes containing polyoxadiazole (POD) functionalized silica nanoparticles, and presenting good performance in fuel cells operating at low relative humidity. As a grafting agent we have used sulfonated, fluorinated polyoxadiazole oligomers (ODF), which provide a good interaction with both the hydrophobic and the hydrophilic phases of these polymers, and compensate for the loss of matrix by adding protogenic species, in the form of $-SO_3H$ groups, and protonable moieties, in the form of oxadiazole rings [12,44]. Both solvent casting and melt extrusion are employed in the membrane fabrication.

Chapter 1. Literature and scientific background

This chapter presents a background on fuel cells, polymer electrolyte membrane fuel cells and the development of polymer electrolyte membranes. The theoretical background for fuel cell performance evaluation is covered, including the measurement of fuel cell performance and hydrogen crossover, and the control of relative humidity for fuel cell characterization. The melt extrusion process for membrane fabrication is also discussed.

1.1 Fuel cells

A fuel cell is an energy conversion device that produces electricity by electrochemical combination of a fuel and an oxidant. The energy produced in this system is clean, since chemical energy is converted directly into electrical energy without giving out toxic combustion byproducts. When fed pure hydrogen, fuel cells produce only water as byproduct. Their efficiency is higher than that of combustion engines, which are limited by the Carnot cycle [45].

1.1.1 Types of fuel cells

Fuel cells are usually classified into six main types based on the electrolytes employed in the cells. The categories differ in the kind of chemical reactions that take place in the cell, catalysts required, operating temperature range, fuel used, and efficiency. These characteristics influence the applications for which these cells are most suitable. Each fuel cell type has its own advantages, limitations, and potential applications. A summary of the classification is shown in Table 1.1.

Table 1.1 Overview of the most extensively studied types of fuel cell and their applications [46].

Fuel cell type	Temp. (°C)	Efficiency (%)	Applications	Advantages	Disadvantages
Alkaline (AFC)	50-90	50-70	- space application	- high efficiency	- CO2 poisoning - corrosion - expensive
Phosphoric acid (PAFC)	175-220	40-45	- stand alone or combined heat and power supply	- tolerant to impure H2 - commercially available	- low power density - corrosion - sulphur poisoning
Molten carbonate (MCFC)	600-650	50-60	- central, stand alone or combined heat and power supply	- high efficiency - near commercial	- electrolyte instability - corrosion - sulphur poisoning
Solid oxide (SOFC)	800-1000	50-60	- central, stand alone and combined heat and power supply	- high efficiency - direct fossil fuel	- high temperature - thermal stress failure - coking and sulphur poison
Polymer electrolyte membrane (PEMFC)	60-100	40-50	- vehicles - small portable	- high power density - low temperature	- intolerant to CO in impure H2 - expensive
Direct methanol (DMFC)	50-120	25-40	- vehicles - small portable	- no reforming - high power density - low temperature	- low efficiency - methanol crossover - poisoning by product

1.1.2 Polymer electrolyte membrane fuel cells

Polymer electrolyte membrane fuel cells (PEMFC)s employ a solid ion exchange polymer as electrolyte. Other names commonly used for this type of fuel cell are ion exchange membrane fuel cell (IEMFC) and solid polymer (electrolyte) fuel cell (SP(E)MFC). They were first developed by the US company General Electric in the 1960s for use by NASA on their first manned space vehicle. PEMFCs work at low temperatures, meaning that they can start quickly. Moreover, as a zero-emission power source, they are environmentally friendly. A further advantage is wide range of possible applications, from portable devices requiring a few watts to transport vehicles needing about 50kW. Apart from the polymer electrolyte membrane (PEM) used for proton conduction between anode and cathode, PEMFCs contain: electrically conductive porous gas diffusion layers (GDLs), electrodes (catalyst layers) sandwiched between the GDLs and the membrane, gaskets for gas sealing and electrical insulation, and cell plates with gas flow channels to carry the fuel or oxidant to the reactive sites. In the cell, the following electrochemical reactions take place [47]:

Anode reaction: $2H_2 \longrightarrow 4H^+ + 4e^-$

Cathode reaction: $O_2 + 4H^+ + 4e^- \longrightarrow 2H_2O$

Over all reaction: $2H_2 + O_2 \longrightarrow 2H_2O$

Hydrogen is catalytically oxidized at the anode providing protons and electrons. The electrons move from the anode through the external circuit to the cathode. The protons pass through the electrolyte to the cathode, where the oxygen gas reacts with the incoming electrons and protons to produce water, as shown in Figure 1.1.

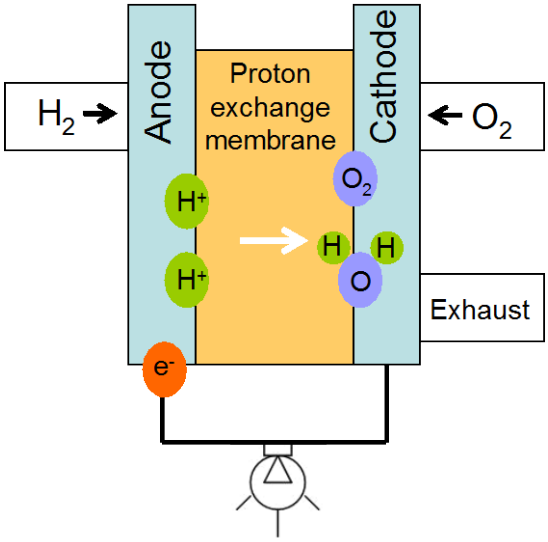

Figure 1.1 Schematic drawing of a hydrogen/oxygen fuel cell.

The PEMFC single fuel cell is only capable of producing a theoretical maximum of 1.23 V which is not large enough for most applications. To produce more useful voltages in a fuel cell, many individual cells are linked together to form a fuel cell stack as presented in Figure 1.2.

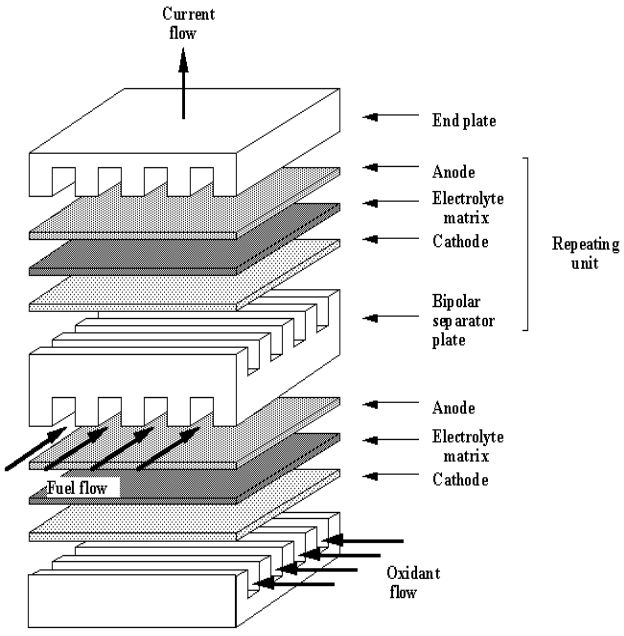

Figure 1.2 Schematic of a fuel cell stack [48].

The basic building block of a fuel cell stack includes anode, cathode, electrolyte and bipolar plates, an additional component required for electrical connections. The

bipolar plates provide electrical contact between the anodes and cathodes of neighboring cells and are also used as the structure which guides reactiant gases and reaction products throughout the cell [49].

1.2 Polymer electrolyte membranes

The polymer electrolyte membrane is the key component in fuel cell system, its main function being proton transport. At the molecular level proton transport is described by two main mechanisms[1]. In the “proton hopping” mechanism, the protons produced from hydrogen at the anode move through the electrolyte membrane by forming a hydronium ion with water, and one different proton from the same hydronium ion jumps to another water molecule. In this system, ionic clusters are swelled by water, contributing to the proton transfer process. In the “vehicular proton transport” mechanism, the electrochemical potential difference causes hydrated proton diffusion through the aqueous medium in the proton conductive membrane. Schemes of both these proton transport mechanisms are shown in Figure 1.3.

To achieve high fuel cell efficiency the polymer electrolyte membranes are expected to have the following desirable properties [4]:

- high proton conductivity to hold up current with minimal resistive losses and zero electronic conductivity;
- sufficient mechanical properties to resist the forces imposed by the membrane electrode assembly process;
- chemical, electrochemical and thermal stability under operating conditions;
- low fuel or oxygen by-pass to maximize columbic efficiency;
- production costs compatible with the intended application.

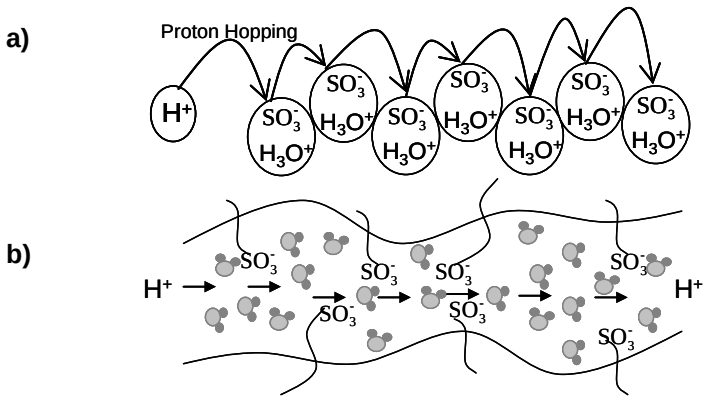

Figure 1.3 Hopping mechanism (**a**) and vehicular mechanism (**b**) (adapted from [1]).

1.2.1 Perfluorinated ionomer polymer electrolyte membranes

The most commonly used polymer electrolyte membrane for PEMFC nowadays is DuPont's Nafion® [50]. It is a perfluorosulfonic acid (PFSA) polymer, consisting of a polytetrafluoroethylene backbone with perfluorovinyl ether pendent side chains terminated by sulfonic groups. The chemical structure of Nafion® is shown in Figure 1.4a.

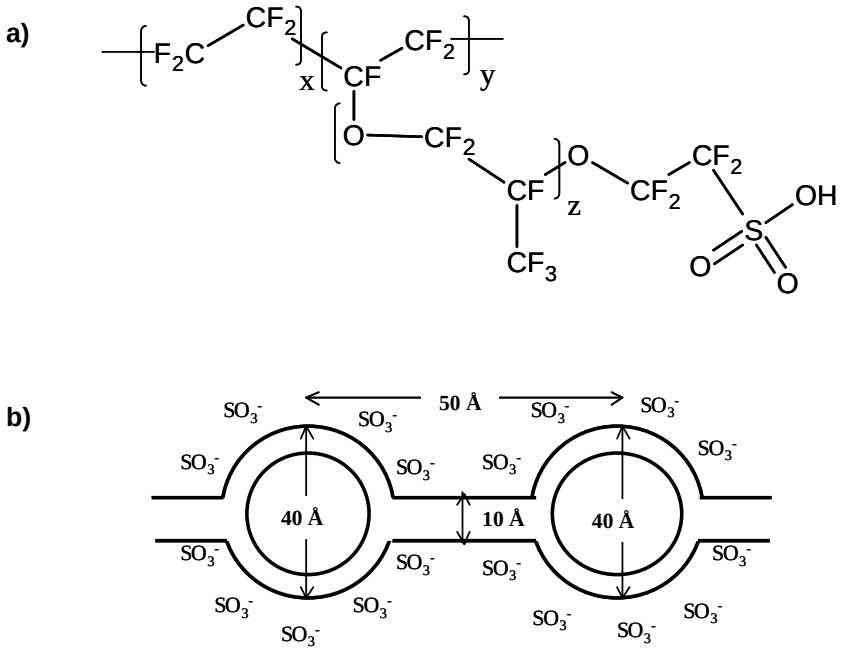

Figure 1.4 Chemical structure (a) and the cluster-network structural model (b) of Nafion®.

The molecular weight of Nafion® is in the range 10^5-10^6 g mol^{-1}. Several structural models have been proposed in order to interpret the results from X-Ray diffraction and scattering experiments on Nafion®. The oldest and better known is the cluster-network model [51,11], which postulates the aggregation of sulfonic groups into "ionic clusters", approximately spherical and with an inverted micellar structure. The clusters, with a 4 nm diameter, are evenly distributed within a continuous fluorocarbon lattice. Small channels about 1 nm in diameter interconnect the clusters enabling ion transport. A representation of this model can be seen in Figure 1.4b. Nafion® has good ionic conductivity, chemical resistivity, mechanical properties and ion selectivity, hence its widespread use for many applications particularly in

electrochemistry. Others companies such as Asahi Chemical, Asahi Glass, and Dow Chemical have developed similar perfluorinated ionomers (Aciplex®, Flemion®).

The major disadvantages [4,52] of these PFSA materials are the high cost of the resulting membranes, safety hazards during their manufacture and use, the requirement of supporting equipment and, most significantly, temperature related limitations. When the operating temperature is over 80 °C Nafion® and other perfluorosulfonic polymers tend to dehydrate, which results in ionic conductivity loss and a decline in mechanical strength.

In the last 15 years, the modification of perfluorinated ionomer membranes for PEMFC and DMFC applications has been increasingly studied. Inorganic oxides such as silicon oxide, titanium oxide and zirconium oxide [53] have been used as fillers to achieve high fuel cell performance at higher operating temperatures.

For example, Nafion® composite membranes containing acidic sulfated zirconia were studied by Zhai, et al. [54]. The ion exchange capacity of composite membranes increased with the content of acidic sulfated zirconia as shown in Figure 1.5. Moreover, the integration of the zirconia also improved the initial degradation temperature by increasing the crystallinity of the composite membranes. Additionally the single cell performance was improved to 1.35 W cm^{-2} at 80 °C when the sulfated ZrO_2 content was 15 wt.% while the pure Nafion® at the same condition gave 1.28 W cm^{-2} as shown in Figure 1.6. The Nafion® composite membranes also showed lower fuel cell internal resistance than pure Nafion® membranes at high temperature and low relative humidity operating conditions.

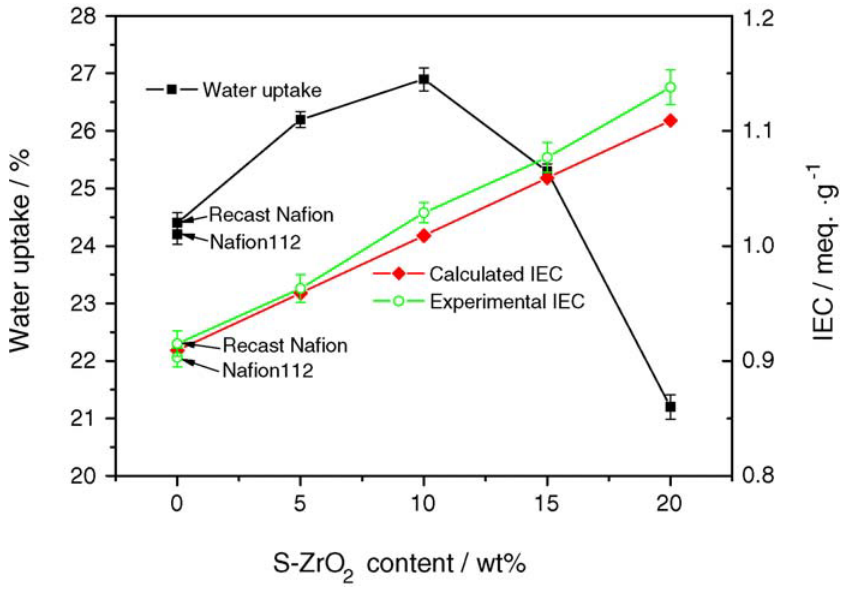

Figure 1.5 Ion exchange capacity (IEC) and water uptake of acidic sulfated zirconia/Nafion® composite membranes [54].

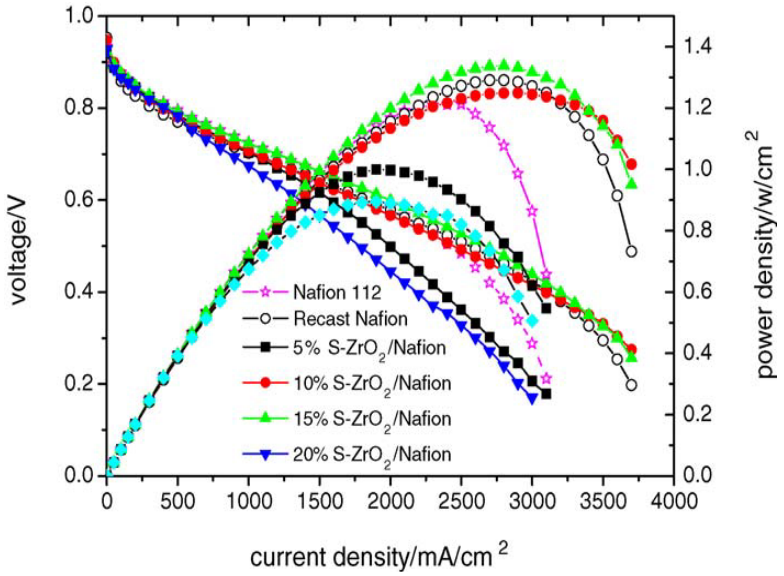

Figure 1.6 Fuel cell performance Nafion® 112, recast Nafion® and acidic sulfated zirconia Nafion® composite membranes at 80 ºC [54].

Composite Nafion® membranes containing directly sulfonated silica of different particle sizes were studied by Gnana Kumar et al. [35]. They obtained better fuel cell performance for composites with 3 and 90 nm SiO_2 particles compared to neat Nafion® as shown in Figure 1.7. The improvement of fuel cell efficiency was attributed to the increased number of proton conducting channels and the better water retention provided by the modified silica.

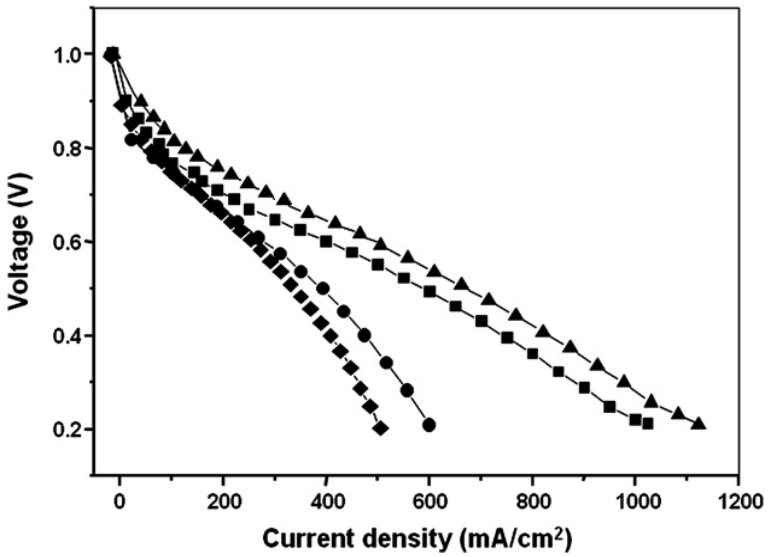

Figure 1.7 PEMFC performance of (►) Nafion-SiO2 (3 nm), (■) Nafion-SiO2 (90 nm), (●) Nafion, and (♦) Nafion-SiO2 (1 µm) composite membranes measured at 80 ºC under 30%RH [35].

An opposite effect was observed for 1µm particles. As explanation for this result they proposed that nanometer-sized modified silica particles are small enough to be trapped inside ionic clusters, thus extending the cluster network, while larger particles disrupt the network.

Many other fillers have been investigated in an attempt to improve the fuel cell performance of perfluorosulfonated membranes. A few examples are montmorillonite [26], polyaniline [55], polypyrrole [56] and Pt/SiO_2, [57].

1.2.2 Poly(ether ether ketone) polymer electrolyte membranes

Poly (ether ether ketone) (PEEK) is a family of polymers with high thermal and mechanical stabilities which make them highly promising for a large number of practical applications, including fuel cells. In sulfonated poly (ether ether ketone) (SPEEK), a fraction of the aromatic rings have a sulfonate group covalently attached: an example of the chemical structure is shown in Figure 1.8. There have been a

number of reports on the applications of sulfonated PEEK in ultra-filtration [58] and fuel cells [59, 60, 61 25, 62]. The proton conductivity of SPEEK depends on the sulfonation degree, which is controlled by the reaction time and temperature of the sulfonation process [63].

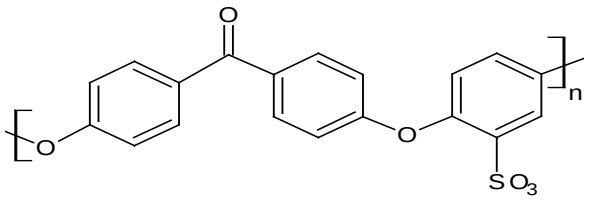

Figure 1.8 Chemical structure of Poly(ether ether ketone).

1.2.3 Poly(oxadiazole) polymer electrolyte membranes

Poly(oxadiazole)s (POD)s, initially described in 1961 [64], are polymers containing oxadiazole units, commonly connected by aromatic units (PODs with aliphatic linkages tend to have lower melting points). Poly(1,3,4-oxadiazole) are high performance polymers, with high chemical and thermal resistance, and have been used to prepare membranes for gas separation [65] and fuel cell [66] applications.

The group of S. Nunes investigated the preparation of proton conducting polyoxadiazole membranes, both by concurrent sulfonation and synthesis of polymers containing sulfonatable aromatic ether moieties[12,13] (Figure 1.9), and by preparation of composites with sulfonated inclusions [14,15]. For polyoxadiazoles without sulfonatable groups, they studied the preparation of acid-doped membranes [44], obtaining good conductivity values at high temperature and low relative humidity conditions. The inclusion of functionalized silica allowed for higher doping levels as well as higher water retention capacity, resulting in better proton conductivities, as shown in Figure 1.10 and Figure 1.11

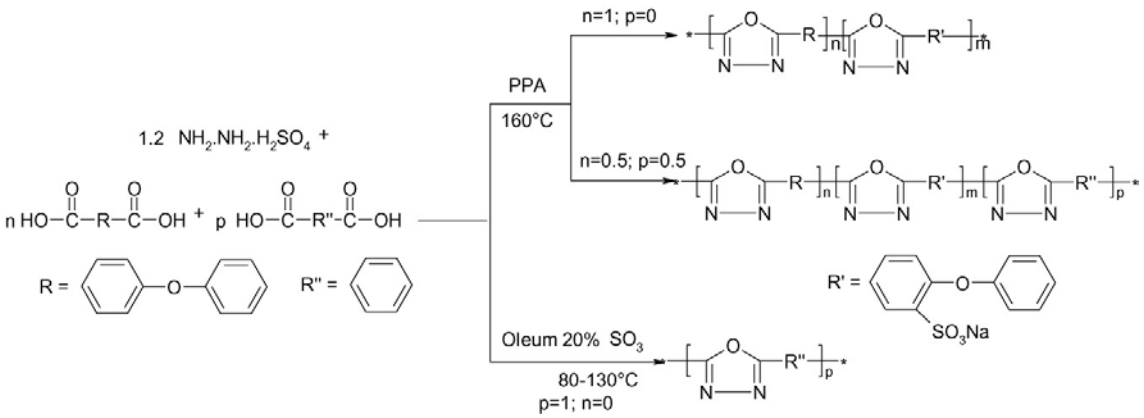

Figure 1.9 Single-step synthesis for sulfonated polyoxadiazoles [13].

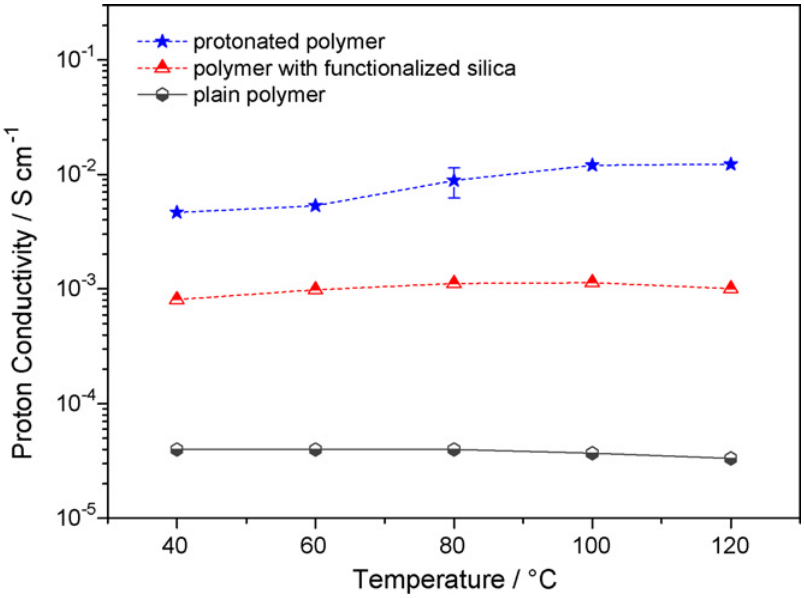

Figure 1.10 Effect of temperature on the proton conductivity for poly(hexafluoropropane-1,3,4-oxadiazole) membranes and composites, at 100% relative humidity [44].

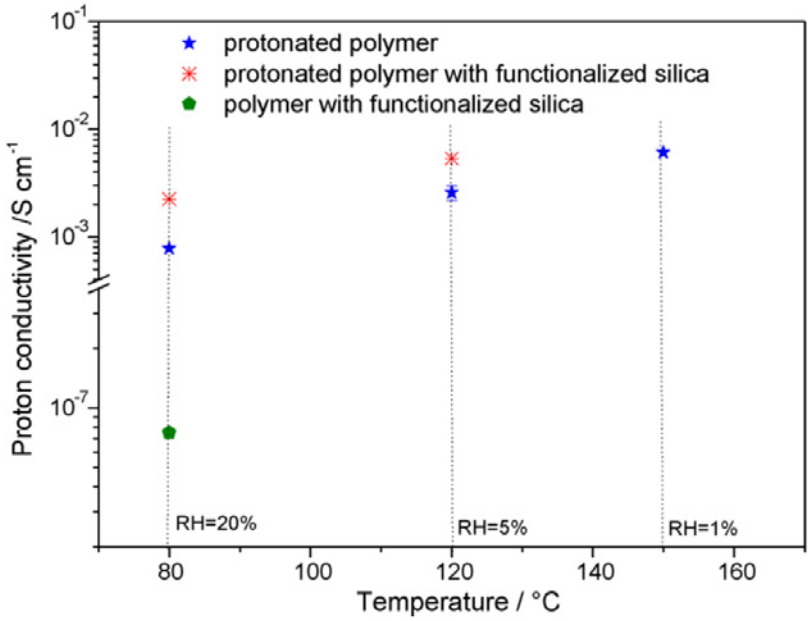

Figure 1.11 Effect of humidity and temperature on the proton conductivity of poly(hexafluoropropane-1,3,4-oxadiazole) membranes and composites [44].

1.3 Fuel cell performance characterization

1.3.1 Polarization curve

The maximum theoretical voltage that a single PEMFC can provide is determined by the Gibbs free energy ($\Delta\bar{g}_f$) released during the global hydrogen-oxygen fuel cell reaction (Section 1.1.2):

$$E = \frac{\Delta\bar{g}_f}{2F}$$

This reversible open circuit voltage (OCV) is about 1.2 V at temperatures below 100°C. Due to irreversible energy losses, on a real fuel cell, the actual OCV is below this value, and the voltage decreases as current is drawn from the cell. A plot of the evolution of the cell voltage with the current density provided by the cell, called a polarization curve, is a useful characterization of a fuel cell's efficiency. It shows the

relationship between the actual voltage and the theoretical maximum of 1.2 V. A typical polarization curve shows several voltage drops, corresponding to the predominant irreversible loss in different current density ranges:

- *Fuel cell crossover,* that is, the diffusion of fuel from the anode to the cathode compartment through the electrolyte, results in a drop in the OCP.
- *Activation losses* are predominant at low current density, where the slow electron transfer rate means some voltage must be lost into driving the electrochemical reactions.
- Ohmic losses are the main cause of voltage drop in the mid-range of current densities, and are due to the resistance of the different fuel cell components (collectors, electrodes, electrolyte) to the flow of charge. This voltage drop is proportional to the current density, that is, it follows Ohm's law.
- *Concentration losses (mass transport losses)* become significant at high current density, when reactants are consumed at high rate, and their concentration is depleted in the vicinity of the surface of the electrodes. The rate of the electrochemical reactions is limited here by the rate of transport of reactants to (and products from) the surface of the electrodes [67].

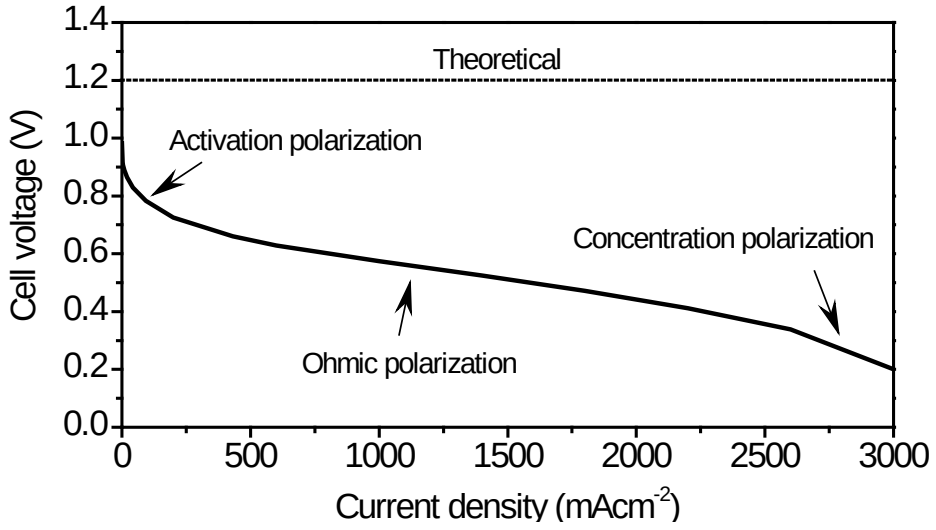

Figure 1.12 Typical polarization curve for a polymer electrolyte membrane fuel cell.

1.3.2 Hydrogen crossover

Hydrogen crossover is the undesirable diffusion of hydrogen fuel from the anode side to cathode side through the MEA. The crossed-over fuel will react at the cathode, thus reducing the fuel cell efficiency. Furthermore, the heat released and the radicals produced by the reaction can cause significant catalyst-layer and membrane degradation [69]. Figure 1.13 shows a simple representation of the hydrogen crossover in a typical MEA, consisting of five layers: anode gas diffusion layer (GDL^a), anode catalyst layer (CL^a), proton exchange membrane (PEM), cathode catalyst layer (CL^c), and cathode gas diffusion layer (GDL^c) [68].

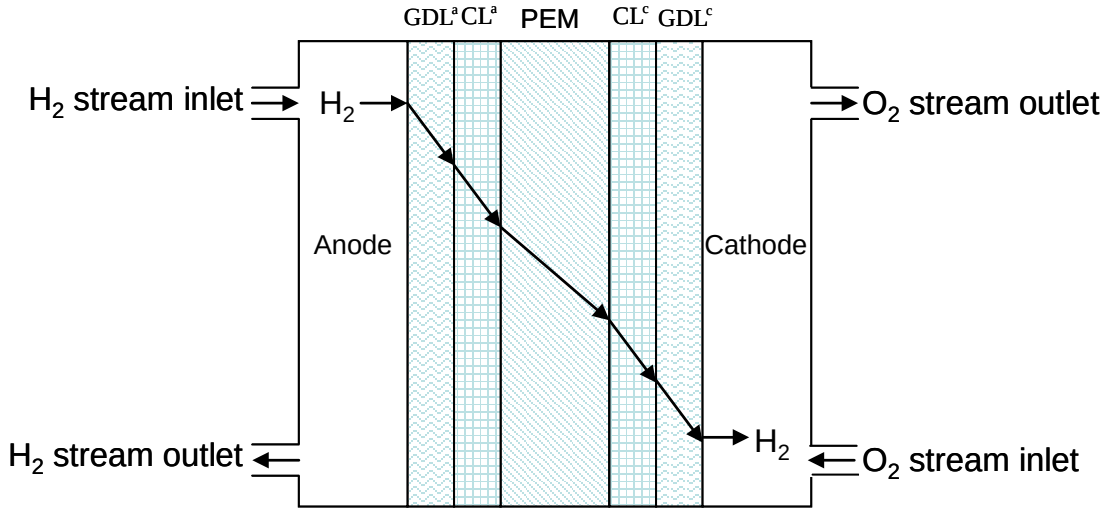

Figure 1.13 Diagram of hydrogen crossover through the MEA in a PEM fuel cell (based on [68]).

The hydrogen crossover can be measured by flushing both compartments with nitrogen, and subsequently allowing hydrogen into the anode compartment. In these conditions, all the hydrogen that has crossed over is oxidized at the cathode. The current produced $I_{H_2}^{cross}$ is directly related to the amount of crossed-over hydrogen [68]. Several constant loads are applied (for example: 0.2, 0.3, 0.4 and 0.5 V) and the corresponding currents are recorded. A plot of the measured currents vs the applied loads gives a straight line which intersects the current axis at the actual hydrogen

crossover current. The hydrogen crossover rate ($J_{H_2}^{cross}$, mol cm^{-2} s^{-1}) can be obtained from Faraday's equation [68]:

$$J_{H_2}^{cross} = \frac{I_{H_2}^{cross}}{nFA}$$

where *n* is the number electrons (=2) for the hydrogen oxidation reaction, *F* is the Faraday constant (~96485 A s mol^{-1}), and *A* is the active area (cm^2) of the MEA.

1.3.3 Relative humidity system in a fuel cell test station

In the operating fuel cell test station used in this work, water vapour was introduced into the cell's anode together with the hydrogen fuel. From the anode side, water electro-osmotically passes through the catalyst layer and PEM into the cathode along with the generated protons. At the cathode, water is produced by the reduction reaction from electrons, oxygen and protons (see section 1.1.2). Some of the generated water diffuses back into the anode as a result of the concentration gradient between the anode and cathode. The excess water on each compartment is drained along with the exhaust gas. The water balance [70] inside an operating PEMFC is shown schematically in Figure 1.14.

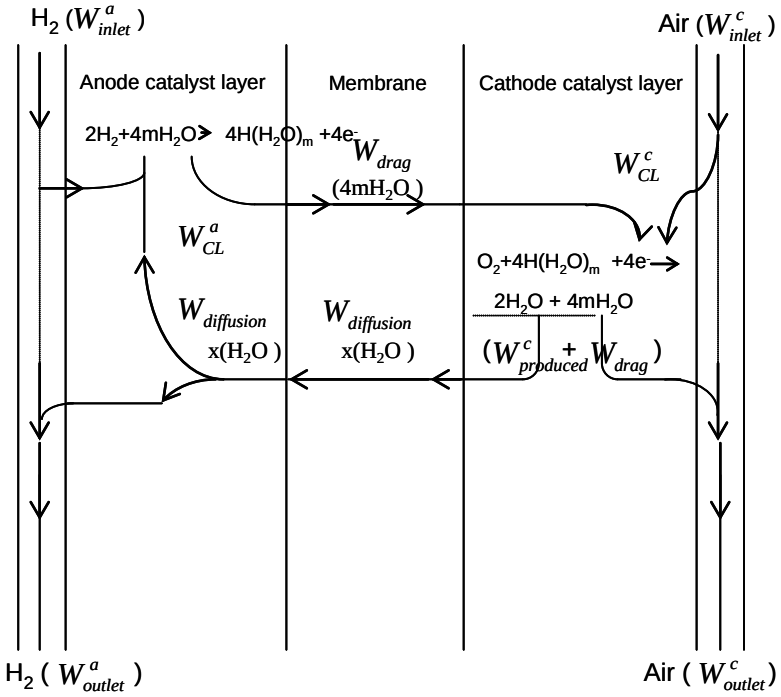

Figure 1.14 Schematic of water balance inside an operating fuel cell (based on [70]). W^{a}_{inlet}, W^{c}_{inlet}, W^{a}_{outlet} and W^{c}_{outlet} are the water flowing into and drained out of the fuel cell at anode and cathode sides, respectively; W^{a}_{CL} and W^{c}_{CL} are the water in the anodic and cathodic catalyst layers of the fuel cell, respectively; $W^{c}_{produced}$ is the water produced at the cathodic catalyst layer; W_{drag} is the water osmotically dragged from anode to cathode; and $W_{diffusion}$ is the water back-diffused from cathode to anode.

The relative humidity (RH) in a fuel cell stream is defined as the percentage ratio of the partial pressure of water vapour in the stream to the saturated vapour pressure of water at a given temperature:

$$\text{RH}(\%) = \frac{P_{H_2O}}{P^{o}_{H_2O}(T)} \text{ x } 100$$

The saturated water vapor pressure $P^{0}_{H_2O}(T)$ can be expressed as a function of temperature [70] by the empirical expression:

$$P^{0}_{H_2O}(T) = 6.02724\times10^{-3} + 4.38484\times10^{-4}(T-273.15) + 1.39844\times10^{-5}(T-273.15)^2 + 2.71166\times10^{-7}(T-273.15)^3 + 2.57731\times10^{-9}(T-273.15)^4 + 2.82254\times10^{-11}(T-273.15)^5$$

where the units of pressure and temperature are atm and Kelvin, respectively. As can be seen in the graphical representation of this expression in Figure 1.15, a fuel cell cannot function at temperatures above 100 °C with 100% RH at 1 atm. In other words, either high pressure or low humidity are required for operation at high temperature (>100 ◦C),

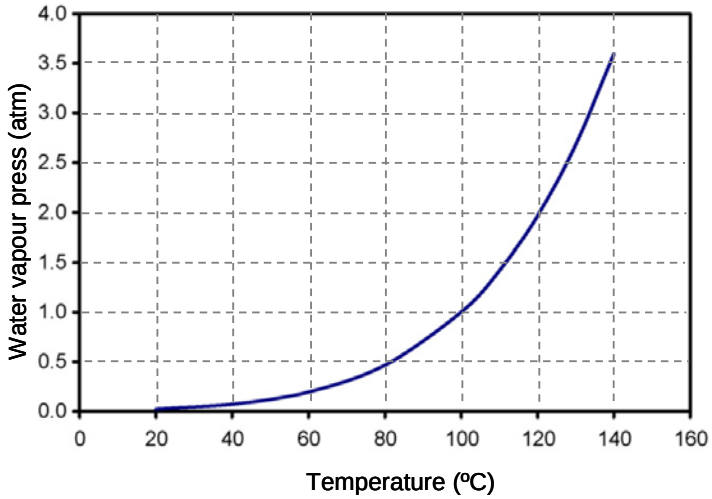

Figure 1.15 Calculated saturated water vapour pressure as a function of temperature [70].

1.4 Melt extrusion

Extrusion is a shaping process that works by pushing a raw material through a die under controlled conditions, usually at high temperature. It is widely used in the polymer industry as a fabrication method. A basic flowchart of an extrusion line is shown as Figure 1.16.

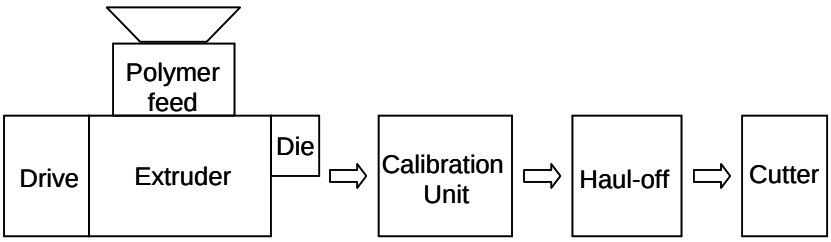

Figure 1.16 The basic components of an extrusion line (based on [71]).

There are essentially 6 parts in an extrusion line: the material feed hopper, the basic extruder, the extrusion die, the calibration units, the haul-off, and the cutting machine (with auxiliary devices for finishing and handling).

The process starts by constantly supplying a raw polymer material in powder, flake or pellet form into the heated extruder. Then the polymer is further heated and pushed by a rotating screw through the die, first compacting the particles, and subsequently melting the contents due to heat and shear forces. The polymer forms a certain shape as it flows through the die, and is then cooled down to give the final shape. Finally the product is drawn along (hauled-off) for finishing.

The two most widely used types of extruders are the single-screw and the twin-screw [72,73], consisting respectively of one or two Archimedean screws rotating in a heated barrel. Twin-screw extruders offer greater control over residence time distribution and mixing than single screw extruders [73], and have superior heat and

mass transfer capabilities. They are generally used to process powder blends as they provide excellent mixing of the material being formed.

A wide range of shapes with constant cross-section can be produced by melt-extrusion, by selecting the appropriate die shape and treatment devices for final finishing [71]. In particular, film extrusion can be achieved by pumping the polymer melt through a long slit die onto highly polished cooled rolls which form and wind the finished sheet [74].

In this study, a 5 mL DSM twin screw micro-extrusion equipped with a wide sheet die (shown in Figure 1.17), was used in a two-step process: composite blend preparation using counter-rotation screws configuration, followed by film preparation using co-rotation screws configuration.

The advantages of extrusion include relatively high production rates, ease of scale-up and excellent repeatability. Nevertheless there are material limitations: high glass transition temperature polymers and polymer degradation during processing are still problematic.

Figure 1.17 The 5cm^3 bench-top twin screw micro-extruder used in this work, equipped with a wide sheet die.

Chapter 2. Functionalizaton of silica nanoparticles

This chapter discusses the preparation and characterization of functionalized silica nanoparticles, to be used as fillers in the composite membranes studied in the rest of this work. The process begins with the synthesis and characterization of the oxadiazole monomer 2,5-Bis(4-fluorophenyl)-1,3,4-oxadiazole. This monomer is then used, together with commercial hydroxyl bisphenol compound, in a polycondensation reaction to produce the functional telechelic oligomer Poly(arylene ether 1,3,4-oxadiazole). The surface of the silica nanoparticles is then prepared by reaction with Bromophenyltrimethoxysilane. Finally the silica nanoparticles are functionalized by grafting the synthesized oxadiazole telechelic oligomer onto the modified surface. Both synthesis and characterization are described in detail for each of these steps.

2.1 Synthesis of 2,5-Bis(4-fluorophenyl)-1,3,4-oxadiazole

The 2,5-Bis(4-fluorophenyl)-1,3,4-oxadiazole monomer was synthesized as summarized in Figure 2.1. Following the synthetic protocol described by Gomes et al. [75], the reaction was carried out from 4-fluorobenzoic acid and hydrazine sulphate in polyphosphoric acid (PPA) solvent. 12.75 g of 4-fluorobenzoic acid, 5.92 g of hydrazine sulphate and 100 g of PPA were added into a round bottom flask fitted with a drying tube. The mixture was heated up to 150 °C and mechanically stirred at 200 rpm for 6 hours under nitrogen atmosphere. Then the temperature was increased to 200 °C for 2 hours. The solution was cooled down to room temperature and precipitated into water. The product was washed several times with deionized water, checking the bath with a pH indicator paper strip until all residual acid was eliminated

. After that the obtained solid was dried in a vacuum oven and recrystallized in ethanol. White needle crystals were obtained with a 78.4% yield.

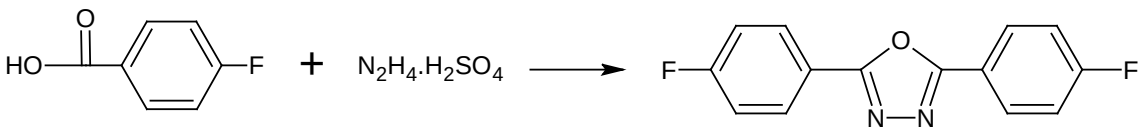

Figure 2.1 Synthesis of 2,5-Bis(4-fluorophenyl)-1,3,4-oxadiazole.

The melting point of the oxadiazole monomer product was determined by DSC to be 208 °C, in good agreement with the value reported in the literature (207 °C in Ref. [75]). Further confirmation of the monomer structure is provided by the ^{1}H-NMR spectrum of the oxadiazole monomer taken in deuterated dimethyl sulfoxide-d6 (DMSO-d6), as shown in Figure 2.2. The signals at 8.2 and 7.4 ppm correspond respectively to protons in positions 1 and 2 in the phenyl ring. No signal of residual hydrazide group is observed in the region 10.0–10.5 ppm [76].

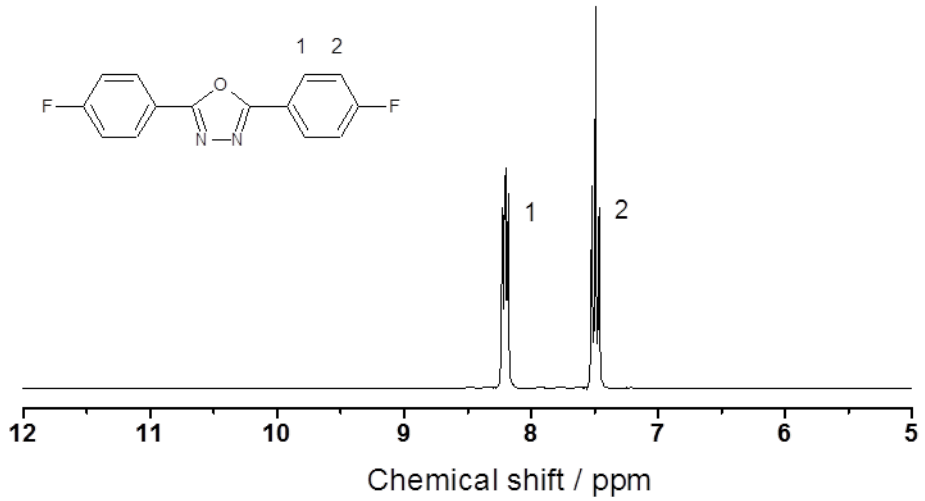

Figure 2.2 ^{1}H NMR spectrum of 2,5-Bis(4-fluorophenyl)-1,3,4-oxadiazole taken in DMSO-d6.

2.2 Synthesis of Poly(arylene ether 1,3,4-oxadiazole) oligomers

The synthesis of oligomers was carried out in a three-neck flask equipped with a dry nitrogen inlet and a Dean-Stark trap fitted with a condenser. 0.93 mol of potassium carbonate was added to a suspension containing 1 mol of bisphenol monomer in 5 mL of NMP and 20 mL of Toluene. The mixture was stirred at 160 °C for 4 hours. During this period, water is produced by phenoxide formation and removed as azeotrope with Toluene. The weak base (K_2CO_3) is added to the reaction system in order to generate the nucleophilic phenoxide from the bishydroxy compound. The nucleophilic aromatic substitution reaction is shown in Scheme 2.2. Afterwards the temperature was increased to 180°C, and 0.93 mol of 2,5-Bis(4-fluorophenyl)-1,3,4-oxadiazole was added. The mixture was kept under stirring for 18 hours, and subsequently cooled down to room temperature. Then the polymer was precipitated into water, filtered, washed by Soxhlet extraction with methanol and dried in vacuum oven. Three different telechelic oligomers were prepared: ODA, ODS and ODF, starting correspondingly with different bisphenol monomers: 4,4′-Isopropylidenediphenol (Bisphenol A), 4,4'-(Hexafluoroisopropylidene)diphenol (Bisphenol AF), and 4,4′-Sulfonyldiphenol (Bisphenol S). The X in Figure 2.3 and in Figure 2.4 represents the groups $–C(CF_3)_2–$, $–SO_2–$ and $–C(CH_3)_2–$, corresponding to the oligomers ODF, ODS and ODA respectively.

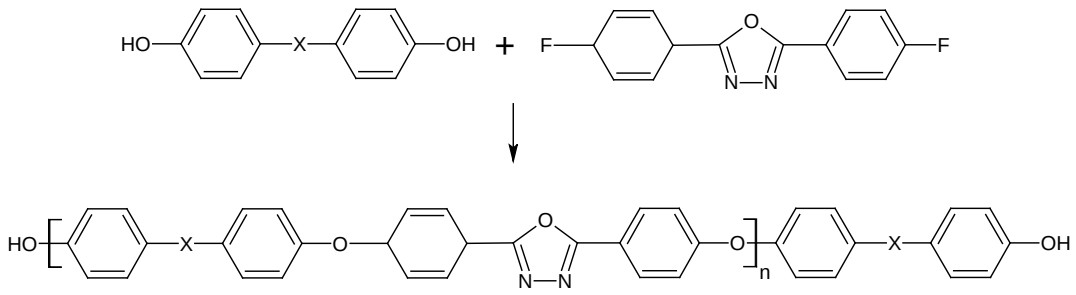

Figure 2.3 Synthesis of Poly(arylene ether 1,3,4-oxadiazole) oligomers (the x represents $-C(CF_3)_2-$, $-SO_2-$ and $-C(CH_3)_2-$, resulting in ODF, ODS and ODA respectively).

The condensation polymerization does not keep going if a weak base, like potassium carbonate, is not involved in the reaction [77]. The molar ratio between bishydroxy compound and K_2CO_3 was kept constant and equal to 0.93 [75]. After the formation of phenoxide, the bifluoro compound is added to the system and the reaction temperature is increased to effect the nucleophilic substitution polymerization, as shown in Figure 2.4. For ODF, ODS and ODA, the number average molecular weights measured by size exclusion chromatography (SEC) in DMAc with polystyrene-standard calibration are 4848, 6124 and 4621 g mol^{-1}, corresponding to polymerization degrees of 8,12 and 10 respectively for these oligomers.

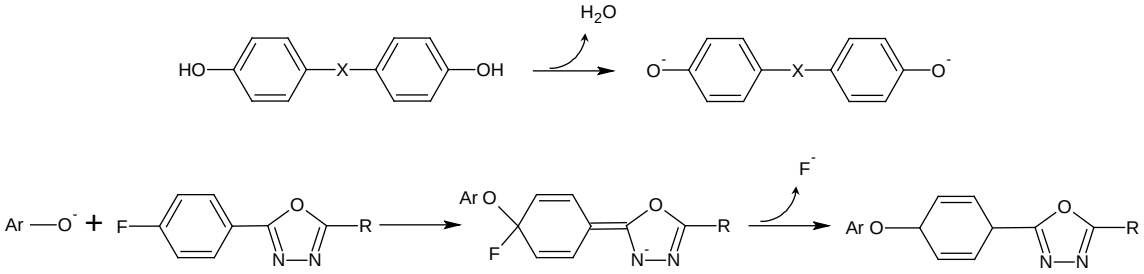

Figure 2.4 Nucleophilic aromatic substitution reaction of an aryl halide with a phenoxide.

The thermal properties of the synthesized oilgomers were determined by thermogravimetric analysis (TGA) and differential scanning calorimetry (DSC). As shown in Figure 2.5, the glass transition temperatures of ODF, ODS, and ODA are 190 °C, 220°C, and 170°C respectively.

Regarding the TGA curves, the first weight loss for all compounds at 120–200 °C corresponds to residual solvents (toluene and NMP), while the second weight loss at 350–600 °C corresponds to the oxadiazole compound. It can be seen that the oligomers are thermally stable up to 350 °C. This allows the use of these telechelics as fillers in fuel cell applications at temperatures up to 300 °C, which is higher than both the PEMFC operating temperature (100–120 °C) and the melt extrusion temperature for Nafion® (240–250 °C [78]).

The chemical composition of the polyoxadiazole oligomers was analyzed by combustion elemental analysis (EA). Table 2.1 shows the experimental and

theoretical contents of hydrogen, nitrogen and oxygen in the synthesized compounds. The experimental data are in good agreement with the calculated values for all three products.

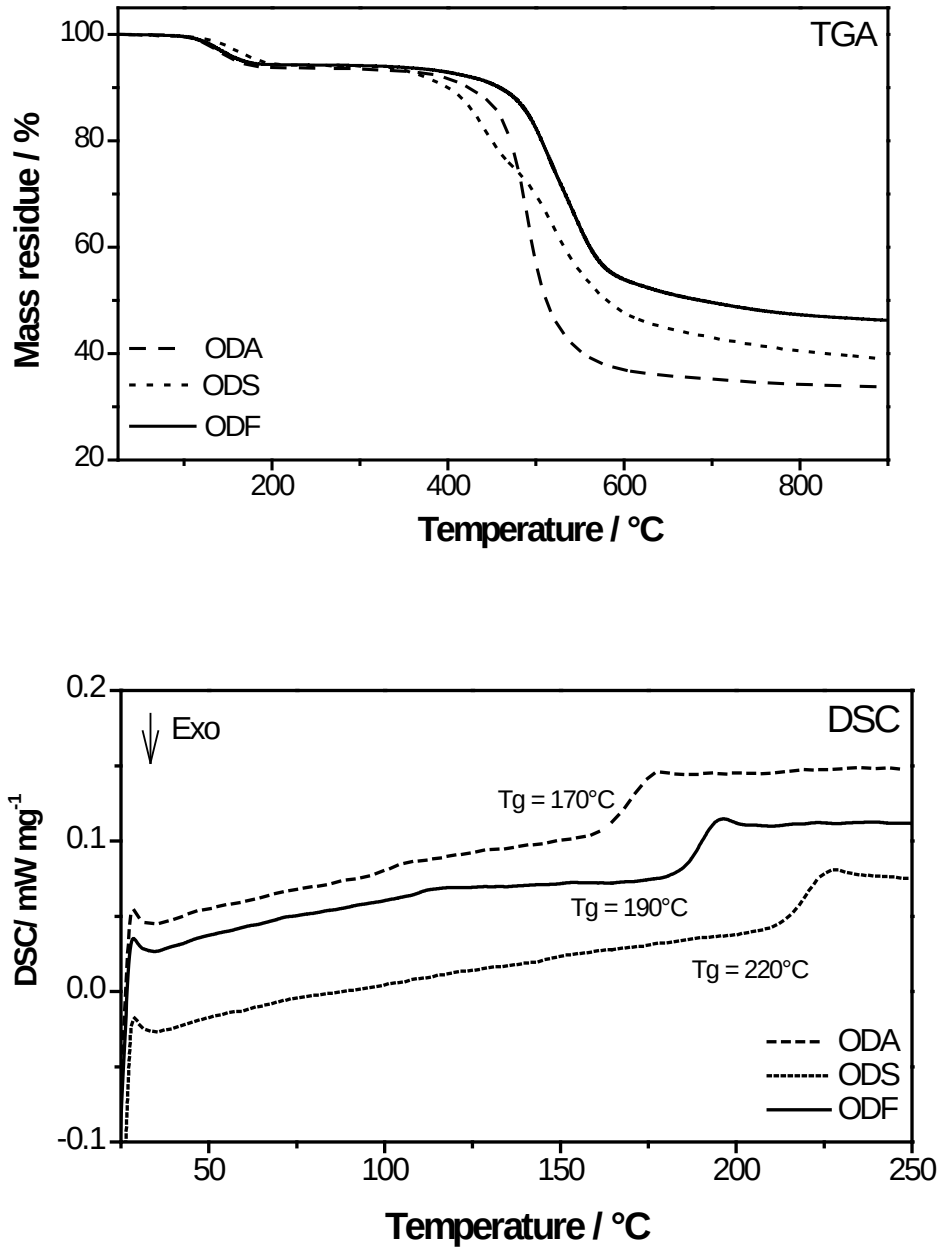

Figure 2.5 TGA and DSC thermograms of poly(arylene ether 1,3,4-oxadiazole) oligomers.

Table 2.1 Elemental analysis data for the synthesized polyoxadiazole oligomers.

	Theoretical (%)			Experimental (%)		
	C	N	H	C	N	H
ODA	78.05	5.97	5.07	79.18 ± 0.23	6.82 ± 0.03	5.31 ± 0.02
ODS	66.20	5.68	3.47	63.90 ± 0.18	6.36 ± 0.06	6.47 ± 0.02
ODF	62.29	4.76	2.91	61.47 ± 0.18	5.68 ± 0.04	3.08 ± 0.05

^{1}H-NMR spectroscopy was employed to confirm the chemical structure of the oligomers. Figure 2.6 shows the 1H-NMR spectrum of each product in DMSO. The two aryl protons on the end-group aromatic rings are labeled **1'** and **3'** for all compounds. **1** and **3** are protons on the corresponding bisphenol rings, while **3** and **4** are protons on the aryl rings bonded to the oxadiazole ring. The chemical shifts and relative intensities of the signals are similar to the values reported in the literature [75] for all the synthesized compounds.

Moreover from ^{1}H-NMR results we can calculate the number average molecular weight of telechelics by the end group analysis method (that is, from the ratio of protons on the end-groups to protons on the polymer chain). In this case the calculated number average molecular weight of ODA, ODF and ODS are 5825, 7982 and 5471 g mol^{-1} respectively.

Finally, all three oligomers displayed good solubility in N-Methyl-2-pyrrolidone. ODS and ODF are soluble in both dimethylacetamide and tetrahydrofuran, while ODA is partially soluble in dimethylacetamide and insoluble in tetrahydrofuran. Considering the TGA, DSC, MNR and EA characterization results, it can be concluded that all three poly(arylene ether 1,3,4-oxadiazole)s were successfully synthesized.

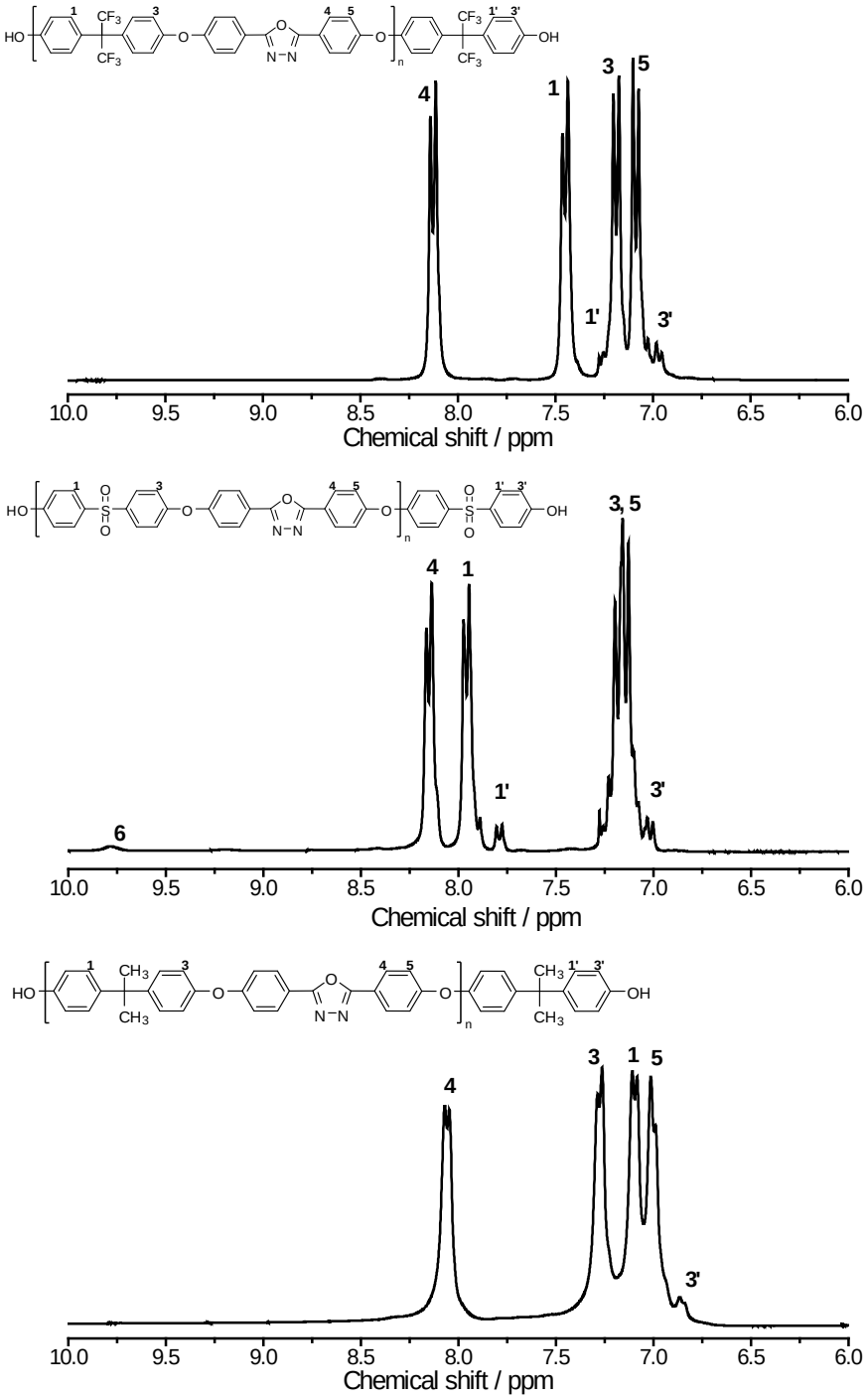

Figure 2.6 ^{1}H NMR spectrum of poly(arylene ether 1,3,4-oxadiazole)s taken in DMSO-d6.

2.3 Silanation

Bromophenyltrimethoxysilane was attached on the surface of fumed silica following Figure 2.7. The Aerosil A380 nanoparticles were first evacuated at 150 °C to eliminate the water adsorbed on the surface. After that a suspension of 4 g of dried silica and Bromophenyltrimethoxysilane in 70 mL of dehydrated Toluene was vigorously stirred at 60 °C for 3 days. The particles were washed several times with Toluene to remove any unreacted silane, using a centrifuge and removing supernatant liquid after each wash. The solid was dried overnight in a vacuum oven at 60 °C [14].

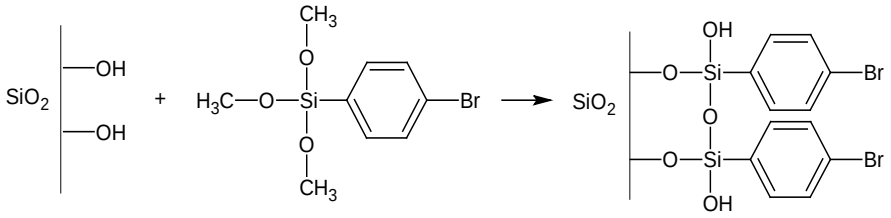

Figure 2.7 Silanation of the silica surface with bromophenyltrimethoxysilane.

Figure 2.8 shows the FTIR spectra obtained for the pristine and modified silica on a Bruker Equinox IFS 55 spectrophotometer in the range 4000–400 cm^{-1}. The samples were mixed (1 wt. %) with dried KBr, and compressed to obtain a translucent disc. The infrared absorption bands with peaks at 1560 cm^{-1} and 1470 cm^{-1} correspond to –C=C– stretching in aromatic rings and to Si–Ar stretching respectively, confirming the presence of silane groups attached to silanol groups on the silica surface.

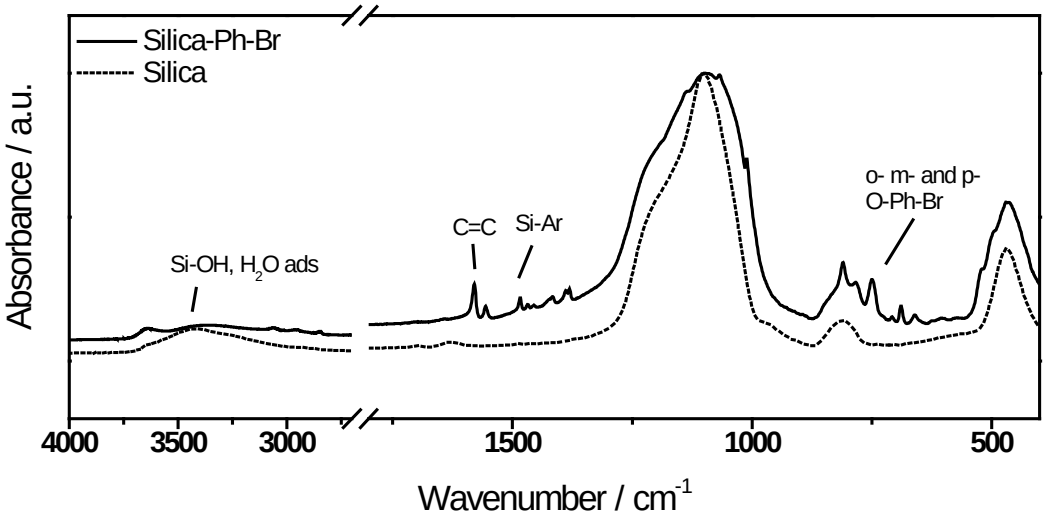

Figure 2.8 FTIR spectrum of neat silica and silane-modified silca.

The bands at 750–700 cm^{-1} are related to Bromine in ortho- and meta- positions on the aryl rings. A significant reduction of intensity is observed for the broad band at 3400–3100 cm^{-1}, corresponding to O–H stretching of silanol and to water adsorbed on the silica shell. This confirms a decrease in the amount of hydroxyl groups on the silica surface due to silane attachment. Additionally the strong absorption band peaking at 1100 cm^{-1} is due to siloxane stretching. The attachment of silane onto silica was further confirmed by the ^{1}H-NMR spectrum of silanated silica taken in Toluene. The commercial bromosilane used in the synthesis is a mixture of isomers, consequently signals for aryl protons in both *meta*- and *para*- positions to a substituted bromide are observable. Details on the infrared band assignment are shown in Table 2.2.

The thermal stability of grafted silica was analyzed by TGA. The weight loss of about 1% in the temperature range 25–110 °C is due to the elimination of adsorbed water, while the loss in the range 130–350 °C can be attributed to residual adsorbed NMP (bp. ~203 °C) and unreacted silane (bp. ~250 °C). Finally, after 350°C the bonded silane is gradually lost [79].

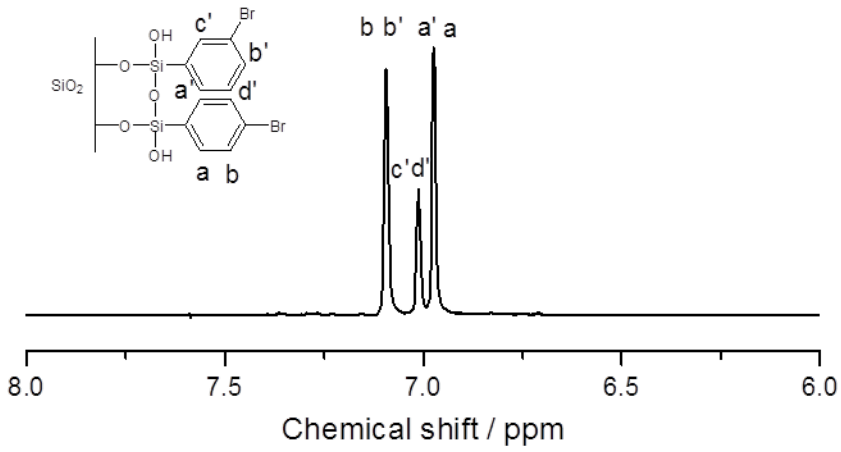

Figure 2.9 ^{1}H-NMR spectrum of silanated silca in toluene.

The attachment of silane onto the silica surface can be studied by varying the proportion of silane and silica in the reaction mixture, and determining the bonded silane on the resulting product by thermogravimetry. When the mole ratio of bromosilane is increased, the amount of grafted silane on the silica surface increases accordingly, until a plateau is reached. The apparent asymptotic maximum is around 7 % (mass of grafted silane to total mass). This maximum corresponds to about 0.37 mmol of silane per gram of silica. For comparison, a series of grafting reactions was performed with 100% *para*-substituted bromosilane. The amount of silane was varied from 2.25 to 13.50 mmol per gram of silica. The maximum mass of grafted silica attained with the pure *para*-bromosilane is similar to that obtained with the isomer mixture.

In both cases about 95% of the asymptotic maximum loading is attained with a mixture of 7 mmol of silane per gram of neat silca, as shown in Figure 2.11 and Figure 2.13 This is the optimal composition of the silanation reaction mixture. At lower ratios of bromophenyltrimethoxysilane to silica, the para-isomer shows higher silanation yield, since it is not affected by the steric hindrance effect of meta-Bromine [80]. For practical applications, however the isomer mixture is preferable, since its can be acquired for a fraction of the cost of the 100% *para*-silane.

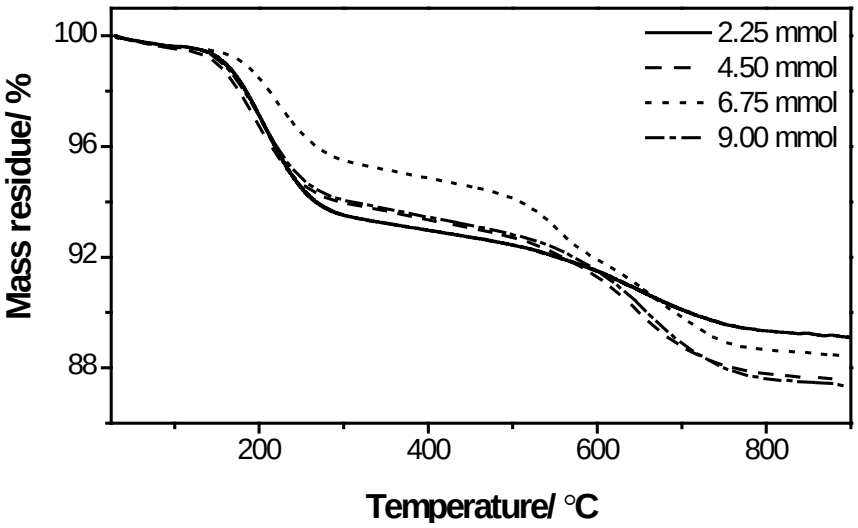

Figure 2.10 TGA thermograms of silica reacted with increasing amounts of a mixture of Bromophenyltrimethoxysilane isomers.

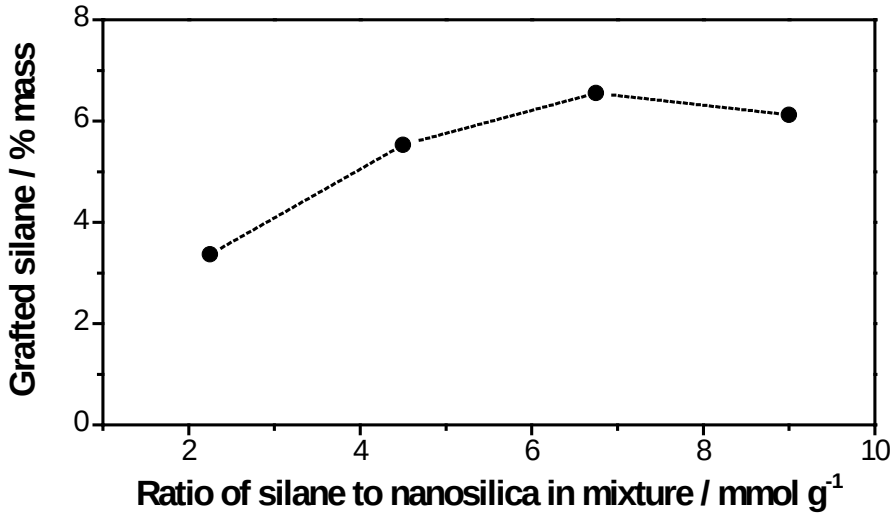

Figure 2.11 Ammount of grafted bromosilane on the silica surface as a function of the ratio of bromophenyltrimethoxysilane to silica in the reaction mixture. Data for the mixture of isomers.

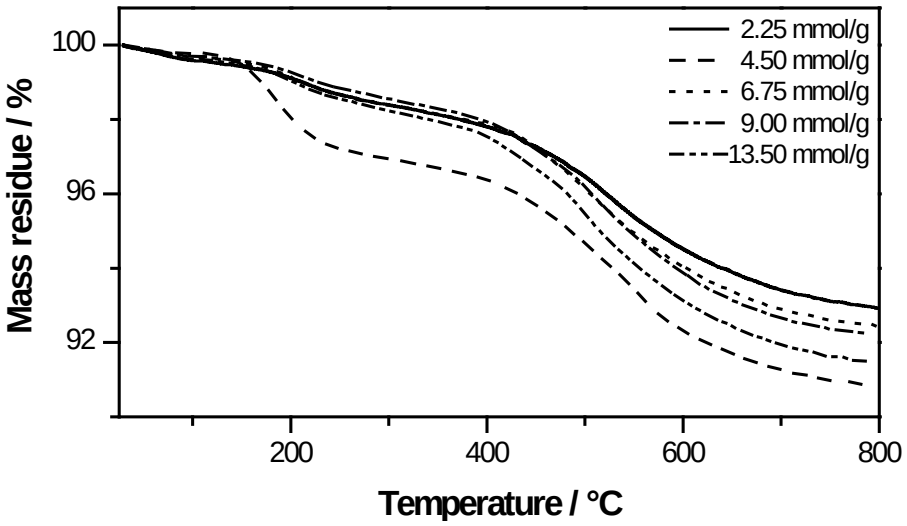

Figure 2.12 TGA thermograms of silica reacted with increasing amounts of a 100% *para*-bromophenyl trimethoxysilane.

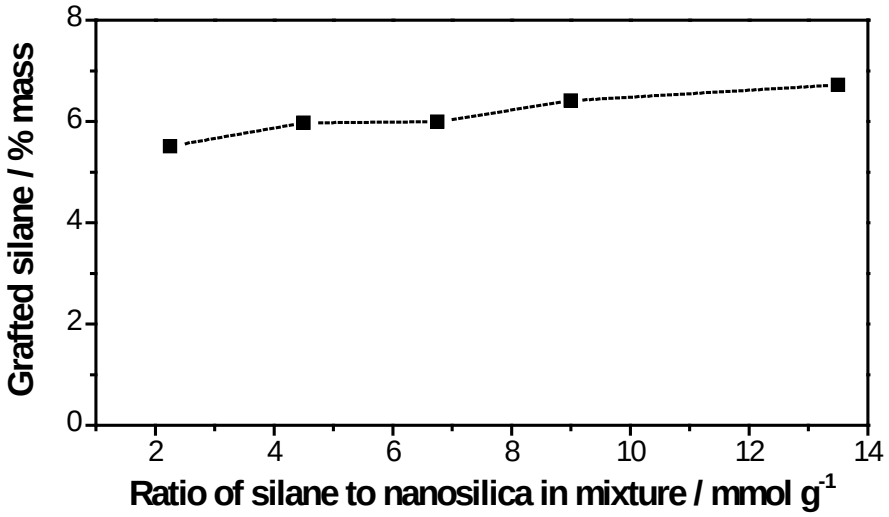

Figure 2.13 Ammount of grafted bromosilane on the silica surface as a function of the ratio of bromophenyltrimethoxysilane to silica in the reaction mixture. Data for the 100% *para*- isomer.

2.4 Functionalization of silica

The functionalization of silica with Poly(arylene ether 1,3,4-oxadiazole) oligomers was carried out as depicted in Figure 2.14, following the protocol described by Gomes et al. [14]. The oligomer and a mixture of 2:1 NMP and Toluene were introduced in a three-neck flask equipped with Dean-Stark trap and distilled at 110 °C for 3 hours under nitrogen atmosphere to eliminate the water formed as an azeotrope with Toluene. Subsequently, bromosilane–modified silica was added, and the mixture was further stirred at the same temperature for 18 hours.

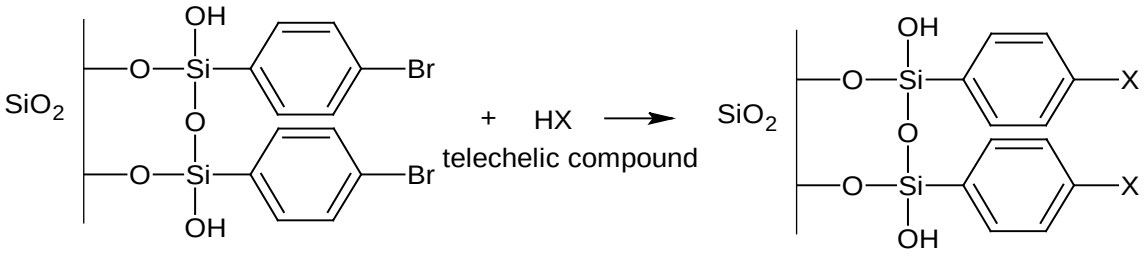

Figure 2.14 Functionalization of silanized silica.

The functionalized particles were washed several times in NMP to remove any unreacted oxadiazole oligomers, each time centrifuging and removing the supernatant liquid. The obtained solid was dried at 60 °C in a vacuum oven for 2 days. ODF, ODS and ODA–functionalized silicas were thus prepared and characterized by FTIR and NMR.

The oxadiazole rings in all samples are evidenced by infrared spectroscopy in the absorption bands at 1400 and 1100 cm^{-1}, which are due to the –C=N– and =C–O–C= stretching, respectively. The bands at 1200, 1070 and 2875 cm^{-1} are asigned to C–F, S=O and $–CH_3$ of the bisphenol groups in ODF, ODS and ODA correspondingly. All three functionalized silicas show the two bands around 900 cm^{-1}, characteristic of oxadiazole rings. Details on the infrared band assignment are shown in Table 2.2.

Table 2.2 Infrared assignments [81].

Frequency (cm^{-1})	Bond	Type of compound
770-730	*v* C–H	Aromatic *ortho*-substitution
810-750	*v* C–H	Aromatic *meta*-substitution
860-800	*v* C–H	Aromatic *para*-substitution
970–920	Si–O–Ar	Silicon, Si–O stretch
1075–1030	*v* C–Br	Aryl carbon
1090–980	*v* C–O–C	Ring breathing of oxadiazole
1130–1000	v_{as} Si–O–Si	Silicon
1200–1120	v_s SO_2	Silicon
1280–1220	*v* C–O–C	Aryl ether
1365–1120	*v* C–F	Alkyl carbon
1430	*v* Si–Ar	Silicon, Ring mode
1600–1500	*v* C=C	Aromatic carbon, Two or three bands
1650–1380	*v* C=N	Ring stretching band of oxadiazole
2850–2810	*v* O–CH_3	Methoxy phenol
3500–3100	*v* Si–OH	Silicon,OH stretch

v, stretch; v_{as}, asymmetric stretch; v_s, symmetric stretch

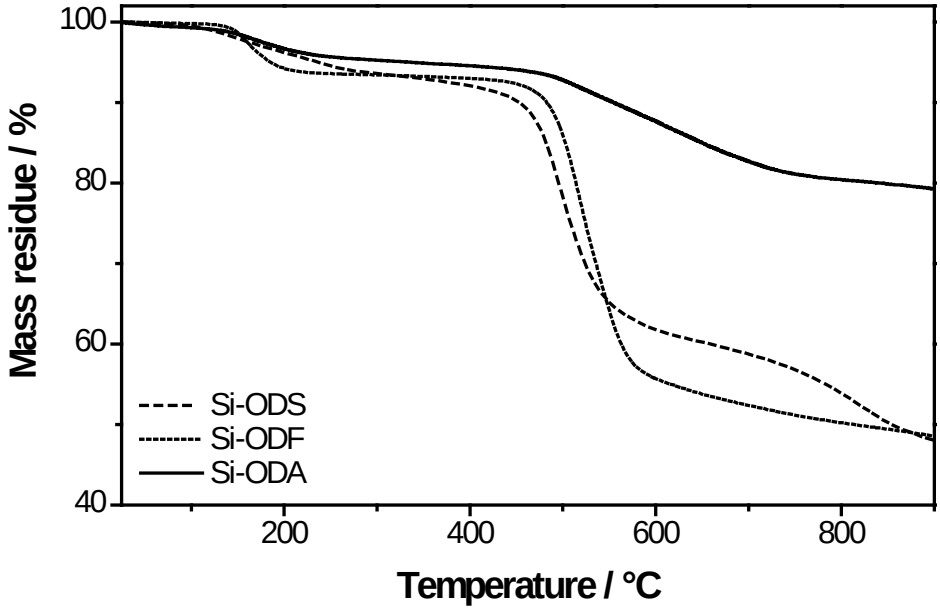

Figure 2.15 TGA thermograms of telechelic-functionalized silica nanoparticles.

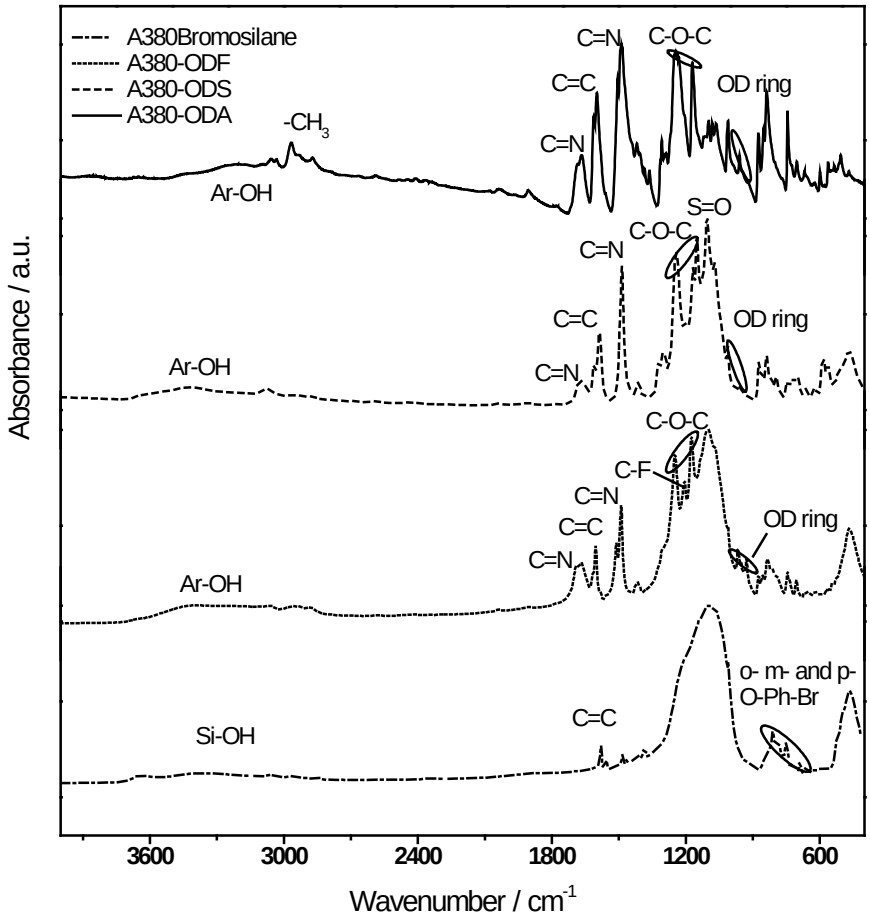

Figure 2.16 FTIR spectra of silica nanoparticles after silanation, and after functionalization with ODF, ODS and ODA.

The thermal stability of these functionalized silicas was characterized by TGA as shown in Figure 2.15. The weight loss in the range 120–200 °C is associated with the elimination of residual Toluene and NMP used in the solvent mixture for the functionalization reaction. The total solvent residue was around 5 wt.%. The weight loss starting at 350–400 °C corresponds to the loss of grafted oligomer ODF, ODS or ODA, and points out to total grafted-oligomer amounts of 40, 34 and 15 wt.% respectivlely. This means the amount of telechelic oligomers ODF, ODS and ODA attached on silica surface per 1 gram of silica are 0.13, 0.08 and 0.04 mmol respectivlely. From the TGA thermogram it can be concluded that the thermal stability of the functionalized nanoparticles is well above that needed for PEMFC application.

2.5 Summary

This chapter described the synthesis of three different oxadiazole-type telechelic oligomers, and their use to prepare functonalized silica nanoparticles, following the protocol developed by Gomes et al. For the silanation step, thermal analysis allowed the identification of the reactant mixture composition necessary to obtain maximum particle loading. The chemical structure of the compounds and functionalized particles was studied by ^{1}H-NMR, EA and FTIR techniques, confirming the success of each synthesis step. In addition the molecular weight of the synthesized telechelics was studied by SEC. For all three cases, the degree of polymerization obtained was around 10. Moreover, the thermal properties of the grafted particles were investigated by TGA and DSC. The functionalized particles show the first degradation steps above 350°C, well beyond the needed thermal stability for PEM fuel cell application.

Chapter 3. Membrane fabrication and characterization

After functionalized silica has successfully been synthesized in chapter 2, in this chapter the grafted silica will be used as filler in composite membranes, in order to improve their properties relevant to fuel cell application. The polymer matrices used in this study are Nafion®, poly(arylene ether 1,3,4-oxadiazole), and fluorinated polyoxadiazole random copolymers. In addition to solvent casting, in the case of Nafion® composites, melt extrusion will also be explored for membrane manufacture. The silica functionalized with fluorinated oxadiazole telechelic oligomer (ODF) will be used for the preparation of composites, as its chemical structure is similar to that of the polymer matrices. Electrochemical, mechanical and thermal properties of the composite membranes are also described in this chapter.

3.1 Membrane fabrication

3.1.1 Solvent cast Nafion® composite membranes

A 5 wt.% Nafion® solution was employed in the preparation of the functionalized silica-Nafion® composite membranes. Since the oligomers attached to the silica surface have a good solubility in DMAc, this solvent was added in a ratio 2:1 to the Nafion® solution in order to improve the nanoparticle dispersion. After that, functionalized silica was added to the mixture. The solutions were then vigorously stirred for 4 h at 50 °C so as to partially evaporate the solvent mixture until a 10 wt.% Nafion® solution was obtained. Subsequently the mixtures were stirred overnight and sonicated for 30 minutes to disperse the silica particles. Finally, a doctor blade with a 650 µm gap was used to cast the solutions on clean glass plates. The cast

membranes were kept at 60 °C overnight and then cooled down to room temperature. Finally, the films were detached from the glass plates, and dried in a vacuum oven at 60 °C overnight. The thickness of the resulting membranes was around 30–40 µm. Photographs of the solvent cast composite membranes are shown in Figure 3.1.

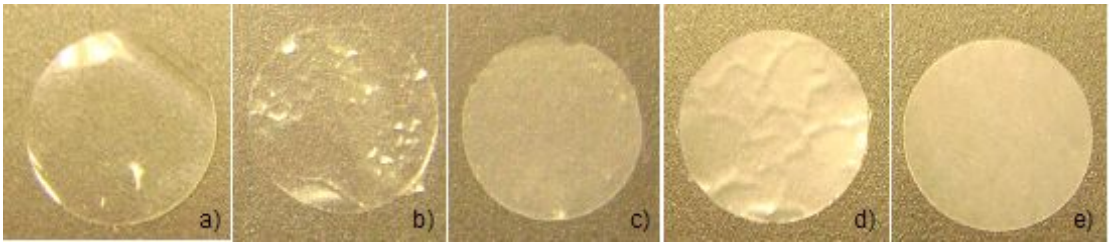

Figure 3.1 Nafion® composite membranes with a) 0, b) 5, c) 10 wt.% of neat silica d) and e) 5 and 10 wt.% of functionalized silica.

3.1.2 Melt extruded Nafion® composite membranes

Blends based on extrusion grade Nafion® in the sulfonyl fluoride ($–SO_2F$) form [82] containing 5 and 10 wt.% of functionalized silica were prepared in a 5 cm^3 DSM micro-twin screw extruder (Figure 1.15) at 240 °C. A two-step extrusion process was applied: nanocomposite blend preparation using counter-rotation screws configuration, followed by film preparation using co-rotation screws configuration. A screw rotation speed raging from 5 to 10.5 rad s^{-1} (~50 to 100 rpm) was used. The extruder was equipped with a 0.1 mm x 3.5 cm die. The thickness of the resulting membranes was in the range 25–35 µm.

The blends containing 10 wt.% silica particles had a high viscosity, resulting in less uniform films when compared to the 5 wt.% blends. Nafion® in the sulfonyl fluoride form does not have cation-exchange properties and must be chemically treated to make it suitable for use in applications requiring proton conduction. The extruded Nafion® film was converted to the salt (K^+) and acid (H^+) forms following a process similar to the one recommended by the manufacturer [83]. The film was hydrolyzed by immersion in a solution of 10% potassium hydroxide, 37% DMSO and 53% de-ionized (DI) water at 40 °C for 30 minutes. Subsequently, the film was thoroughly

washed with DI water, by soaking three times in room-temperature DI water for 30 minutes, in order to remove all traces of unreacted KOH. Finally the membrane was dried in vacuum oven at 60°C for 12 hours. The hydrolyzed film was changed to the H^+ form by exchanging the K^+ for H^+ ions in a 15% solution of nitric acid (HNO_3). This step was repeated three times with fresh nitric acid, including a fresh DI water rinse after each acid treatment. After that, the film was immersed three times in room-temperature DI water for 30 minutes. Finally the membrane was dried out in vacuum oven at 60 °C for 12 hours.

3.1.3 Poly(arylene ether 1,3,4-oxadiazole) composite membranes

The synthesis of poly (arylene ether 1, 3, 4-oxadiazole) was carried out following the protocol described by Vetter et al. [98] (Figure 3.2).

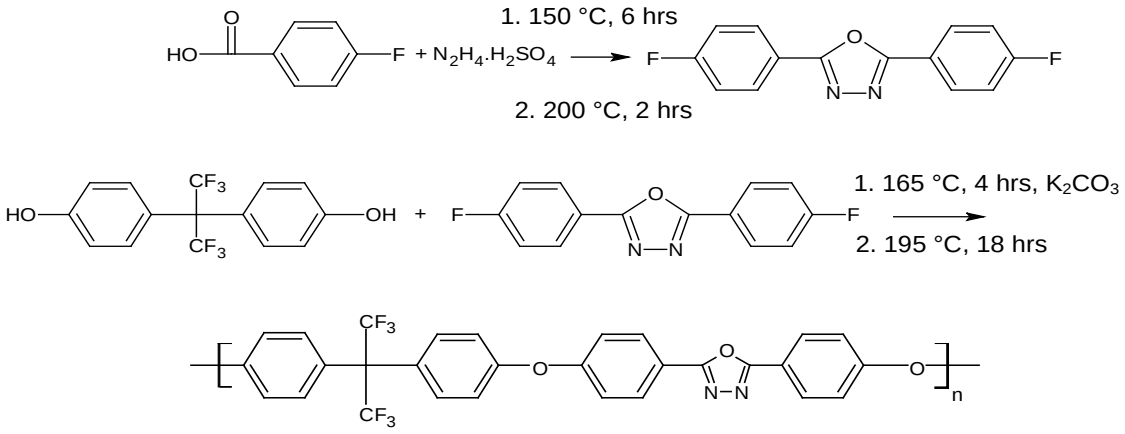

Figure 3.2 Synthesis of poly(arylene ether 1,3,4-oxadiazole).

The bisfluoro-oxadiazole monomer was synthesized in polyphosphoric acid as described in Chapter 2, giving white crystals with needle shape after recrystallization. For the the reaction between the oxadiazole monomer and bisphenol AF, 2.58 grams of 2,5-bis(4-fluorophenyl)-1,3,4-oxadiazole, 3.36 g of 4,4'-(Hexafluoroisopropylidene) diphenol and excess of potassium carbonate (3.32 g) were added to a three-neck flask connected with dried nitrogen inlet and a Dean–Stark trap fitted with a condenser. 40 ml of NMP and 15 ml of toluene were used as solvent. The mixture was stirred and the toluene refluxed at 165 °C for 4 hours and after that the reaction

was carried out at 195 °C for 18 hours. Then it was cooled down to room temperature. Finally the polymer was precipitated into water, filtered, washed with methanol and dried in vacuum oven at 80 °C overnight.

The successful synthesis of polyoxadiazole polymer was confirmed by 1H and 13C NMR. The corresoponding spectra are shown in Figure 3.3. In the 1H NMR spectrum, obtained in CDCl3 solution, the signal at 8.15 ppm can be assigned to 4 aromatic protons in position ortho to the oxadiazole ring; at 7.45 ppm the signal results from 4 aromatic protons in position meta to the perfluorinated isopropylidene moiety; the signal at 7.21 ppm refers to 4 aromatic protons in meta to the oxadiazole ring and finally at 7.10 ppm, the signal corresponds to 4 aromatic protons in ortho to the hexafluoroisopropylidene moiety. For the 13C NMR spectrum, the carbon signals at chemical shifts 164, 119.7, 129, 119.6, 159, 157, 118.5, 132, 128.5, and 78 ppm are assigned to carbons in position 1 to 10 respectively.

Size exclusion chromatography (GPC) analysis was employed to determine the molecular weight of the synthesized polymer, using polystyrene as standard polymer and chloroform as eluent solvent. The number average molecular weight (Mn) obtained was 17300 (17289) g mol-1, with a weight average molecular weight (Mw) of 41000 (41025) g mol-1, and a polydispersity index (PDI) of 2.373.

The thermal properties of the polymer were evaluated by differential scanning calorimetry (DSC) and thermogravimetric analysis (TGA). As shown in Figure 3.5, the glass transition temperature (Tg) of this polyoxadiazole polymer is around 210 °C. On the TGA thermogram the first weight loss at 50-120°C can be assigned to elimination of adsorbed methanol and water, while the second weight loss at 150-200 is probably due to adsorbed NMP (from the polymerization reaction mixture). The third weight loss corresponds to polyoxadiazole degradation, and reveals for this polymer a thermal stability of up to 400 °C.

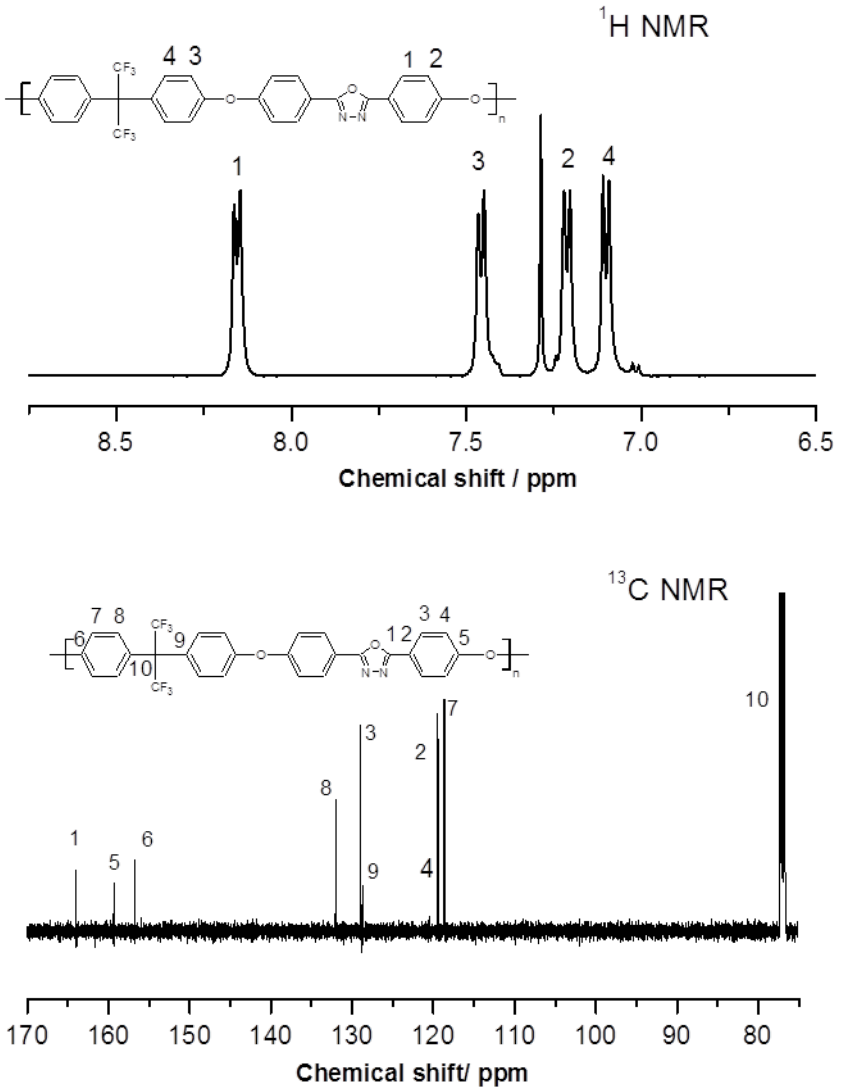

Figure 3.3 ^{1}H and ^{13}C NMR spectrum of poly(arylene ether 1,3,4-oxadiazole) in $CDCl_3$.

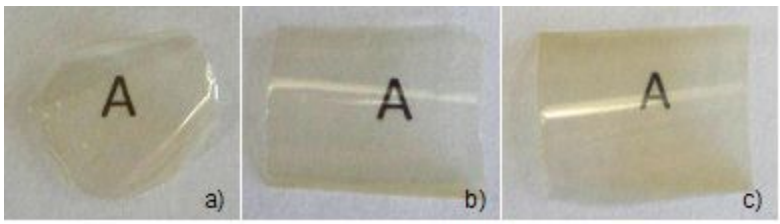

Figure 3.4 Poly(arylene ether 1,3,4-oxadiazole) membranes: a) pure polymer, b) membrane with 10 wt% neat silica c) membrane with 10 wt.% grafted silica.

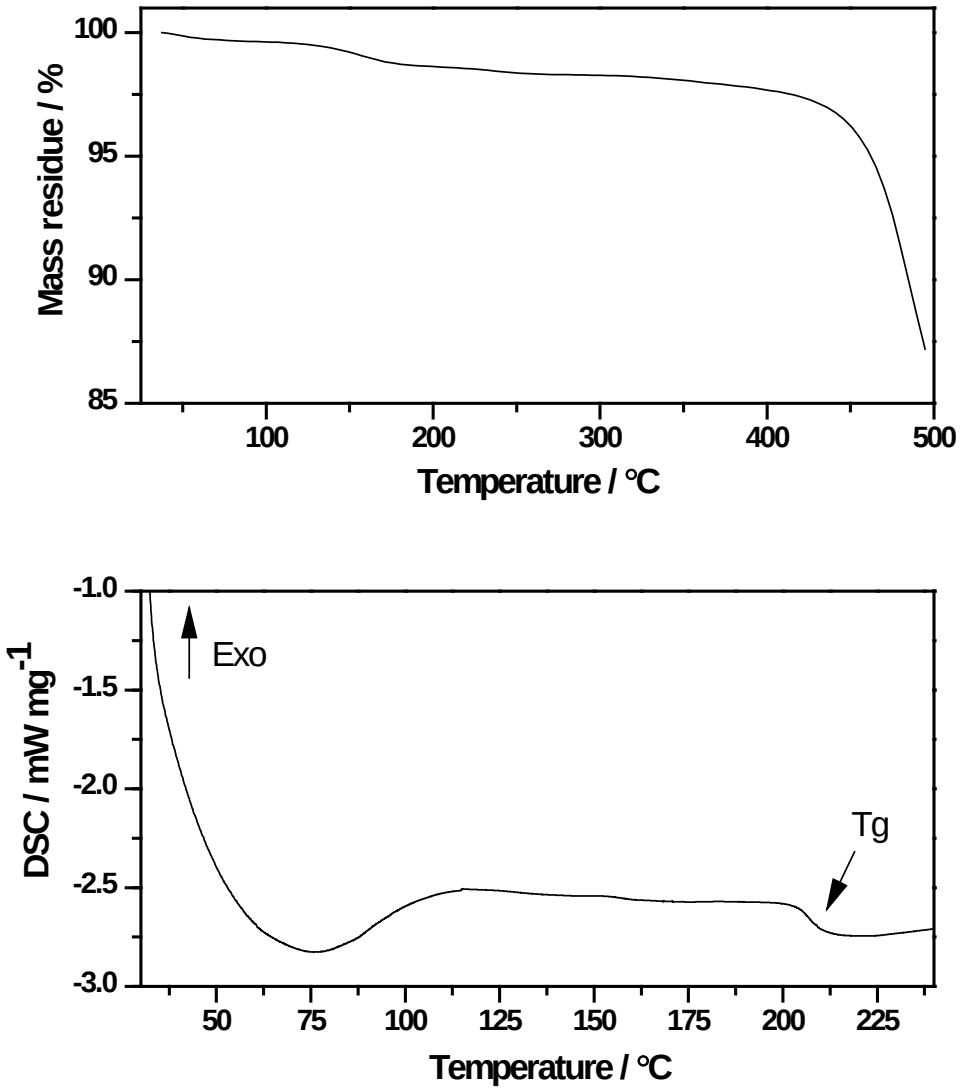

Figure 3.5 TGA and DSC thermograms of poly(arylene ether 1,3,4-oxadiazole).

Membranes from this polyoxadiazole were prepared by solvent casting, from solutions 10 wt.% of polymer in DMAc. The solutions were first vigorously stirred for 1 hour at room temperature. After filtering, 5, 10 and 15 wt.% functionalized silica was added. The particles were dispersed by mechanically stirring for 3 hours and sonicating for 15 minutes. Subsequently the solutions were cast onto glass plates using a ~75 µm (3 mil) bird bar plus ~250 µm (10 mil) tape spacer. The cast plate was left in the oven at 50 °C overnight and then it was cooled down to room temperature. Finally the membranes were dried out in vacuum oven at 60 °C overnight. Thickness of the obtained membranes was around 30 ± 5 µm.

Photographs of the resulting poly(arylene ether 1,3,4-oxadiazole) composite membranes are shown in Figure 3.4.

3.1.4 Fluorinated polyoxadiazole random copolymer composites

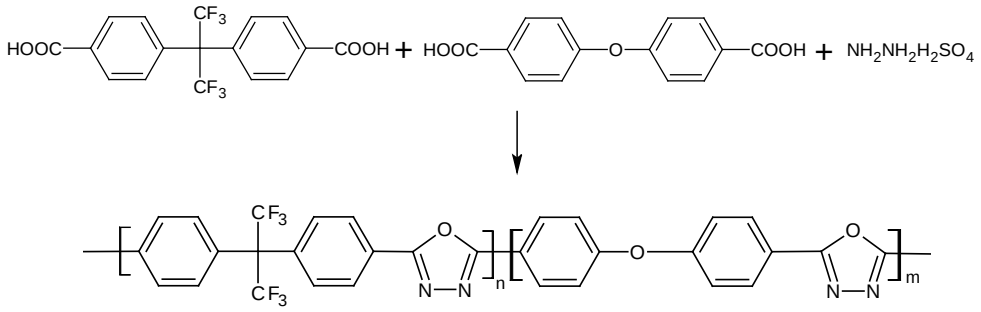

Figure 3.6 Synthesis of fluorinated polyoxadiazole random copolymers.

For comparison with the two polymer matrices described above, a series of four fluorinated polyoxadiazole random co-polymers were obtained from a sister research line in the WT Institute at HZG. They were synthesized at HZG following Figure 3.6, with molar ratios of 2-(diphenyl ether)-1,3,4-oxadiazole (ODBA) to 2-[4,4'-(Hexafluoroisopropylidene)diphenyl]-1,3,4-oxadiazole (FDBA) equal to 0.5, 1.0, 2.0 and 3.0 (called "PODOcoF-A", "PODOcoF-B", "PODOcoF-C", and "PODOcoF-D", respectively). For membrane preparation, 10 wt.% copolymer solutions in NMP were prepared by virgorously stirring the corresponding polymer-solvent mixtures for 2 days at 50 ºC. After filtering the solutions, 5 and 10 wt.% of grafted silica nanoparticles were added. The nanoparticles were dispersed by mechanically stirring for 2 days and sonicating for 30 minutes. After that the solutions were cast onto glass plates using a doctor blade with a 650 µm gap. The coated plates were left in the oven at 50 °C overnight and then cooled down to room temperature. The membranes were then detached from the glass plates and dried in vacuum oven at 60 °C overnight. The thickness of the resulting membranes was around 40 ± 5 µm.

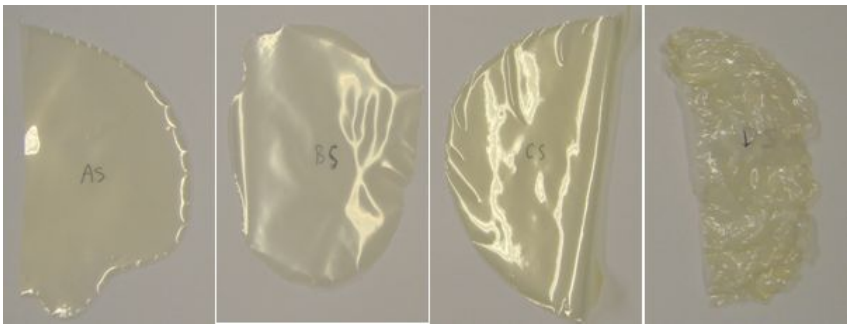

Figure 3.7 Fluorinated polyoxadiazole random copolymer membranes.

3.2 In-situ post-sulfonation of the functionalized filler

In order to attach sulfonic acid groups onto the telechelic chains grafted on the silica nanoparticles, the composite membranes were subjected to a post-sulfonation treatment, by soaking the membranes in 50 wt.% H_2SO_4 at room temperature overnight. After that, the residual acid was washed out by rinsing the membranes with DI water and then immersing them in fresh DI water for 30 minutes. The washing procedure was repeated several times, checking the wash water with pH paper strips, until a pH ~7 was obtained. Finally, the membranes were dried at 60 °C overnight in vacuum oven.

3.3 Membrane characterization results

3.3.1 Nafion® composites

The main function of the polymer electrolyte membrane in a fuel cell is proton transport. In sulfonic acid based membranes, the proton conductivity depends on the amount of accessible acid groups and their dissociation potential in water [41]. Thus, ion exchange capacity and conductivity can provide insight into the ability of a membrane to transport protons.

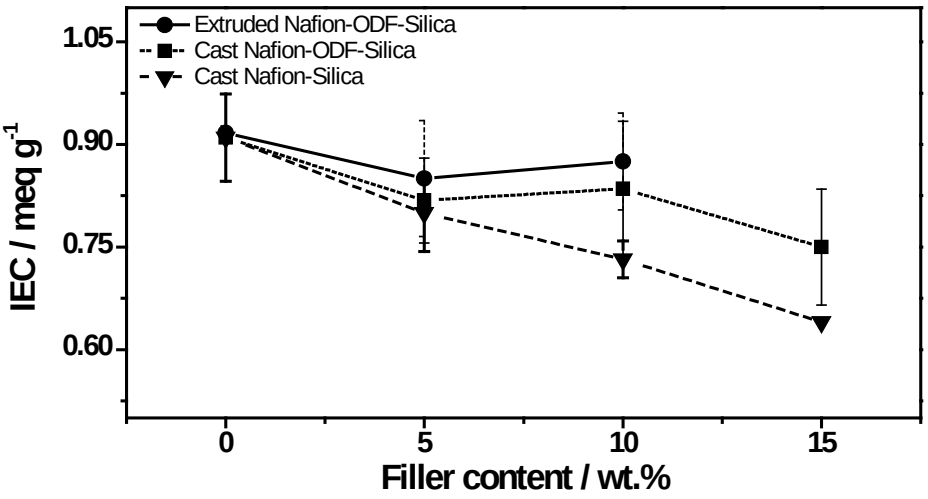

Figure 3.8 Ion exchange capacity of Nafion® composite membranes as a function of filler content.

Figure 3.8 shows IEC values for the Nafion® composite membranes as a function of filler content. For solvent-cast membranes, introducing 5 wt.% of silica nanoparticles causes a reduction in the IEC: from 0.91 down to 0.80 meq g^{-1} for neat silica, and a slightly lower decrease for functionalized silica, down to 0.82 meq g^{-1}. However, for membranes containing 10 wt.% of functionalized filler, the IEC stabilizes, even slightly increasing back from 0.81 to 0.84 meq g^{-1}, as the sulfonic acid groups in the oligomers compensate for the loss of sulfonated matrix. This is in contrast with 10 wt.% neat silica composites, for which the IEC continues to decrease down to 0.73 meq g^{-1}. Nevertheless, with a further increase in the loading of functionalized silica to 15 wt.%, the IEC drops down again, probably due to the agglomeration of filler particles, which makes a large portion of the oligomer-bonded sulfonic acid groups inaccessible.

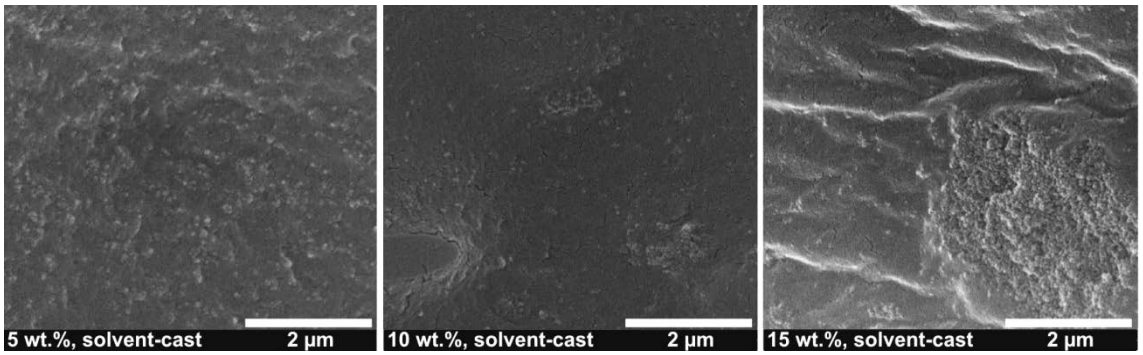

Figure 3.9 SEM micrographs of solvent-cast Nafion composite membranes containing 5, 10 and 15 wt.% functionalized silica.

As evidenced by the scanning electron microscopy (SEM) photographs in Figure 3.9 filler agglomeration in the solvent-cast membranes is already observable at 10 wt.% loading, and significant at 15 wt.%. A similar trend is found for the extruded, functionalized-silica composite membranes. IEC decreases to 0.85 meq g-1 for 5 wt.% loading, but stabilizes and slightly increases back to 0.88 meq g-1 for films with 10 wt.% filler content.

The through-plane conductivities of solvent-cast and extruded composite membranes with increasing loadings are shown in Figure 3.10. For our solvent-cast pure Nafion® membranes, the conductivity was around 56 mS cm-1. 5 wt.% loadings of neat and functionalized silica reduce this value to 24 and 36 mS cm-1 respectively. For the 10 wt.% composites, the proton conductivity increases again to 49 mS cm-1 for functionalized silica particles, but continues to drop for membranes with neat silica.

The dependency of conductivity values on filler type and content is similar to the trend observed for IEC values. The presence of sulfonate groups on the ODF-functionalized silica compensates for the loss of sulfonated polymer matrix [36]. Furthermore, the oxadiazole groups contain a basic nitrogen (-N=) which can contribute to the charge transport by exchanging protons with sulfonic acid groups (-SO_3H) [15]. The decline in conductivity towards 15 wt.% grafted silica content can be similarly explained by nanoparticle agglomeration, with the consequent loss of sulfonate group accessibility.

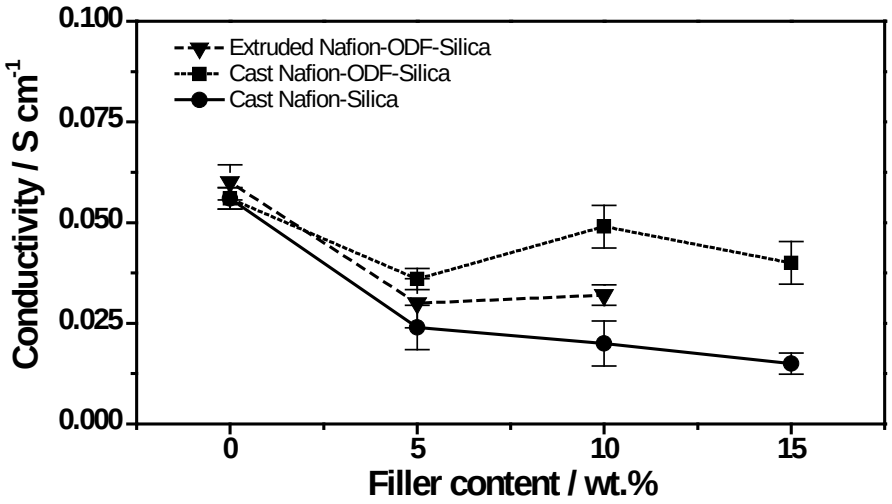

Figure 3.10 Proton conductivity of the Nafion® composite membranes as a function of filler content.

The average IEC values for the ODF-silica composites prepared by solvent casting are similar to the values for the extruded membranes. However, higher proton conductivity values are observed for solvent-cast membranes when compared to extruded membranes with the same filler content. A possible explanation is the better dispersion achieved in the solvent-cast membranes, as shown by the SEM micrographs in Figure 3.11. Solvent-cast membranes show a number of macroaggregates, the largest of which tend to accumulate towards the bottom side of the membrane. Nevertheless, a significant fraction of filler in still distributed in well-dispersed very small aggregates. Conversely, extruded membranes present a large number of evenly distributed medium-size agglomerates. While proton-exchange groups in the core of moderately size agglomerates are still accessible for ion exchange, and thus contribute to the global IEC of the membrane, only the groups on the agglomerate surface, in intimate contact with the protogenic matrix, contribute significantly to the proton conductivity of the composite.

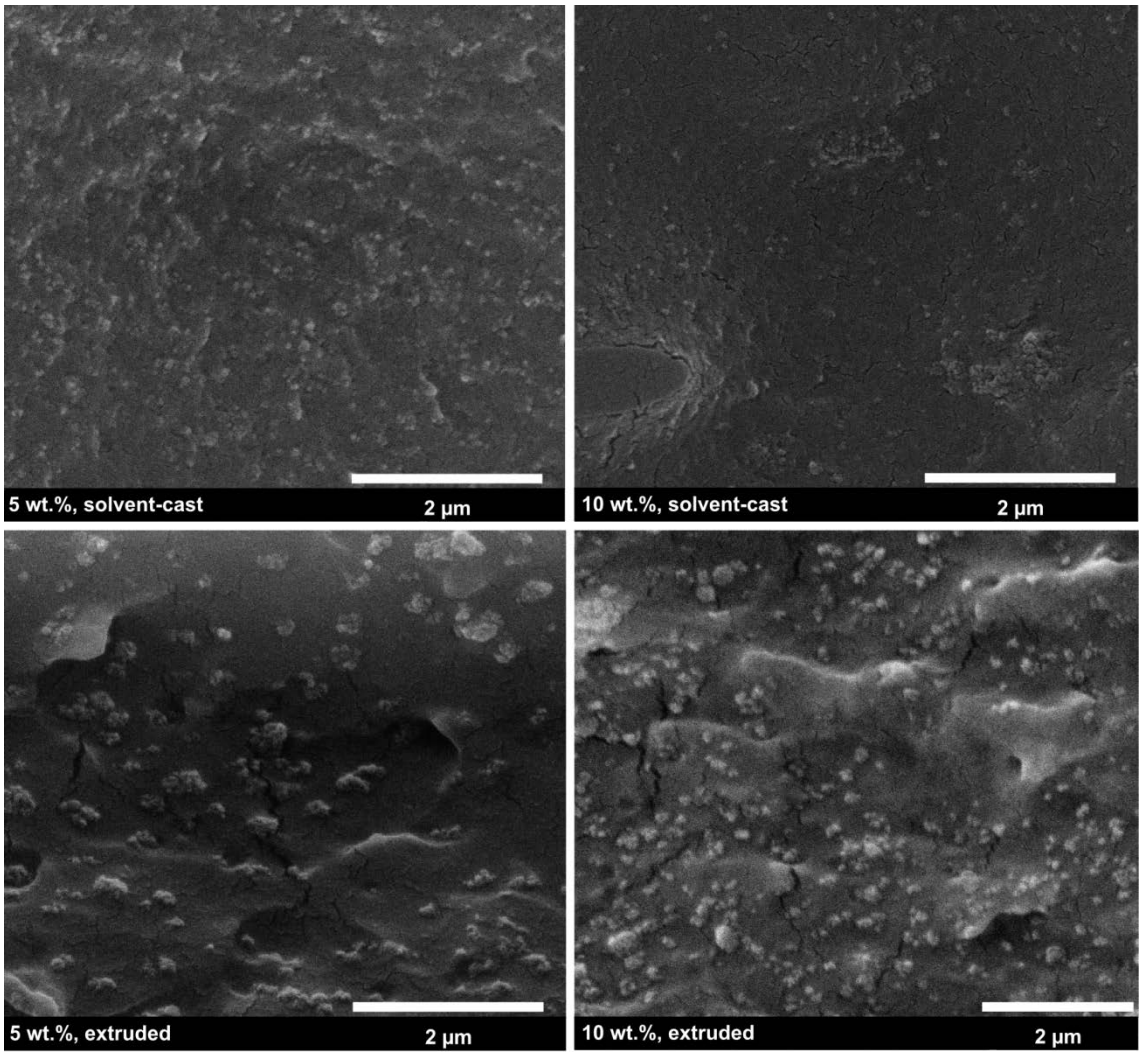

Figure 3.11 SEM micrographs of 5 and 10 wt.% solvent-cast (above) and 5 and 10 wt.% extruded (below) Nafion® composite membranes containing ODF-functionalized silica nanoparticles.

For solvent-cast ODF-functionalized silica composites, water uptake drops from the 58% of pure Nafion® down to 35% for membranes containing 5 wt.% of filler. For higher filler contents the water uptake slowly increases up to 42% for membranes with 15 wt.% loading. While a similar trend is observed for the solvent-cast composites containing neat-silica, the latter presents higher water uptakes at all loadings (down to 43, and then up again to 50 and 57%, for composites with loadings of 5, 10 and 15 wt.% respectively).

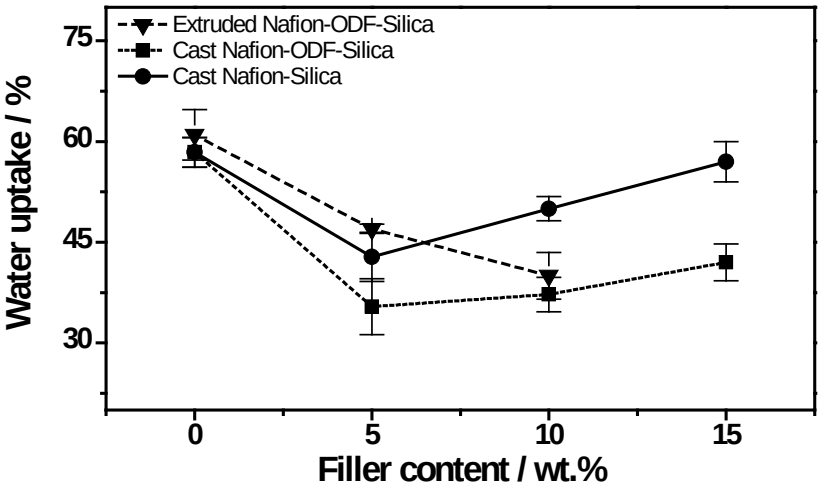

Figure 3.12 Water uptake at room temperature and 100% RH for Nafion® and composite membranes as a function of filler content. Figure 3.10 and Figure 3.11 show respectively the evolution of water uptake and of thickness expansion, at room temperature and 100% RH, for Nafion® composite membranes with increasing filler contents.

A probable explanation for the initial drop in water uptake is the reinforcement effect of the particulate fillers. The nanoparticles act as physical crosslinks, significantly reducing swelling. As filler aggregation increases for the composites with higher loadings, the specific surface area of the fillers is reduced, and consequently the interaction with the matrix is less effective. Additionally, the ODF-functionalized silica particles contribute to the water uptake as they carry sulfonic acid groups. The drop in water uptake is less marked in the extruded membranes, as agglomeration is significant already at 5 wt.% loading.

Compared to the ODF-functionalized silica, the neat-silica particles have a lower affinity for the perfluorinated matrix. This originates a lower initial decrease in water uptake for the 5 wt.% neat-silica composites, and also in a faster increment in water uptake at higher filler contents, as agglomeration increases, and the interaction with the matrix is less efficient.

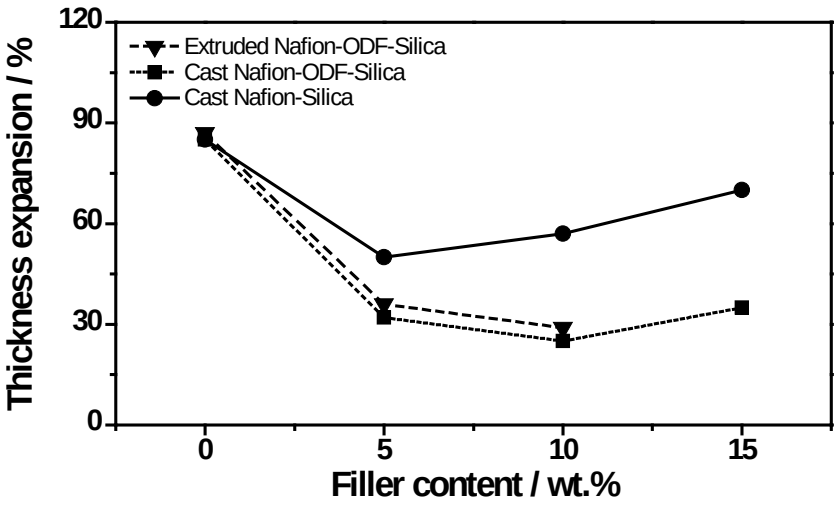

Figure 3.13 Thickness expansion at room temperature and 100% RH for Nafion® and composites as a function of filler content.

Analogously, for ODF-functionalized silica composites, both solvent-cast and extruded, the thickness expansion (Figure 3.13) drops from ~85% for pure Nafion®, down to ~35% for the membranes with 5wt.% filler content, and remains relatively stable at higher contents. This is in agreement with a strong interaction between the particles and the matrix. In contrast, for the neat-silica composites, with a weaker matrix-particle interaction, the thickness expansion increases again at higher loadings, as particle aggregation reduces the specific area of the fillers.

Thermogravimetric analysis curves for composite membranes studied in this work are shown in Figure 3.14. The mass residues after each thermal decomposition step, as well as the temperatures of the maxima of the derivative curves (DTG) for relevant steps, are given in Table 3.1 for solvent-cast and extruded Nafion® composites.

An initial mass loss (I) in the range 25–180 °C (not shown in the figure), with a derivative maximum around 120 °C, can be attributed to the elimination of adsorbed water, most of which is adsorbed in the ionic clusters of the Nafion® matrix [84].

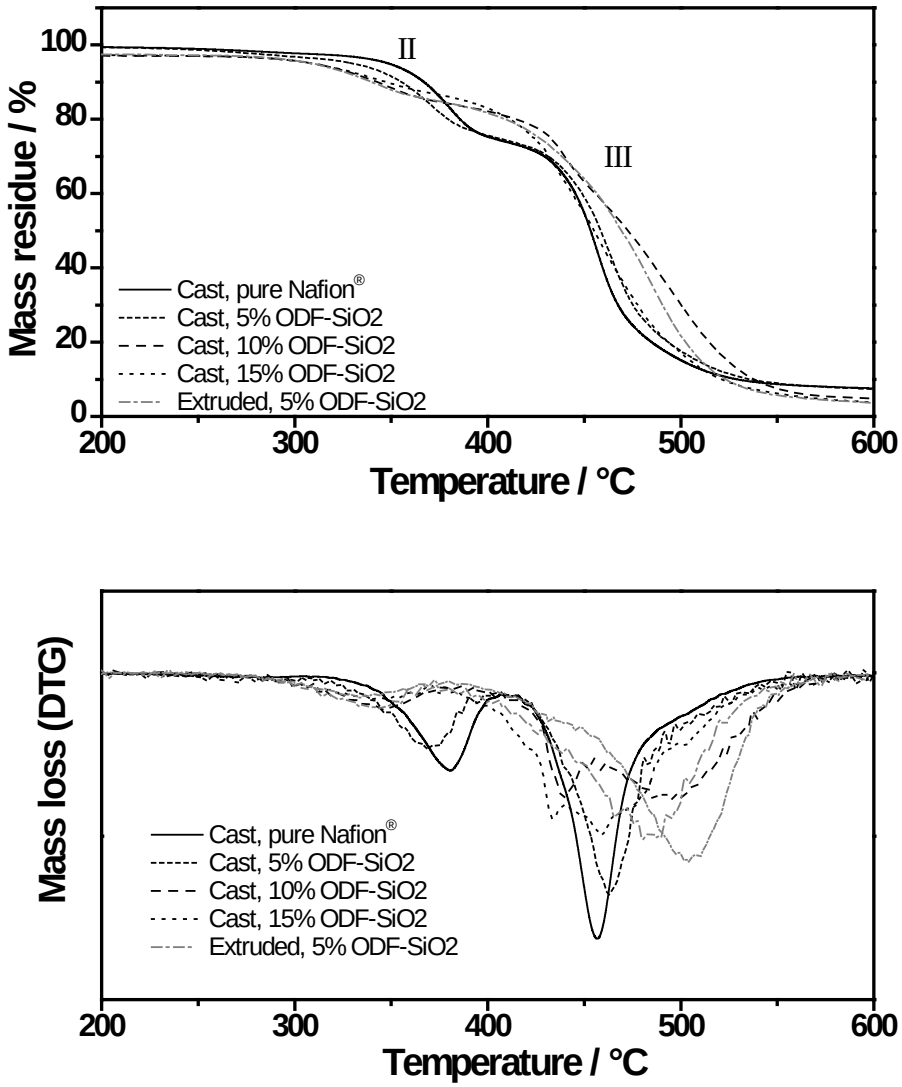

Figure 3.14 TGA curves obtained for solvent-cast and extruded Nafion® composites studied in this work. The derivative curves (DTG) are shown on the right side. See the text for a description of the mass loss step nomenclature.

The second mass loss step (II), in range of 300–400 °C, with DTG maximum in the range 340–380 °C, corresponds to the partial loss of sulfonic acid groups [85,86].

A net tendency is observed for the composites, with a shift of the DTG maximum to lower temperatures, as the content of grafted silica increases, probably due to contribution from the degradation of filler particles. However, the total mass loss is significantly lower in this step for the highly loaded composites. Three phenomena may account for this effect: firstly, at high filler loadings, the amount of Nafion® sulfonic acid groups is lower due to the decreasing fraction of polymeric matrix in the

composite. Secondly, while the matrix-bonded -SO_3H groups might, as they decompose, catalyze the degradation of the filler nanoparticles exposed to the matrix, at high loadings, due to agglomeration, a significant amount of filler is "protected" inside the agglomerates, and only contributes to mass loss at higher temperatures. Finally, *on average*, the -SO_3H groups present higher thermal stability, and decompose at higher temperatures, mainly due to the limitation on side chain mobility caused by the dispersed ODF-SiO_2 nanoparticles. A similar stability increase in the matrix -SO_3H groups was observed by Deng et al. [87] for Nafion® composites containing *in-situ* generated, post-functionalized SiO_2.

The third mass loss step (III), ranging from 420 to 550 ºC, consists of the complete oxidative degradation of the C-O-C moieties along with the fluorocarbon backbone in Nafion®, and of any remaining sulfonic acid groups [85,88]. The derivative of the thermogram evidences two stages for this step, with maxima in the ranges 430–470 (IIIa) and 480–520 (IIIb). For the composites, these last steps also include the degradation of the grafted oligomer backbone that is not in direct contact with the Nafion® matrix, which occurs in two consecutive steps as well, with DTG maxima at 515 °C and 540 °C. The thermogravimetric analysis curve for the pure non-sulfonated ODF oligomer is shown in Figure 3.15.

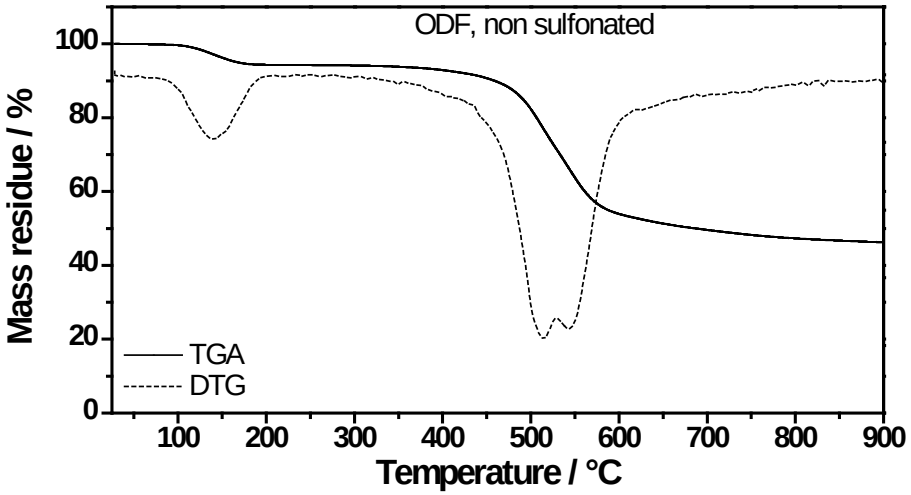

Figure 3.15 TGA curve (solid line) and its derivative (dotted line) for the non-sulfonated ODF oligomer.

Table 3.1 Mass loss for each of the three main steps in the thermograms of Nafion® ODF-Silica composite membranes.

Membranes	Mass loss / %			Temperatures of DTG maxima / °C	
	I	II	III	II	III
Cast Nafion®	0.58	25.30	69.60	380.4	455.9
Cast Nafion®, 5% ODF-SiO_2	0.50	24.28	70.22	370.2	463.4
Cast Nafion®, 10% ODF-SiO_2	2.84	13.04	80.93	348.9	439.7; 493.2
Cast Nafion®, 15% ODF-SiO_2	2.77	10.07	84.23	344.4	432.8; 460.2
Extruded Nafion®, 5%ODF-SiO_2	2.50	11.87	83.38	341.8	484.8
Extruded Nafion®, 10%ODF-SiO_2	2.50	9.35	86.21	334.9	503.7

Infrared analysis of the gases evolved during thermal decomposition provides further information regarding the effect of the ODF-SiO_2 particles on the structure and thermal stability of Nafion®. For solvent-cast pure Nafion®, telechelic oligomer ODF (post-sulfonated ex-situ with the same protocol applied to the composites and described earlier), and for the solvent-cast composite with 10 wt.% ODF-SiO_2, a series of FTIR spectra were obtained, at constant temperature intervals, from the volatile products generated during thermogravimetric runs in inert atmosphere. The thermograms were carried out on dry membranes, with an initial 15 min isotherm at 110 °C performed in order to further eliminate adsorbed water. Figure 3.16 shows the resulting spectra at 335, 440, 485 and 530 °C.

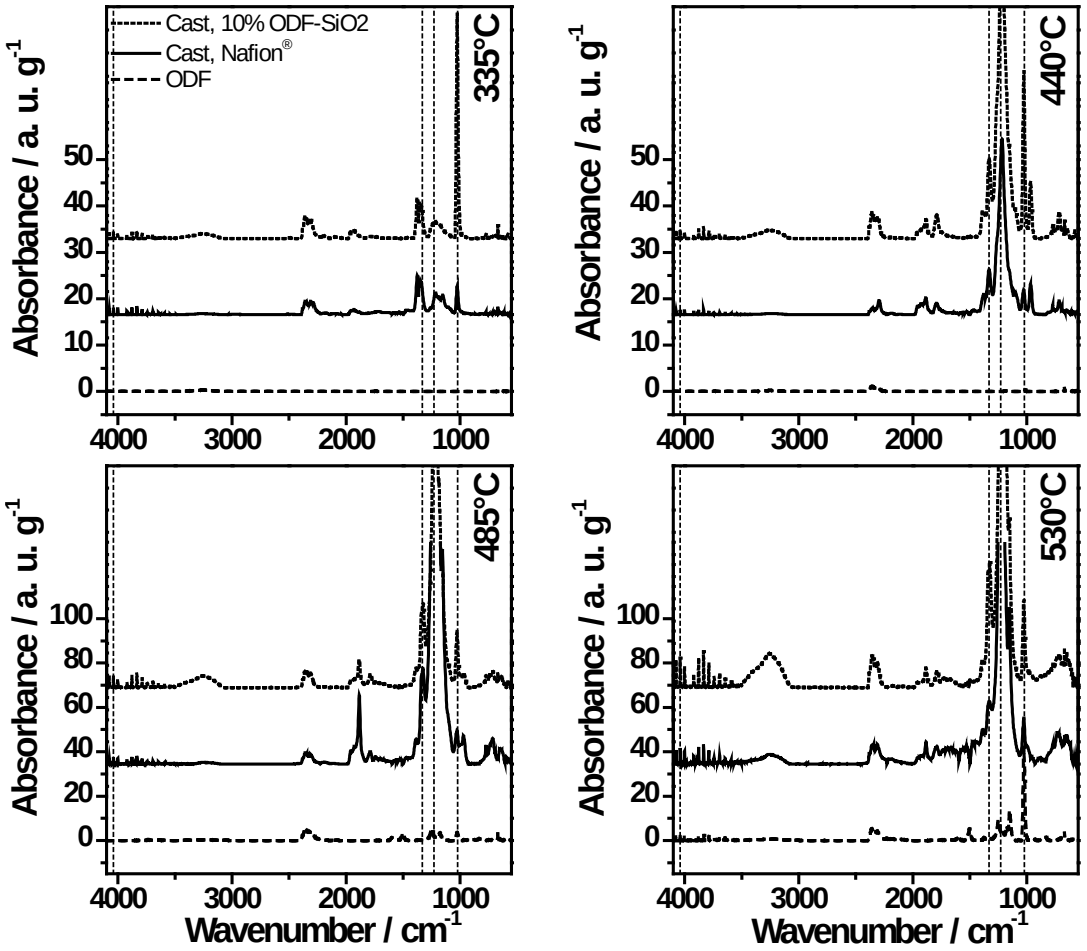

Figure 3.16 Infrared spectra of the volatile thermal decomposition products at 335, 440, 485 and 530 °C, for solvent-cast pure Nafion®, telechelic oligomer ODF, and the solvent-cast composite with 10% ODF-SiO_2. The vertical lines mark the wavenumbers 1022 (SiF_4), 1230 (RCF2R'), 1330 (SO_2) and 4040 cm^{-1} (HF). The spectra in each plot are depicted to the same scale, but vertically displaced to facilitate comparison.

For both pure cast Nafion® and its composite, the most significant absorption bands correspond to SO_2 (1330 cm^{-1}), and SiF_4/CF_3CFCF_2 (1022 cm^{-1}) in agreement with previous observations on SiO_2-Nafion® composites [87]. Both decompose to give gaseous mixtures with medium to strong absorptions for CO_2 (2320–2360 cm^{-1}) and substituted carbonyl fluorides (RC(=O)F) (1960, 1930, 1880 cm^{-1}) as well as a broad complex band in the range 1100–1300 cm^{-1}, corresponding to CF_2 stretching absorptions in several fluorinated degradation products. A further band at 1790 cm^{-1}, attributed to -CF_2CF_2- [87], is also present at high temperatures.

A hydrogen fluoride (HF) band with rotational structure centered around ~3900 cm^{-1} is already present at 335 °C for Nafion® and its composite, but only observable beyond 450 °C for the pure ODF oligomer. At higher temperatures, pure ODF displays very clear bands at 1500, 1600, 1735 cm^{-1}, which can be attributed to phenyl isocyanates (PhNC) and phenyl nitriles (PhCN), previously reported in the degradation of aryl oxadiazoles [89] and of other polyoxadiazole-based polymers [90]. The high-temperature degradation of ODF also yields gaseous fluorinated hydrocarbons with absorptions peaks in the range 1000–1300 cm^{-1}.

The evolution profiles for different thermal decomposition products can be obtained by plotting the absorbance (normalized by the residual solid sample mass at each point) as a function of temperature, for absorptions at relevant infrared frequencies. Figure 3.17 shows the decomposition profiles at wavenumbers 1022, 1230, 1330 and 4040 cm^{-1}, indicatives of the evolution of SiF_4/CF_3CFCF_2, RCF_2R', SO_2 and HF respectively.

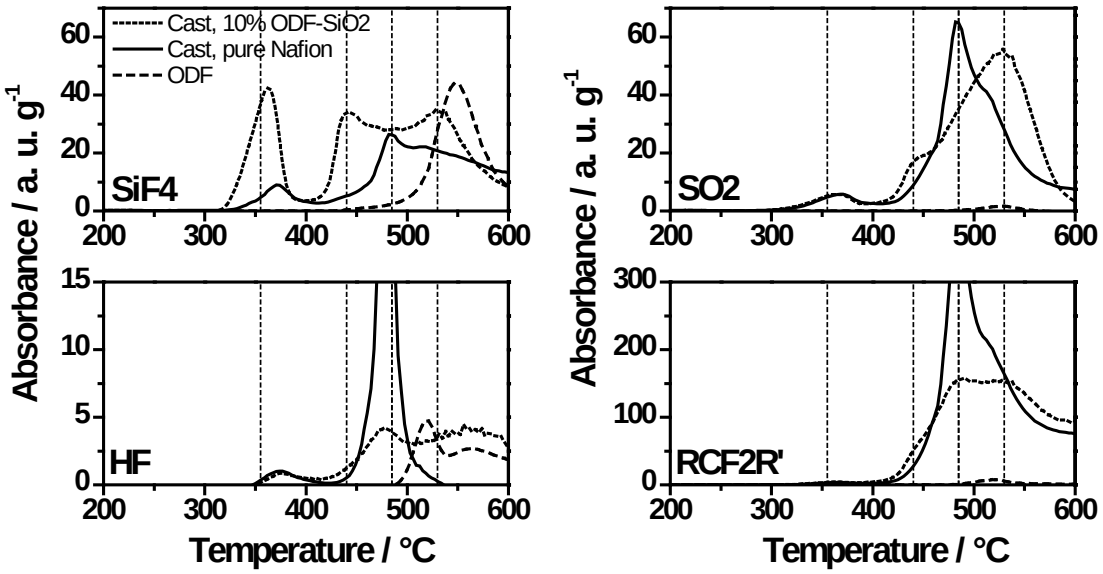

Figure 3.17 Thermal decomposition profiles at wavenumbers 1022 (SiF_4), 1230 (RCF2R'), 1330 (SO_2) and 4040 cm^{-1} (HF), for solvent-cast pure Nafion®, telechelic oligomer ODF, and the solvent-cast composite with 10% ODF-SiO_2. The vertical lines mark the temperatures 355, 440, 485 and 530°C, for which the full spectra are shown elsewhere in this thesis.

Wilkie et al. [91] proposed a degradation mechanism for Nafion® involving an initial cleavage of the C-S bond, resulting in a carbon-based radical and a SO_3H radical. The latter breaks down into SO_2 and an OH radical, while the former suffers further degradation. In agreement with observations by Deng et al. [92] for sol-gel synthesized SiO_2-Nafion® composites, the highest SO_2 profile is obtained for pure Nafion®, as expected from the greater content of sulfonic acid groups. For both Nafion® and its composite, the profile for SO_2 corresponds directly with the thermogram derivative peaks from two broad peaks are clearly distinguishable, confirming the presence of $-SO_3H$ groups in at least two different chemical environments. The first peak, with a maximum around 365°C, can be modelled by a single Gaussian distribution function. It can be assigned to the $-SO_3H$ in the dry Nafion® matrix. Sulfonic acid groups associated in clusters, are stabilized by strong interactions, and would start to decompose at higher temperatures, explaining the further complex peak in the SO_2 evolution profile. For the composite, reduced mobility due to the presence of nanoparticles is also a stabilizing factor, and allows a fraction of the matrix sulfonic acid groups to tolerate higher temperatures, and thus contribute to the second SO_2 evolution peak.

SiF_4 is produced by reaction between the evolved HF, and SiO_2 present in the filler nanoparticles ($4\ HF + SiO_2 \rightarrow SiF_4 + 2\ H_2O$) [92]. Wilkie et al. assigned the absorption band at 1022 (1030) cm^{-1} to SiF_4. For the decomposition products of pure Nafion®, they attributed this band to the quartz walls of their TGA sample tube. While our setup contains no quartz parts, we nevertheless observed this absorption during the decomposition of pure Nafion® samples. Hexafluoropropene (CF3-CF=CF2), which also absorbs strongly at this wavelength [93], was proposed as a thermal degradation product by Samms et al. [94]. It is generated through an anionic decomposition mechanism, and its presence points to concurrent radical and anionic mechanisms in the thermal decomposition of Nafion®. Starting towards 500 °C, the degradation products of the ODF oligomer show a strong absorption band at this wavelength as well.

As shown in Figure 3.15, both for Nafion® and its composite, there are two main SiF_4/CF_3CFCF_2 and HF evolution steps, corresponding to the TGA degradation steps

II and III. This behaviour, parallel to the SO_2 evolution, indicates that the sulfonic acid group degradation is always accompanied by some backbone degradation. This is corroborated by the close similarity between the SO_2 and the RCF_2R' evolution profiles. The HF profile corresponds to the portion of hydrogen fluoride that has not reacted with SiO_2 in the system. Consequently, there is a "delay" between the two profiles, with the SiO_2 being evidenced at lower temperatures, as initially all generated HF reacts before it can be detected. The presence of silicon oxide available for reaction in the composite membrane results in both an earlier start and a much higher magnitude for each of the decomposition steps, in comparison to pure Nafion®. At even higher temperatures, the decomposition of the oligomer "shells" results in a clear second maximum at 530 °C for the composite's SiF_4/CF_3CFCF_2 evolution profile.

Figure 3.18 shows differential scanning calorimetry results for the dry composites. A first run, not shown in the figure, was carried out from room temperature to 150 °C at a heating rate of 10 °C min^{-1}, in order to eliminate adsorbed water and to impose a similar thermal history across all samples. Subsequently, the sample was cooled down to -150 °C at 30 °C min^{-1}, and finally a second run at 10 °C min^{-1} was performed up to 280 °C.

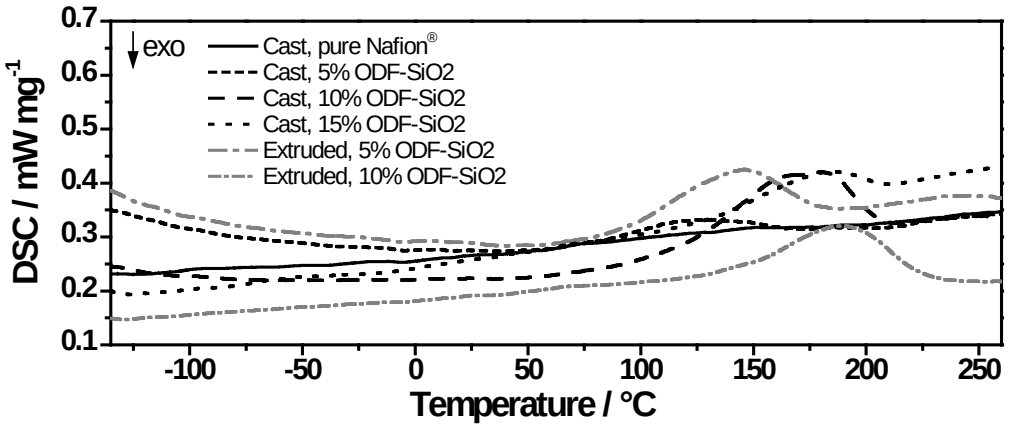

Figure 3.18 DSC curves (2nd run) for solvent-cast and extruded Nafion® composites studied in this work, obtained from -135 to 260 °C at 10 °C min^{-1}. The first run from room temperature to 150 °C is not shown.

A weak transition (not shown in the figure) is observable around -110 °C for the pure cast Nafion® membrane. Corti et al. [84] have assigned this transition to the gamma relaxation observed in dynamic mechanical studies [95], attributed to motion of the Nafion® backbone. This transition is almost undetectable in the composite membranes, as would be expected from reduced matrix mobility caused by the highly dispersed ODF-SiO_2 nanoparticles.

For all our samples, the first heating up to 150 °C was enough to eliminate most of the freezable water, resulting in the absence of any significant water melting peak [96, 97] around 0 °C. In the case of pure cast Nafion®, the pre-heating run was also sufficient to eliminate all water trapped in the ionic clusters (non-freezable water), as evidenced by the absence of a peak [84] in the range 100–200 °C, in the second run. The enhanced water-retention in the composite membranes is substantiated by the endothermic peak at temperatures above 100 °C also in the second run. Increasing the amount of ODF-SiO_2 filler results both in an increased area and a shift to higher temperatures in this peak, in agreement with the observations of Chen et al. [55] for silica-Nafion® composites. Mathematical decomposition of this peak reveals two Gaussian components: if the lower temperature component (Ia) can be assigned to the ionic cluster-bonded water in Nafion®, then the higher temperature component (Ib) probably arises from water more strongly retained by the filler particles. Table 3.2 shows the peak temperatures for the Gaussian components of this desorption peak.

Table 3.2 Peak temperatures for the Gaussian components of the DSC desorption peak (2nd run) observed in the range 100–200 °C.

Membranes	Peak Temp. / °C	
	Ia	Ib
Cast Nafion®	0	0
Cast Nafion®, 5% ODF-SiO_2	121	148
Cast Nafion®, 10% ODF-SiO_2	161	185
Cast Nafion®, 15% ODF-SiO_2	165	187
Extr. Nafion®, 5% ODF-SiO_2	130	152
Extr. Nafion®, 10% ODF-SiO_2	161	191

3.3.2 Poly(arylene ether 1, 3, 4-oxadiazole) composite membranes

Poly(arylene ether 1,3,4-oxadiazole) membranes must be post-sulfonated, in order to attach to their backbone the sulfonic acid groups, which will be the main contributors to proton conductivity. An attempt at sulfonation using concentrated sulfuric acid resulted in redisolution of the composite membranes. The very mild sulfonation conditions of 50 wt.% sulfuric acid at room temperature for 2 days resulted in sulfonated membranes with in-plane conductivity around 1.4 mS cm-1, which is not practical for fuel cell appication. Finally, relatively good conductivity values were obtained by rising the temperature of the sulfonation reaction to 80 °C while still using 50 wt.% sulfuric acid. The resulting conductivity was studied as a function of time in order to further optimize the sulfonation conditions. Table 3.3 shows the influence of sulfonation time on the membranes' IEC, water uptake and conductivity. Each membrane property was measured every one hour for the first 7 hours, and one final time on the following morning. We found that IEC and in-plane conductivity of the sulfonated membranes was enhanced by increasing sulfonation time. The samples that were sulfonated overnight presented slightly higher IEC values, but resulted in membranes too brittle for proton conductivity and water uptake to be measured. This can be explained by degradation of the polymer chains (with the resulting reduction

of molecular weight) due to acid-catalyzed cleavage of the diphenyl ether functions [90]. Consequently the sulfonation in 50 wt.% sulfuric acid at 80 °C for 7 hours is an optimal post-sulfonation condition set, conveying the poly(arylene ether 1,3,4-oxadiazole) membranes acceptable conductivity without significantly compromising their mechanical stability.

In an effort to increase the physical stability of the poly(arylene ether 1,3,4-oxadiazole) membranes without losing the proton conductivity, nanocomposites were prepared containing silica particles functionalized with oxadiazole telechelics. The optimum post-sulfonation conditions from the previous experiment were used on the composite membranes. The results are shown in Table 3.4. The nanocomposite membranes prepared with 10 wt.% functionalized silica presented higher proton conductivity than the plain membrane, in agreement with previous work carried out by the group of S. P. Nunes, when functionalized silica was added to poly(hexafluoropropane-1,3,4-oxadiazole) [44] and sulfonated PEEK [14]. This effect can be partially attributed to the amphoteric character of the sulfonated oxadiazole oligomeric parts containing both sulfonic acid groups and basic nitrogen sites. The pyridine-like nitrogen sites near sulfonic groups can be seen as additional points for proton hopping. Nevertheless, the IEC of the sulfonated polymer composites was still very low considering that for PEM fuel cell application the target proton conductivity is around 0.1 S cm-1.

Table 3.3 IEC, in-plane conductivity and water uptake of poly(arylene ether 1,3,4-oxadiazole) membranes as a function of sulfonation time using 50 wt.%, sulfuric acid at 80 °C.

Time (hours)	Membrane characterization		
	IEC (mmol/g)	Conductivity(mS/cm)	Water uptake (%)
1	0.242	3.04	6.2
2	0.239	2.72	5.2
3	0.236	2.49	9.1
4.5	0.210	5.06	12.9
6	0.308	8.83	19.3
7	0.409	9.92	20.4
overnight	0.507	*	*

* Cannot be characterized since the obtained membranes are too brittle.

Table 3.4 IEC, in-plane conductivity and water uptake of polyoxadiazole membranes sulfonated in 50 wt.% sulfuric acid at 80 °C for 7 hours.

Amount of filler (%)	In-plane conductivity (mS cm-1)	IEC (mmolg-1)	Water uptake (%)
0	7.88	0.358	22.91
5	6.10	0.344	21.24
10	9.12	0.361	22.50

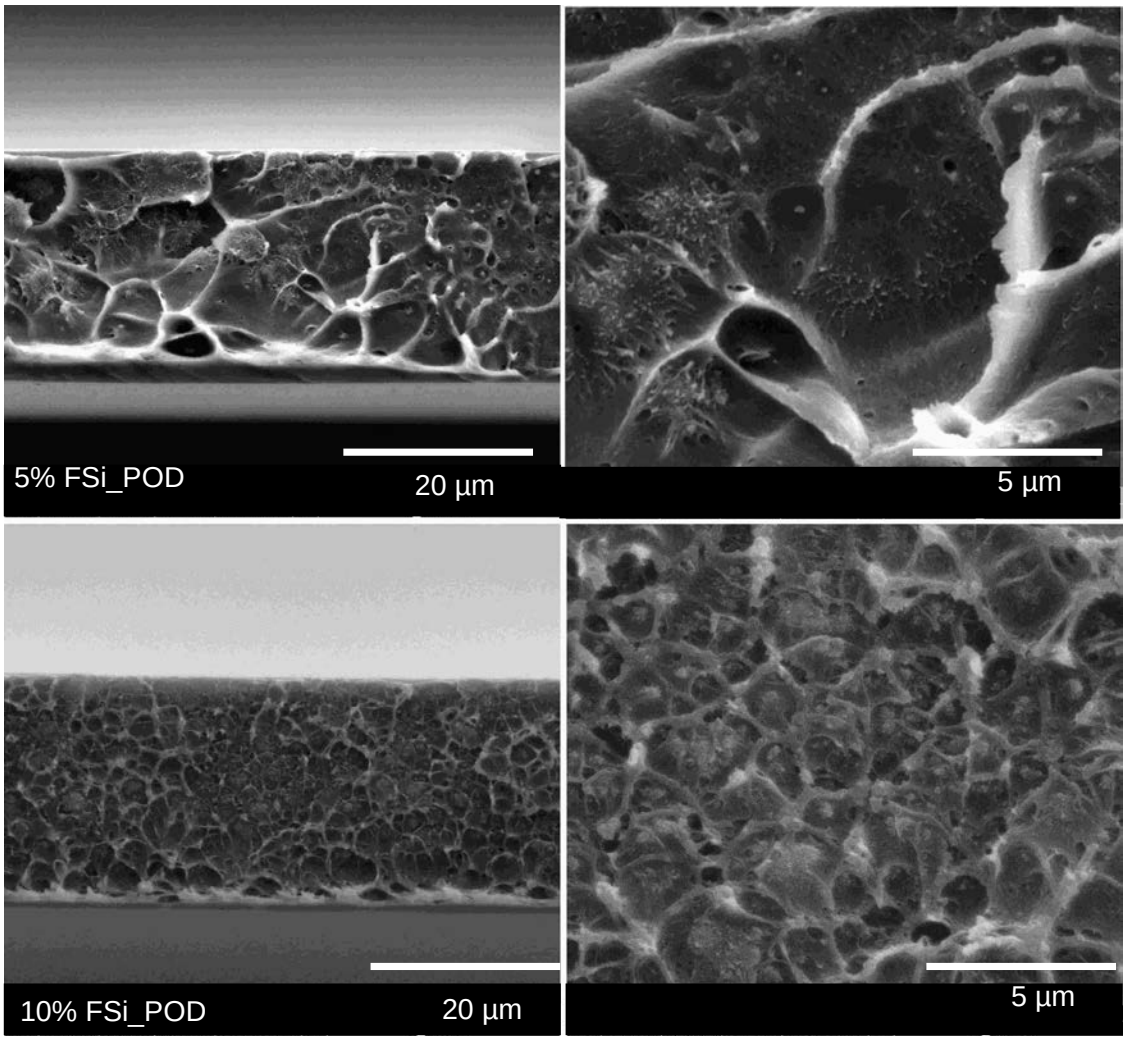

Figure 3.20 SEM micrographs of poly(arylene ether 1,3,4-oxadiazole) composite membranes containing 5 and 10 wt.% of ODF-silica.

The SEM micrographs (cryofracture) of composite membranes shown in Figure 3.20 reveal a tendency of the functionalzed silica particles to segregate from the polymer matrix, similarly to what has been observed on composites with perfluorinated oxadiazole [44]. The result is a sponge-like structure with closed cells containing silica aggregates. This microstructure results from the high hydrophobicity of the polymer prior to post-sulfonation, and may explain the relatively modest improvement in transport properties provided by the nanoparticles: as the inclusion network is mostly discontinuous, transport must still rely on percolation across the matrix.

The thermal stability of poly(arylene ether 1,3,4-oxadiazole) composite membranes was determined by TGA (Figure 3.21). The first mass loss, in the temperature range

of 50–200 °C corresponds to sorpted water and residual solvent (DMAc, b.p. 164-166 °C [81]). This step is more significant for the composites, as expected from the increase in water uptake afforded by the hydrophilic inclusions. The second (and third) mass loss steps in the range 400-600 °C result from the partial loss of sulfonic groups [85] and the degradation of the oxadiazole [99] backbone. The appearance of a second DTG maximum starting at slightly lower temperatures is also observed for these composites, as in the case of Nafion® composite membranes described in the previous sections. The mass loss values for all these decomposition steps are given in Table 3.5.

Table 3.5 Decomposition patterns and Tg of polyoxadiazole composite membranes.

Membranes	Mass change (%)			Tg
	I	II	III	
POD	1.87	46.07	-	201
5% ODF_SiO2 POD	3.90	15.05	32.10	211
10% ODF_SiO2 POD	3.00	53.32	-	245
15% ODF_SiO2 POD	3.12	15.11	31.01	-

As in the case of Nafion® composites described previously, DSC thermograms of these composites evidence reduced chain mobility compared to the pristine polymer. Indeed, the Tg transitions of the composites are both broader and shifted to high temperatures (Tg~201 °C for the pure polymer, and ~211 and ~245 °C for the 5 and 10 wt.% composites respectively).

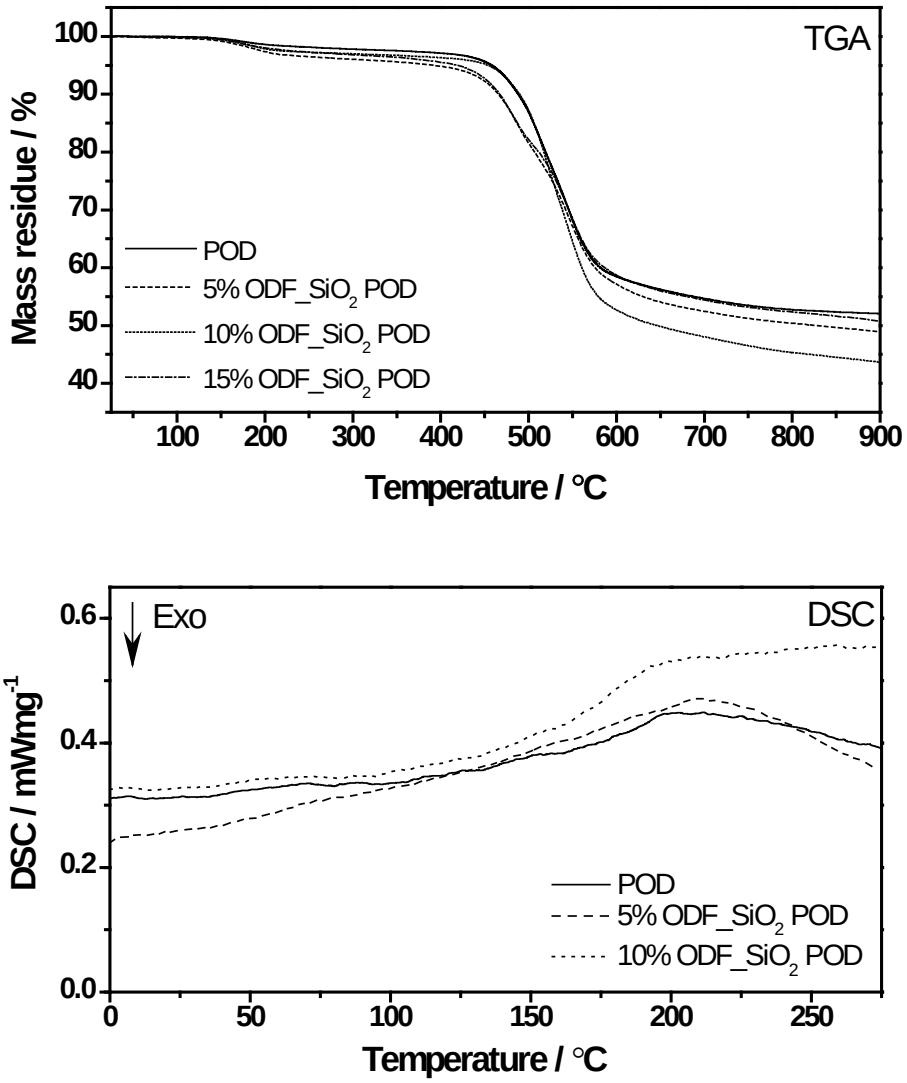

Figure 3.21 TGA and DSC results obtained for poly(arylene ether 1,3,4-oxadiazole composite membranes showing thermal degradation and glass transiton temperatures.

3.3.3 Fluorinated polyoxadiazole random copolymers composites

For the fluorinated polyoxadiazole random copolymers, composite membranes were prepared with ODF-silica loadings of 5 and 10 wt.%. In this section, the random copolymers with ratios of 2-(diphenyl ether)-1,3,4-oxadiazole (ODBA) to 2-[4,4'-(Hexafluoroisopropylidene)diphenyl]-1,3,4-oxadiazole (FDBA) equal to 0.5, 1.0, 2.0 and 3.0 will be referred to as PODOcoF-A, PODOcoF-B, PODOcoF-C and

PODOcoF-D respectively. Analogously, PODOcoF-AS, PODOcoF-BS, PODOcoF-CS and PODOcoF-DS denote the corresponding sulfonated copolymer membranes. These membranes were characterized in the same manner as the composite membrane systems described in the previous sections. Figure 3.22 shows the experimental data from water uptake measurements. As expected, membranes with a higher ODBA ratio show higher water uptake. This is because the sulfonation reaction can only modify the diphenylether moieties in the ODBA repeating units. These units posess a deactivating oxadiazole (OD) ring, but also an ether bond, which allows a sulfonation attack on the benzene rings attached to it. The FDBA unit is completely deactivated, due to both the OD ring and the perfluorinated isopropyl, and thus does not react under normal sulfonation conditions. Furthermore, the water uptake of the DS membranes could not be measured, as the extensive sulfonation results in excessive swelling and ultimately dissolution in water.

For highly sulfonated copolymers (ODBA:FDBA > 1), the introduction of ODF-silica particles mitigates the swelling considerably, with a more significant effect obtained for the membranes with 10 wt.% loading. Nevertheless, the effect of the inclusions is not strong enough to prevent the dissolution of membranes prepared with the PODOcoF-DS.

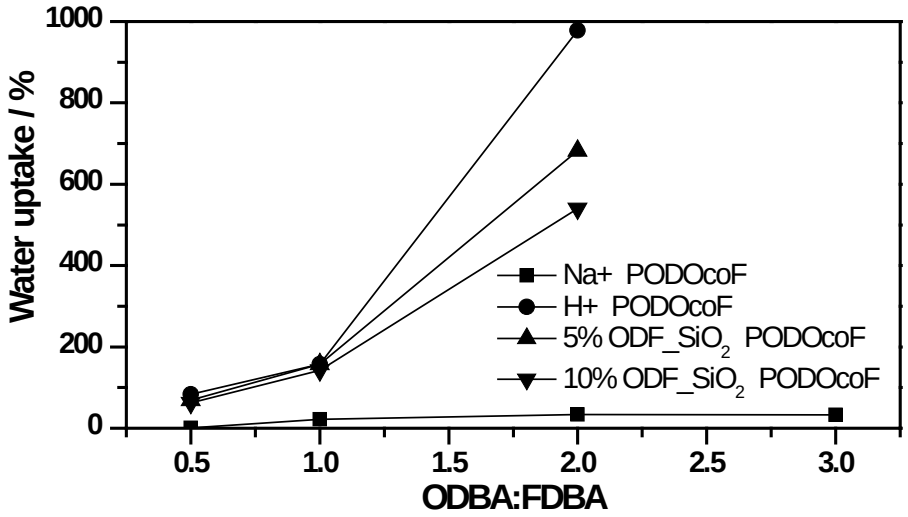

Figure 3.22 Water uptake of membranes fluorinated polyoxadiazole random copolymers and composites as a function of ODBA:FDBA ratio.

IEC characterization of these random copolymers and composite membranes are shown in Figure 3.23. The IEC values of sulfonated membranes are comparable to those of Nafion® composites (however, due to their excessive swelling, the mechanical stability of these polymers in is much lower). For the copolymers with high sulfonic group content, the IEC of both 5 and 10 wt.% composites is lower than that of the pure copolymer. This indicates that the reduction in swelling described above must be to a certain extent due to the partial elimination of sulfonated copolymer matrix. As observed for the Nafion® composites, there is no significant difference in IEC between the membranes loaded with 5 and 10 wt.% ODF-silica, due to compensating effect of the exchange groups introduced with the functionalized particles.

The proton conductivity values (Figure 3.24) for these membranes follow the behaviour observed for the IEC. The compensation provided by the ODF-particle "shells" means the decrease in conductivity for the composites is negligible (the 5 wt.% is even slightly higher than for the pure polymer). The values for these copolymers and their composites, while higher than those of poly(arylene ether 1,3,4-oxadiazole) discussed previously, are still about one order of magnitude below those of Nafion®-based membranes.

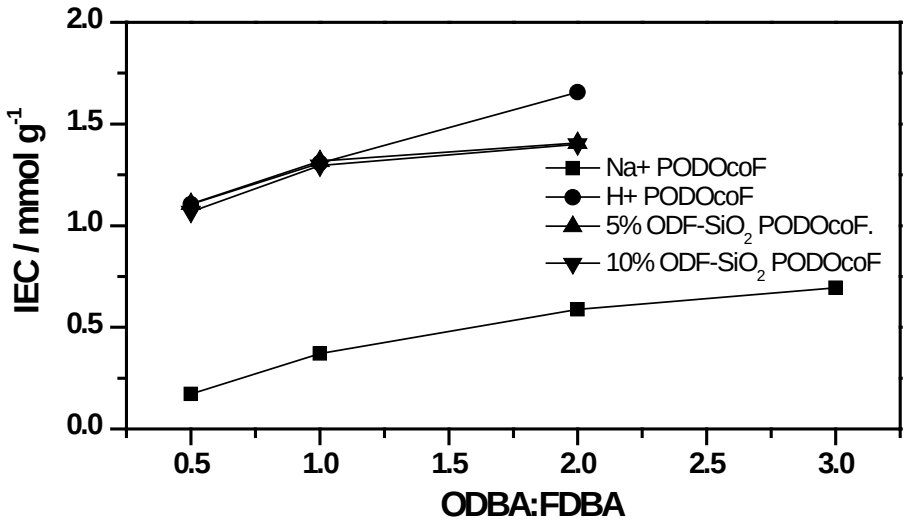

Figure 3.23 IEC of fluorinated polyoxadiazole random copolymers and composites as a function of ODBA:FDBA ratio.

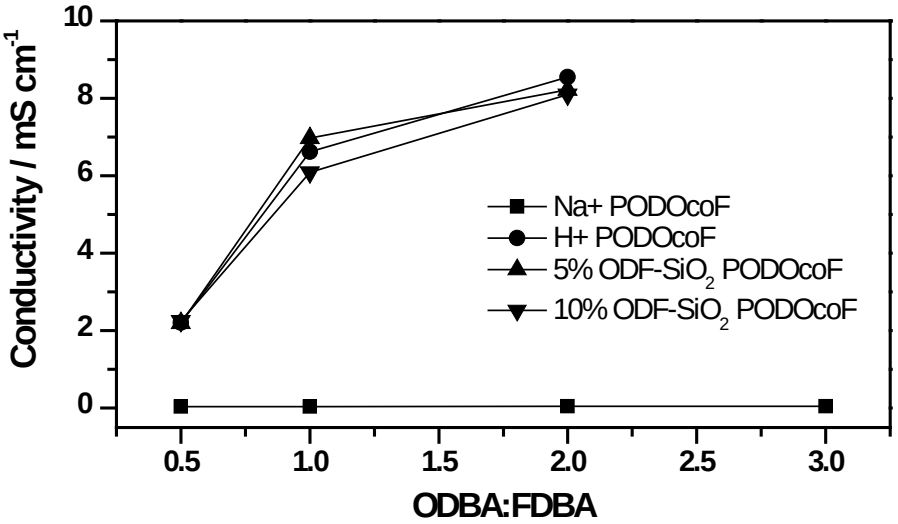

Figure 3.24 Conductivity of fluorinated polyoxadiazole random copolymers and composites as a function of ODBA:FDBA ratio.

The morphology of the sulfonated composite membranes is shown in the SEM micrographs (cryofracture) in Figure 3.25. The PODOcoF-AS, being the less sulfonated (more hydrophobic) of the series, shows a certain degree of segregation, similar to what was observed for poly(arylene ether 1,3,4-oxadiazole). As we increase the sulfonation degree, this phenomenon becomes less significant and finally nonexistent for the highly sulfonated PODOcoF-CS membranes. As observed for Nafion® composites, macroaggregates are already present at 5 wt.% loading, and their number is more significant for the 10 wt.% membranes.

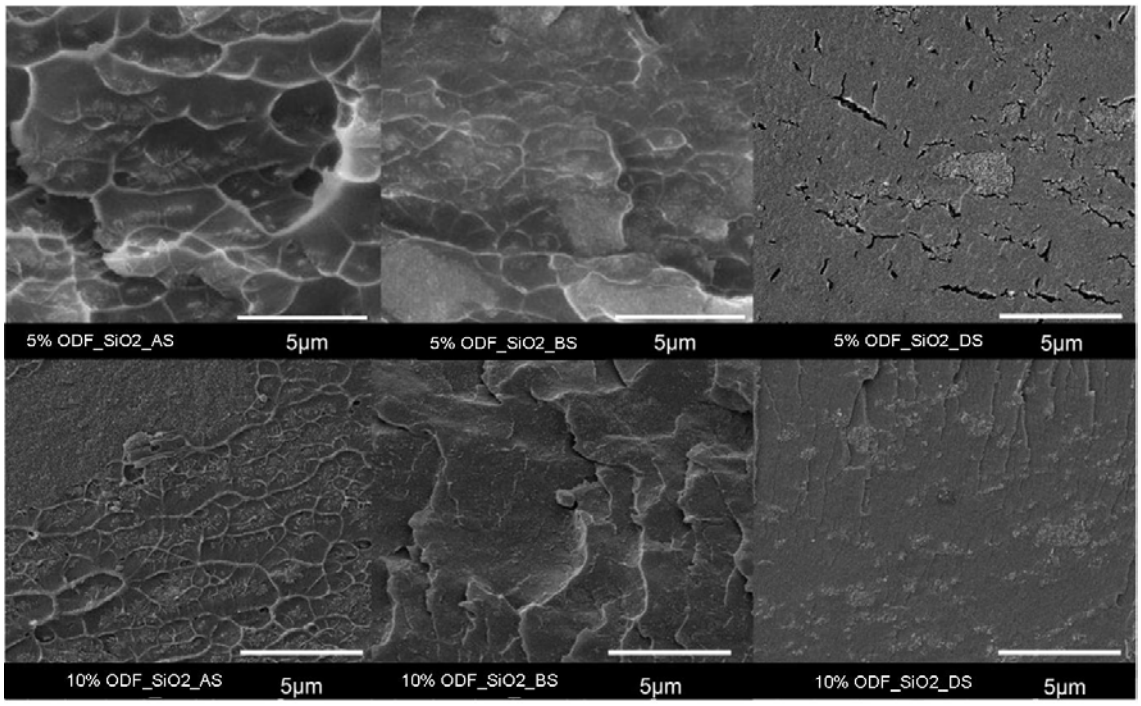

Figure 3.25 SEM micrographs of random copolymer composite membranes of increasing sulfonation degree (AS, BS and DS) containing 5 and 10 wt.% ODF-silica.

In the thermogravimetric analysis data shown in Figure 3.27, the amount of sorpted water eliminated in the first mass loss (50-150 °C) is directly related to the fraction of sulfonatble moieties, due to the more hydrophilic nature of the diphenylether unit, and to a small number of sulfonic groups introduced during the synthesis [12]. The post sulfonated copolymers also follow this trend, but display more significant mass loss steps, as expected from their enhanced water-uptake. Similarly, for the composites, increased content of functionalized silica results in greater mass loss in this region, as can be seen for the case of PODOcoF- AS in Figure 3.27.

The gradual mass loss in the range 170-320 °C (denoted II in Figure 3.27) can be assigned to partial degradation of diphenylether-bonded sulfonic groups, probably accompanied by elimination of residual casting solvent. Most of the copolymer backbone is finally lost in the third degradation step in the range 450-650°C, starting with the breaking of the diphenyl ether bond [90]. This bond breaking might be catalyzed by the filler particles, as evidenced by the shift towards lower temperatures (2~5 °C) of the third mass loss step for the composites. The addition of 5 wt.% of functionalized filler does not have a significant effect on the second mass loss step.

The decomposition patterns of fluorinated polyoxadiazole random copolymers and their composite membranes are shown in Table 3.6.

Table 3.6 Decomposition patterns of fluorinated polyoxadiazole random copolymers and their composite membranes.

Membrane	Mass change (%)				Tg
	I	II	III	IV	
PODOcoF-A	1.00	9.32	49.42		237.4
PODOcoF-B	1.45	10.56	45.71		234.2
PODOcoF-C	4.52	11.72	39.17		225.0
PODOcoF-D	3.30	10.88	40.95		208.5
PODOcoF-AS	1.97	13.04	38.93		240.0
PODOcoF-BS	3.67	11.04	37.22	13.24	230.0
PODOcoF-CS	4.51	6.87	31.77	14.01	195.0
5% PODOcoF-AS	2.98	11.61	44.61	-	241.4
5% PODOcoF-BS	3.89	12.52	41.09		235
5% PODOcoF-CS	6.52	6.61	42.14		218.4
5% PODOcoF-DS	8.88	30.33	16.98		*
10% PODOcoF-AS	3.95	11.62	43.72		278.2
10% PODOcoF-BS	8.00	5.92	39.91		317.5
10% PODOcoF-DS	10.52	27.92	15.62		*

* Membrane dissolved.

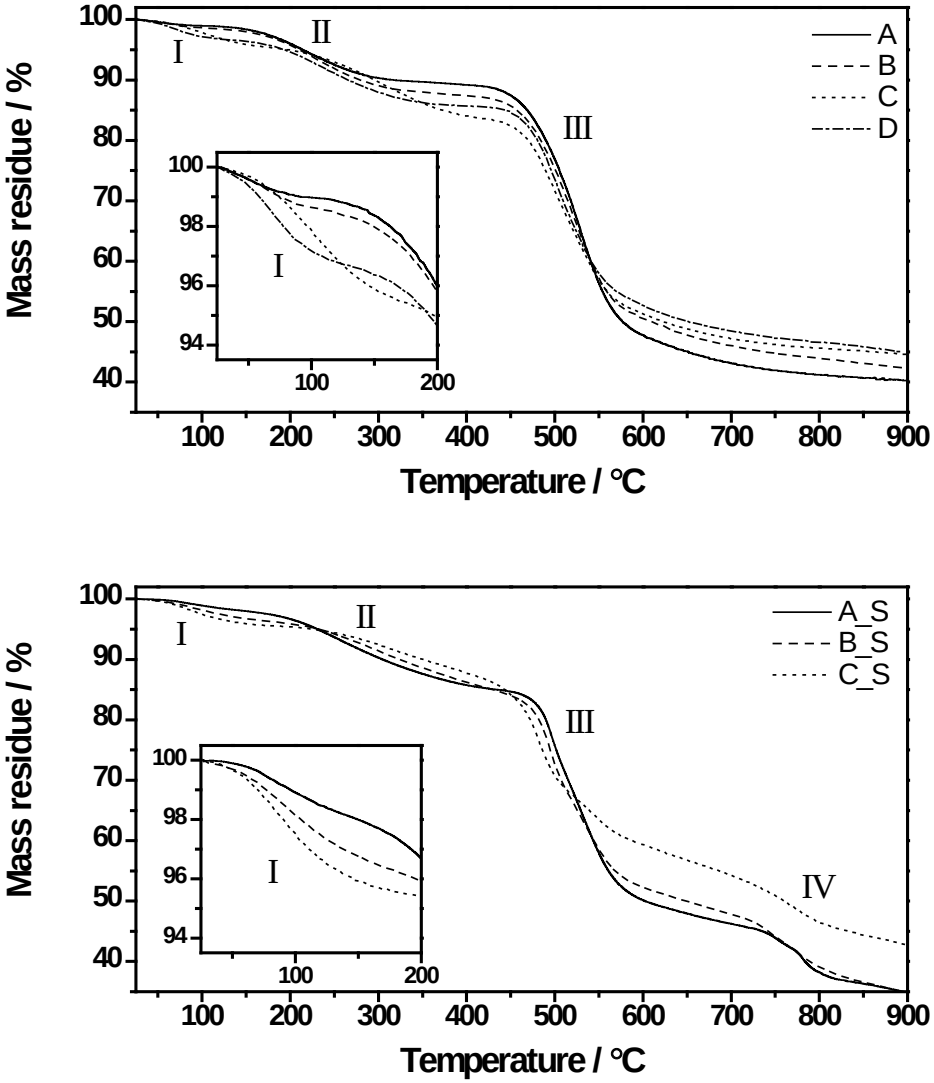

Figure 3.26 Thermogravimetric analysis of random oxadiazole copolymers before (above) and after post-sulfonation (below).

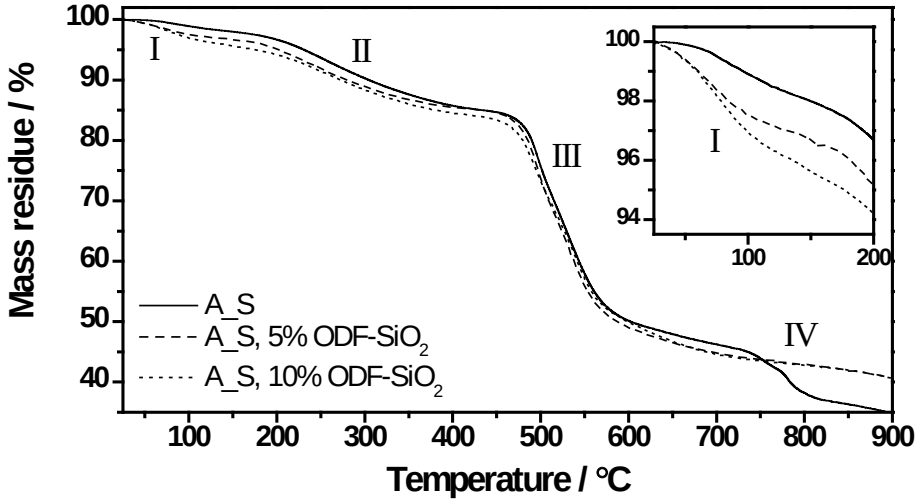

Figure 3.27 Thermogravimetric analysis of AS and its composites with ODF-SiO2.

The DSC thermograms in Figure 3.28 were obtained after a first run up to 120°C was carried out in order to eliminate adsorbed water. Glass transitions are observed for these copolymers in the range 200-300 °C. With the addition of ODF-Silica, these transitions move to higher temperatures, and become fainter due to the reduced chain mobility, in agreement with the observations on Nafion® composites in the previous section. The shift towards higher temperatures is proportional to the filler content (see Table 3.6).

Dynamic mechanical analysis of these membranes was performed in the range 40-200°C. Figure 3.29 shows the plot of E' (storage modulus) and E" (loss modulus) versus temperature for AS and its composites. For temperatures between 40 and 100°C, the E' and E" are relatively constant and in the range 2.5-3.5 GPa in agreement with reports for polyoxadiazoles with similar structure [100]. For the pure copolymer, a dramatic drop in storage modulus in is observed in the range 90-200 °C. The possible causes for this are the increased proton-transport, which might induce backbone mobility as in the case of Nafion, and the loss of adsorbed water and its plasticizing effect. This drop is efficiently mitigated with the addition of functionalized silica filler, due to both physical cross-linking, and better water retention.

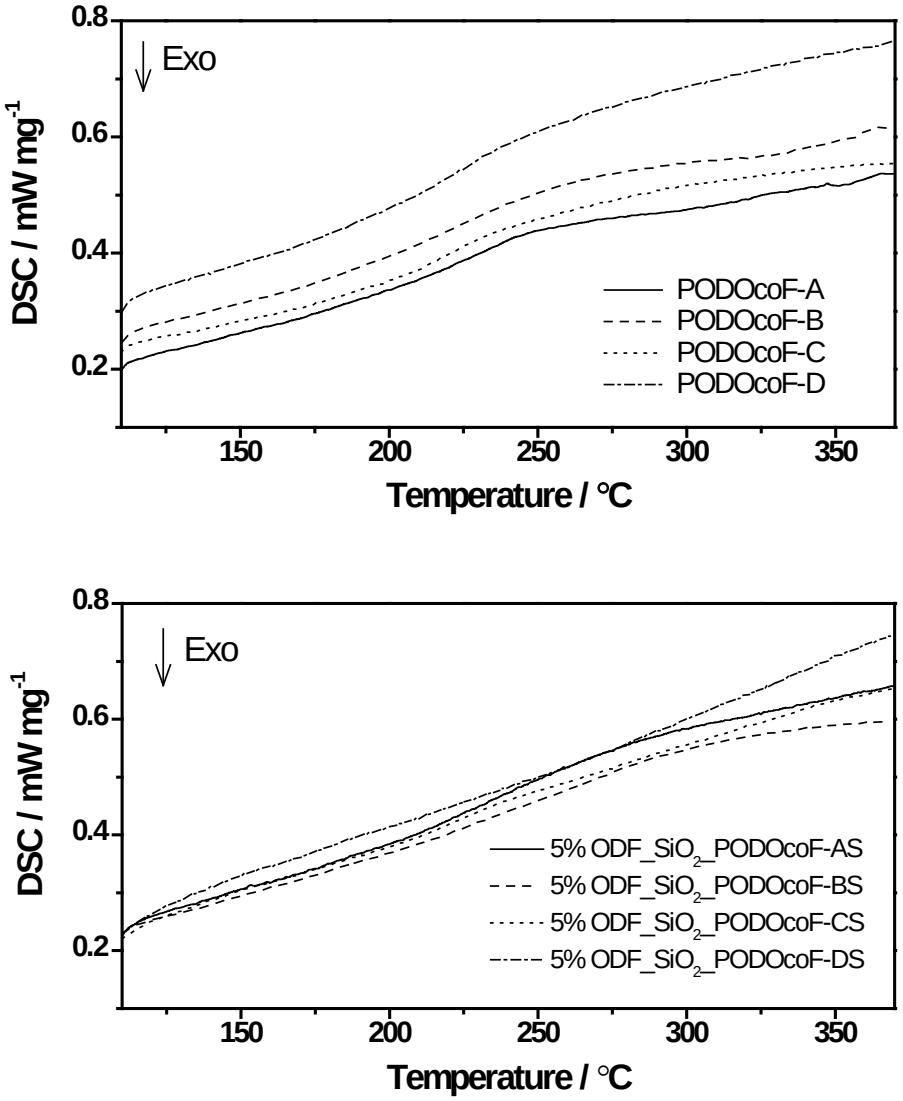

Figure 3.28 DSC thermograms of random oxadiazole copolymers and composite membranes.

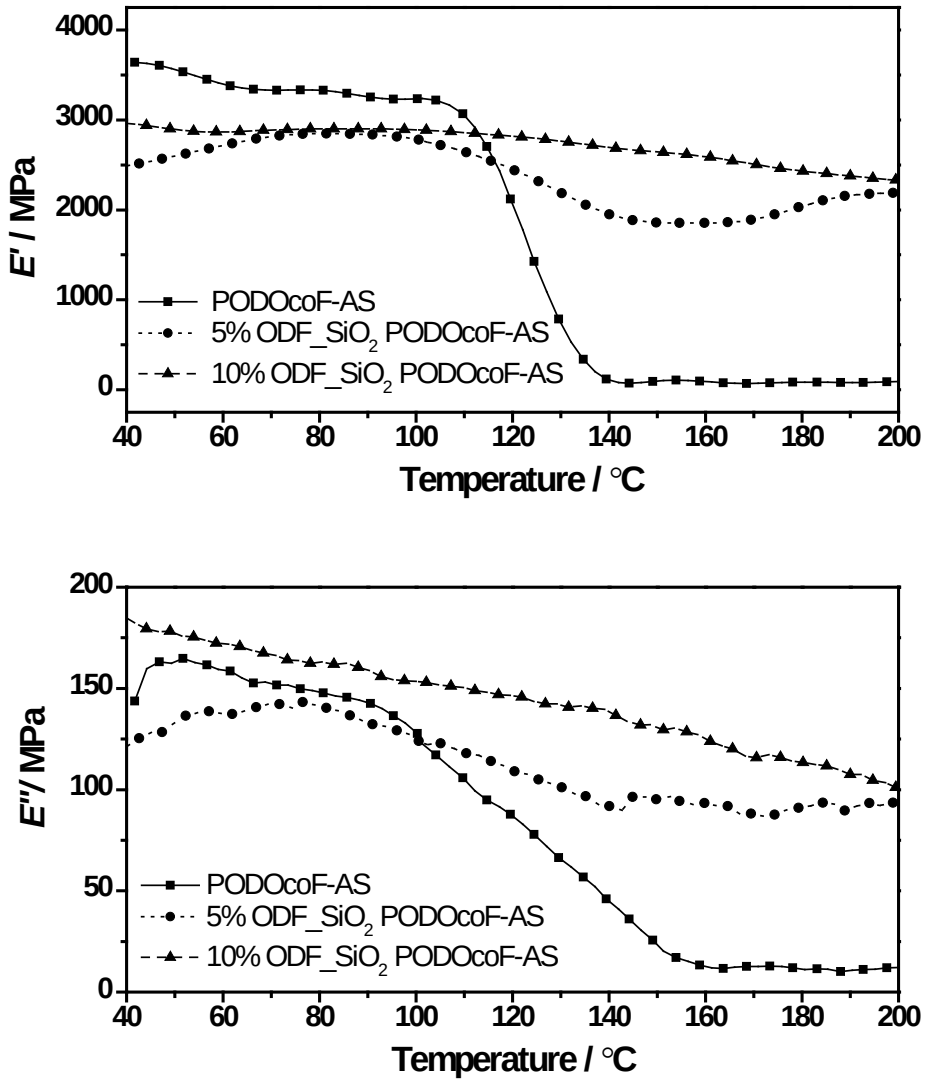

Figure 3.29 Dynamic mechanical analysis of AS copolymer and its composites.

3.4 Summary

A series of Nafion®-functionalized silica composite membranes were prepared by solvent casting and melt extrusion processes, and their properties relevant to fuel cell application were thoroughly characterized. It was found that the inclusion of nanoparticles proved beneficial, mainly due to a reinforcement effect and an improvement in water retention. Moreover, due to their higher affinity for the matrix, the functionalized nanoparticles perform better than the pristine silica particles. For the same filler loading, better nanoparticle dispersion was achieved for solvent-cast membranes, which in turn results in higher proton conductivity. The composite membranes showed excellent thermal stability, allowing for PEM fuel cell operation at temperatures higher than pure Nafion®.

Furthermore poly(arylene ether 1,3,4-oxadiazole) and fluorinated polyoxadiazole random copolymer composite membranes with functionalized silica were also prepared and characterized. The inclusion of functionalized silica was shown to improve the mechanical stability of these membranes without significantly losing IEC or proton conductivity. Nevertheless, their proton conductivity values were low when compared to current commercially available polymer electrolyte membranes.

Chapter 4. Fuel cell performance evaluation

In this chapter we discuss the fuel cell performance measured on single cells assembled using polymer electrolyte membranes prepared and characterized in the previous chapter. Additionally, the hydrogen crossover measured in operation conditions is discussed, as it is an important parameter to assess the viability of polymer membranes for practical application to fuel cells.

4.1 Characterization methods

4.1.1 Membrane electrode assembly and fuel cell testing

The gas diffusion electrodes (GDEs) were prepared by auto-spraying a homogeneous catalyst ink, consisting of carbon powder-supported platinum (Pt), Nafion® solution, and iso-propanol, onto a gas diffusion layer (GDL). The GDL consists of PTFE-treated carbon paper (SGL-24BC), impregnated with a PTFE and carbon black microporous layer (MPL). The total Pt loading for both anode and cathode was 0.4 mg Pt cm^{-2}. The total Nafion® loading in the catalyst layer (CL) was 30 wt.%. The 5 cm^2 area membrane electrode assemblies (MEAs) were prepared by hot pressing the anode GDE, Nafion® composite membrane, and the cathode GDE together at 135 °C at ~4 MPa for 3 minutes. Then the MEA was cooled down under constant pressure to 30 °C for 5 minutes. Both bipolar plates had identical serpentine flow fields with a nominal area of 5 cm^2. The depth and width of the channels and the width of the ribs on the flow fields were all 0.84 mm.

The MEAs were characterized in a Teledyne 125 W test station under atmospheric pressure, with relative humidity (RH) ranging from 34 to 100%. Before the test, the cell was conditioned by drawing current at 0.6 V for 12 hours, in order to activate the

electrochemical reaction sites in the catalyst layers of both anode and cathode. Afterwards, polarization data were collected as a function of RH, by varying the cell temperature, and keeping the saturator temperature constant at 64 °C. The resulting temperature-humidity pairs are shown in Table 4.1.

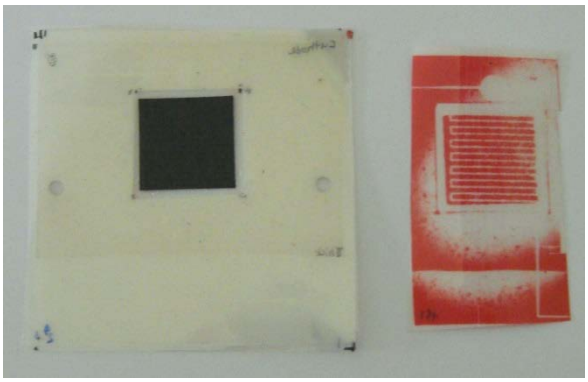

Figure 4.1 Photograph of an MEA (left) with the corresponding gaskets. The pressure sensitive film used to verify the cell assembly is shown on the right side of the picture.

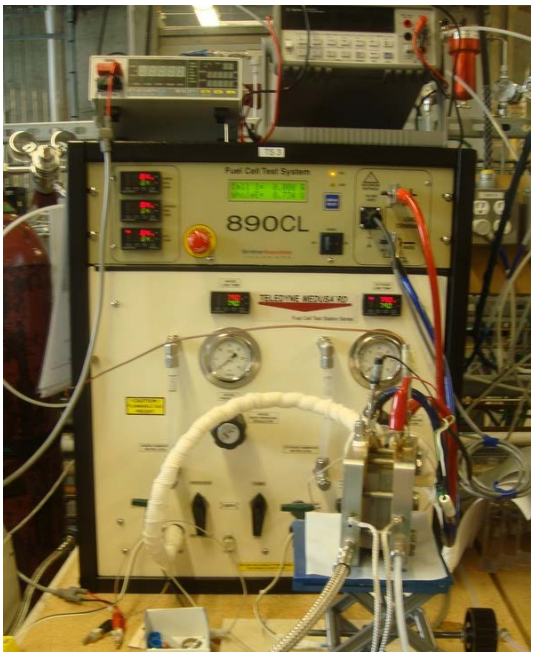

Figure 4.2 Photograph of the Teledyne 125 W fuel cell test station used in this work.

Table 4.1 Cell temperatures/relative humidity pairs in the fuel cell test protocol followed in this work.

Cell temperature /°C	Relative Humidity / %
64	100
68	84
72	70
75	62
80	50
85	41
90	34

Cell voltage and cell resistance were recorded as a function of RH under a 1 A cm^{-2} current density, after 1 hour stabilization at the same load. The gas streams of pure H_2 and O_2 were controlled by their respective mass flow controllers and the flow rates were kept at 0.2 L min^{-1} (at standard conditions of 1 atm and 25 °C). Before H_2 and O_2 were fed into the anode and cathode, they were humidified by passing through their corresponding humidifiers at 64 °C.

4.1.2 Hydrogen crossover measurement

In order to measure the H_2 crossover, an MEA was assembled into a cell and conditioned for 12 hours under load at 0.6 V and 100% RH. After that the load was removed, and a humidified N_2 stream at 1 L min^{-1} was applied to the cathode side to purge any oxygen traces. Once a stable cell voltage was obtained (~0.1 V), the N_2 flow rate was changed back to 0.2 L min^{-1}. Then a Solartron 1287 potentiostat was connected to the fuel cell, with the working electrode probe joined to the cathode, and the counter/reference electrode probes connected to the anode. CorrWare software was used to apply four potential steps in the range 0.2–0.5 V, and record the corresponding current values after stabilization (about 15 min). In this potential range, all H_2 that has crossed over from the anode to the cathode should be

completely oxidized, giving a current indicative of the amount of H_2 that has crossed over. The reported crossover value is obtained from extrapolation to open circuit potential [9].

4.2 Characterization results

4.2.1 Fuel cell performance and hydrogen crossover of Nafion® composites

Figure 4.3 and Figure 4.4 shows typical fuel cell polarization curves of single cells with solvent-cast and extruded 5 and 10 wt.% ODF-Silica Nafion® composite membranes. Fuel cell performance of both extruded and solvent cast composite membranes decreases with decreasing the relative humidity.

The highest power densities achieved for 5 wt.% and 10 wt.% solvent-cast films are 0.97, 1.05 W cm^{-2} respectively, while for 5 and 10 wt.% extruded, the highest values are 0.88 and 0.84 W cm^{-2} respectively. The power density for all the membranes decreased significantly as the humidity was lowered to 34%. The humidity affects not only membrane conductivity, but also reactant (O_2 and H_2) partial pressures, and consequently the fuel cell reaction thermodynamics and kinetics [70].

Better performance is observed for solvent cast composite membranes, compared to extruded composites with the same functionalized filler loading. This behaviour can be correlated to the evolution in conductivity values, and probably explained by unavailability, under fuel cell operating conditions, of filler-grafted exchange functions for membranes with poor dispersion. For the extruded composite membranes the performance peaks at 5 wt.% loading. For the solvent cast composites, where agglomeration is less significant, the performance continues to improve towards 10 wt.% loading.

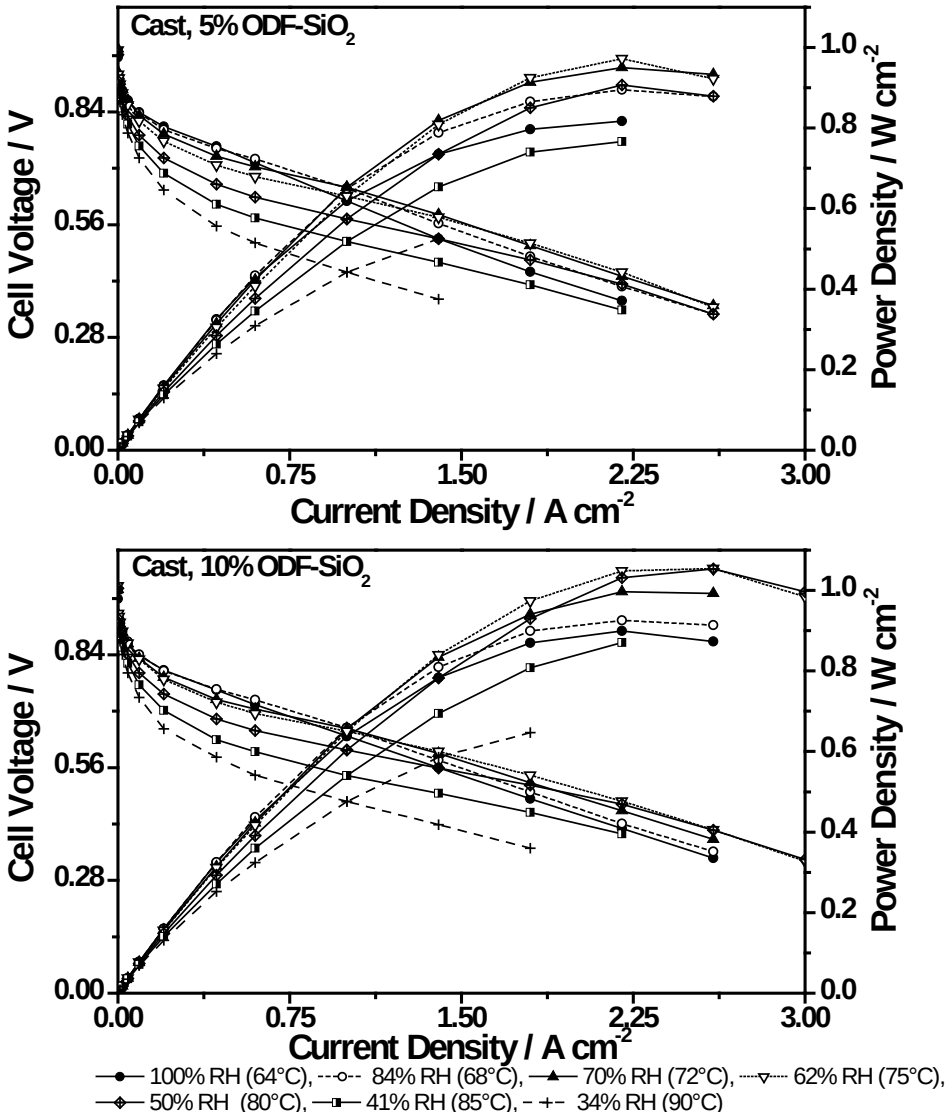

Figure 4.3 Fuel cell performance of 5 and 10 wt.% ODF-SiO_2 solvent-cast Nafion® composites at different temperature and relative humidity values. For each plot, abscissa is current density in A cm^{-2}, right ordinate is power density in W cm^{-2}, and left ordinate is cell voltage in V.

Figure 4.5 and Figure 4.6 show respectively the fuel cell resistance and voltage values for cells assembled with Nafion® and composite membranes, after 1 hour of operation at 1 A cm^{-2}. The cell resistance comprises the contributions from the membrane, the electrodes and the membrane-electrode interfaces, as well as the terminal connections. In order to achieve high fuel cell performance, the cell resistance must be as low as possible.

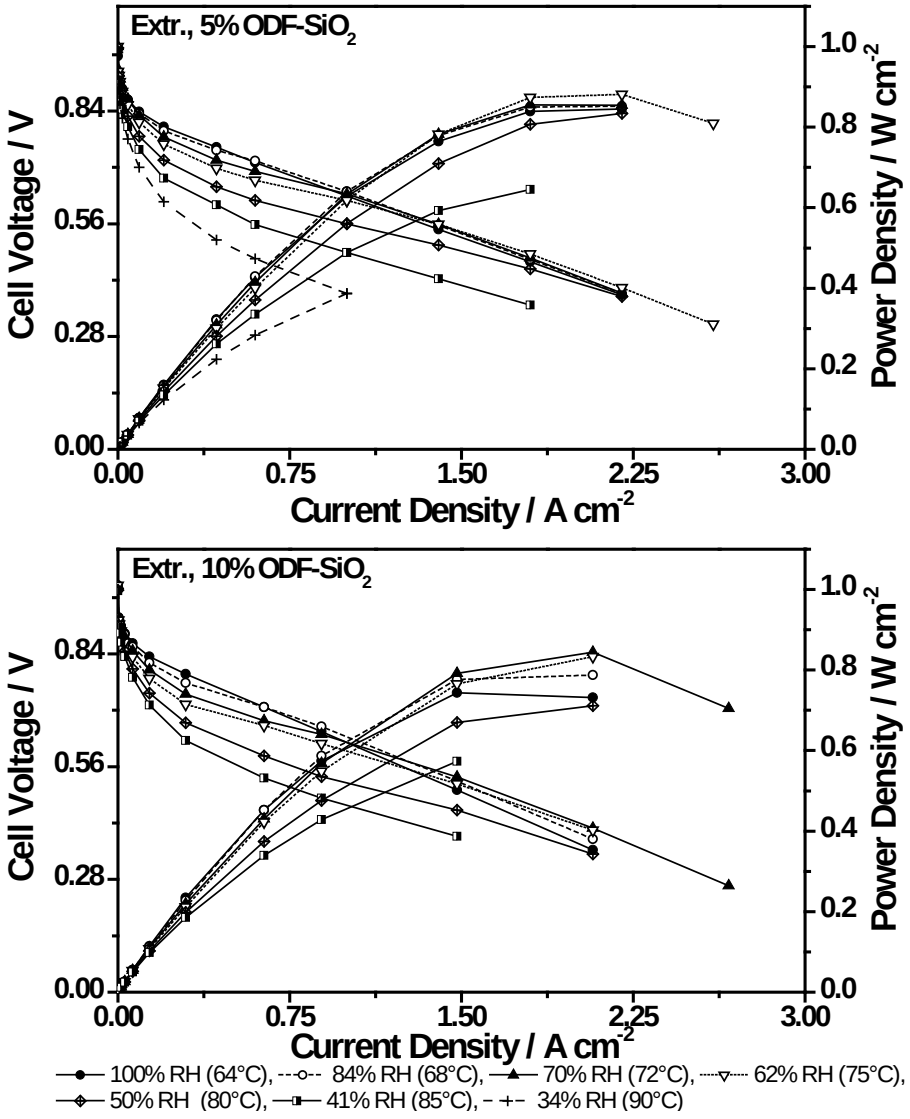

Figure 4.4 Fuel cell performance of 5 and 10 wt.% ODF-SiO_2 extruded Nafion® composites at different temperature and relative humidity values. For each plot, abscissa is current density in A cm^{-2}, right ordinate is power density in W cm^{-2}, and left ordinate is cell voltage in V.

The cell voltage is related to the resistance by Ohm's law, a lower resistance giving a higher cell voltage and consequently a higher power density for a given current density. For both extruded and cast membranes, cell resistance is diminished by the addition of fillers: even the solvent-cast membrane containing 5 wt. % of non functionalized silica shows lower resistance (higher voltage) values than pure cast Nafion®. A reduced thickness expansion due to reinforcement is most likely the main reason behind this improvement. This beneficial effect is however counteracted at high loadings, as the loss of sulfonated matrix becomes more significant. The lowest

resistances (highest voltages) are obtained for 10 wt. % ODF-silica loadings; in the case of solvent cast membranes.

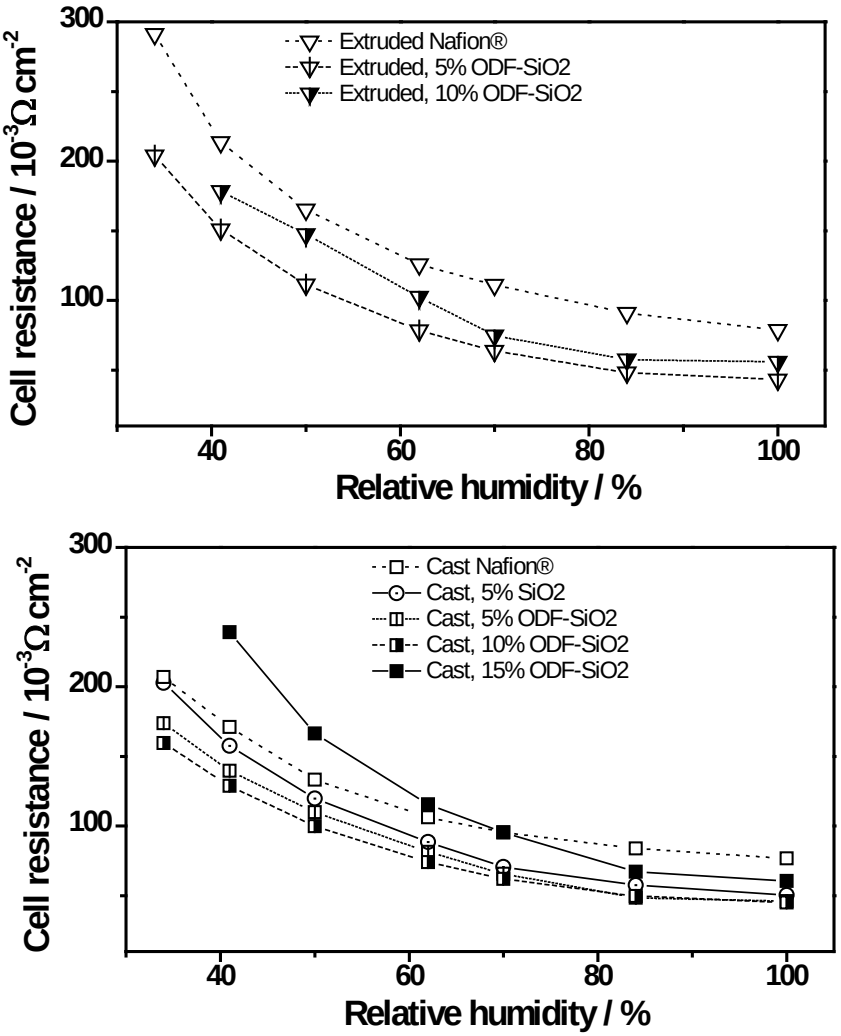

Figure 4.5 Fuel cell resistance at 1 A cm^{-2}, for extruded and solvent-cast Nafion® and composite membranes at increasing relative humidity.

For extruded membranes, the optimal composition is 5 wt. %, due to the previously mentioned difference in filler dispersion within the matrix.

Figure 4.7 shows the hydrogen crossover for the composite membranes in the relative humidity range 34–100 %. A slight decrease is observed at high RH values (lower temperature), due mainly to the corresponding temperature reduction in our test conditions, as expected from reports in the literature relating crossover to cell temperature [68,101].

The measured hydrogen crossover was higher for all composite membranes than for pure Nafion®, though the crossover values for composites with different loadings were not significantly different. Cong et al. [103] have proposed the existence of porosity at the particle-matrix interface to explain the permeability increase in silica-polymer composites. In our case, this would result in reduced crossover for membranes with higher loadings, due to the diminished particle-matrix interface area. However, as agglomeration increases, the intra-aggregate porosity might compensate for this effect, resulting in similar permeabilities for composites with high and low particle contents (Figure 4.8). An improved compatibilizing agent would be required for better affinity between the particles and the matrix, which in turn would decrease both interfacial porosity and agglomeration, thus reducing hydrogen crossover.

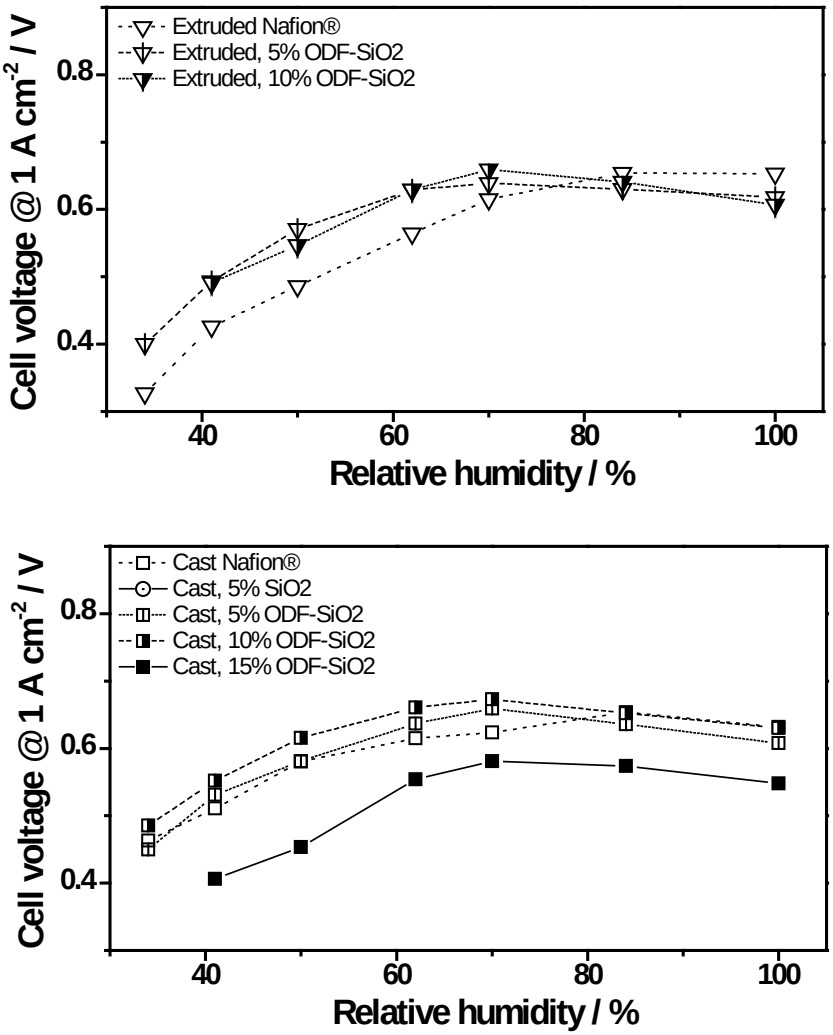

Figure 4.6 Fuel cell voltage at 1 A cm^{-2}, for extruded and solvent-cast Nafion® and composite membranes at increasing relative humidity.

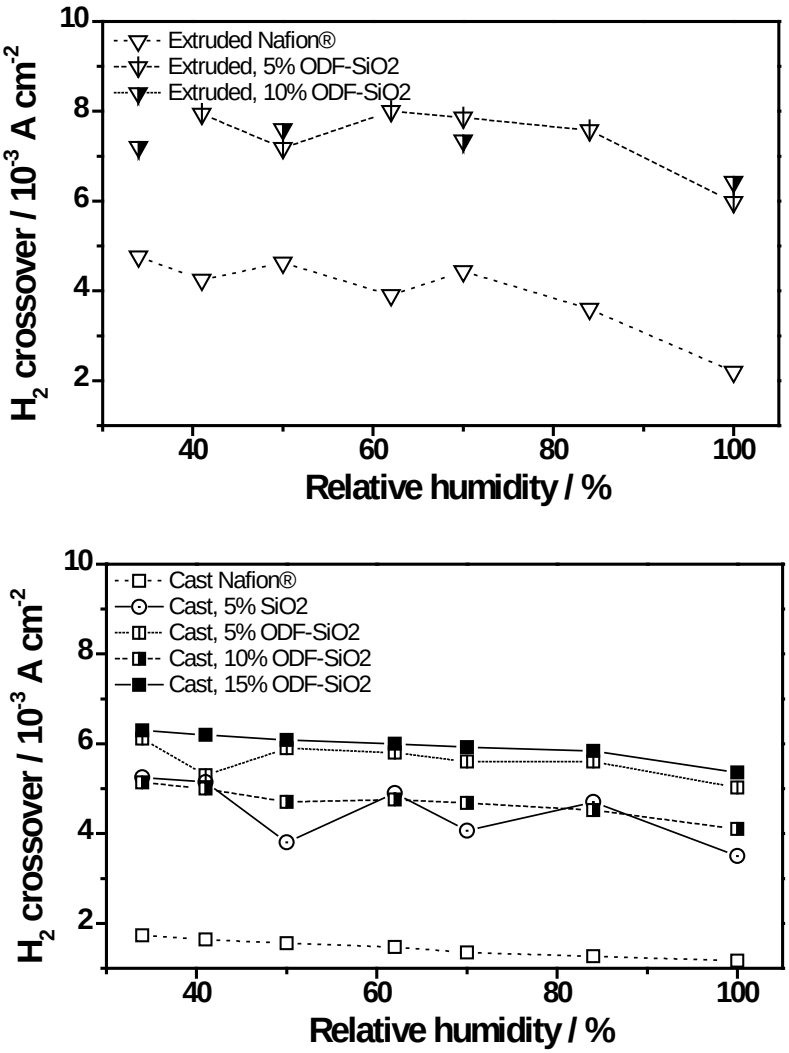

Figure 4.7 Hydrogen crossover for extruded and solvent-cast Nafion® and composite membranes at increasing relative humidity.

A higher hydrogen crossover was observed for extruded composite membranes. For example at 100% RH the hydrogen crossover of solvent-cast 5 wt.% ODF-silica composite membranes was 5 mA cm^{-2} while that of extruded membranes was 6 mA cm^{-2}. Nevertheless, the crossover increase from the pure polymer to the composite membranes was similar for cast and extruded films (around 3–4 mA cm^{-2}).

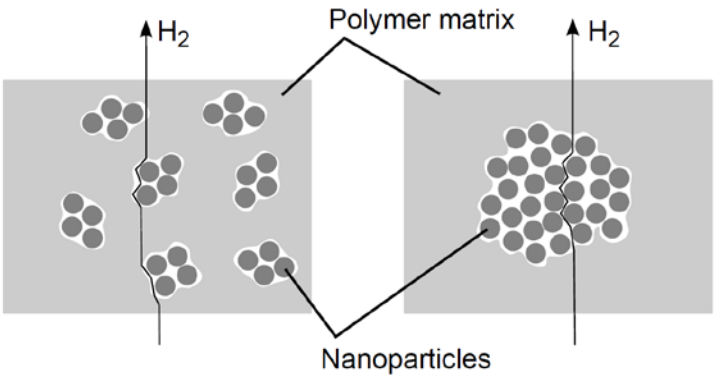

Figure 4.8 Porosity at the particle-matrix interface could explain the permeability increase in silica-polymer composites.

4.2.2 Fuel cell performance evaluation of fluorinated polyoxadiazole random copolymer membranes

In the case of aromatic hydrocarbon polymer membranes, the catalyst-coated membrane method (CCM [102]) was used for the manufacture of membrane electrode assemblies (MEAs). An isopropanol-based ink composed of carbon supported catalyst (46.4 wt.% Pt/C) and Nafion® ionomer (30 wt.%) was spray-deposited directly on both sides of proton conducting membranes (the total Pt loading for both anode and cathode was 0.4 mg Pt cm^{-2}). Subsequently the membrane was sandwiched between GDLs. The CCM process was chosen since it provides better adhesion between polymer membrane and catalyst layer in the case of high melting point aromatic hydrocarbon polymers [104].

One issue with the sulfonated oxadiazole random copolymer membranes prepared was their poor dimensional stability: they would swell excessively in high humidity conditions. The swelling was more dramatic for the membranes with the highest ODBA:FDBA ratio (highest sulfonic group content). Thus only PODOcoF-AS (ODBA:FDBA=0.5) showed enough dimensional stability for MEA manufacture.

Accordingly, we prepared a catalyst-coated membrane from PODOcoF-AS polymer and assembled this MEA into a single cell in order to evaluate the viability of this polymer electrolyte membrane for practical PEMFCs. Unfortunately, in dry conditions,

this polymer has the poorest mechanical properties of the series, becoming very brittle. The testing thus was first carried out at 100% relative humidity to avoid degradation. Before the test, the cell conditioning to activate the catalyst layer was also carried out at 100% RH. Figure 4.9 shows a typical fuel cell polarization curve of a single cell with PODOcoF-AS sulfonated fluorinated oxadiazole random copolymer membrane.

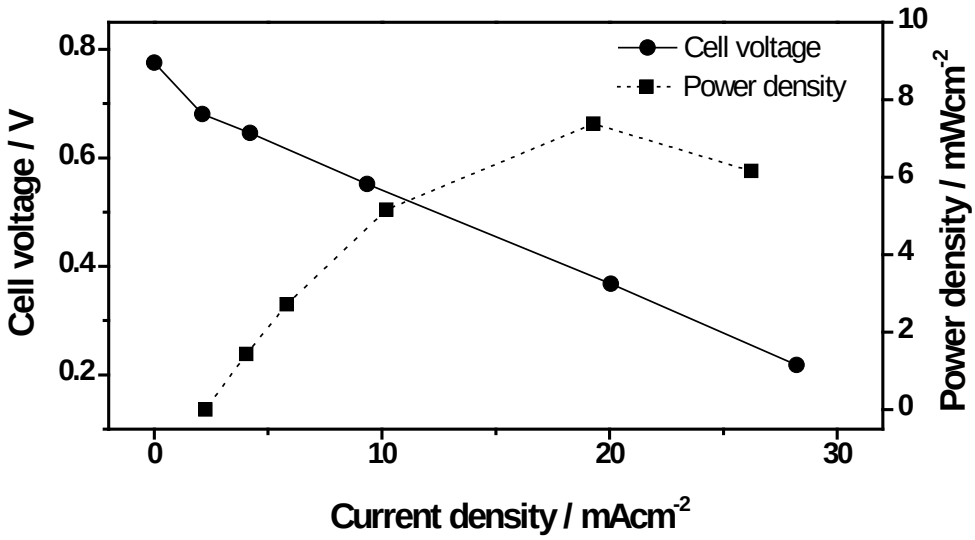

Figure 4.9 Polarization curve for PODOcoF-AS at 100 RH after 10 hours conditioning.

The highest power densitiy achieved at 0.5 volts was 7.5 mW cm^{-2}, at 100% relative humidity. We found that by increasing the conditioning time from 1 to 6 and 10 hours the power density increased from 1.0 to 4.0 and 7.5 mW cm^{-2} at 0.25, 0.44 and 0.50 volts, respectively. However this power density is still rather low for practical fuel cell application. Furthermore, when we keep running the fuel cell station at a load giving initially 0.6 Volts, the operating cell voltage was stable only for 24 hours. Afterwards, the measured hydrogen crossover was 20.0 mA cm^{-2}. This value is rather high, and points to fracturing and pinhole formation in the membrane during fuel cell operation. The deficient fuel cell performance can be explained by the low conductivity of this membrane. The durability issue, however, is more probably related to poor dimensional stability, due to local humidity variations during fuel cell operation.

In a previous study by Gomes et al. [44] on fluorinated oxadiazole homopolymers (containing no sulfonic groups), phosphoric acid doping was found to give good

conductivity to solvent-cast membranes. In order to explore this possibility with our non sulfonated oxadiazole copolymers, a series of phosphoric acid doped membranes was prepared, attempting loadings from 5 to 20%. The highest loading without visible aggregation was 15 wt.%, obtained for the copolymer PODOcoF-C (ODBA:FDBA=2). A fuel cell was built following the same protocol used for the previous polymer.

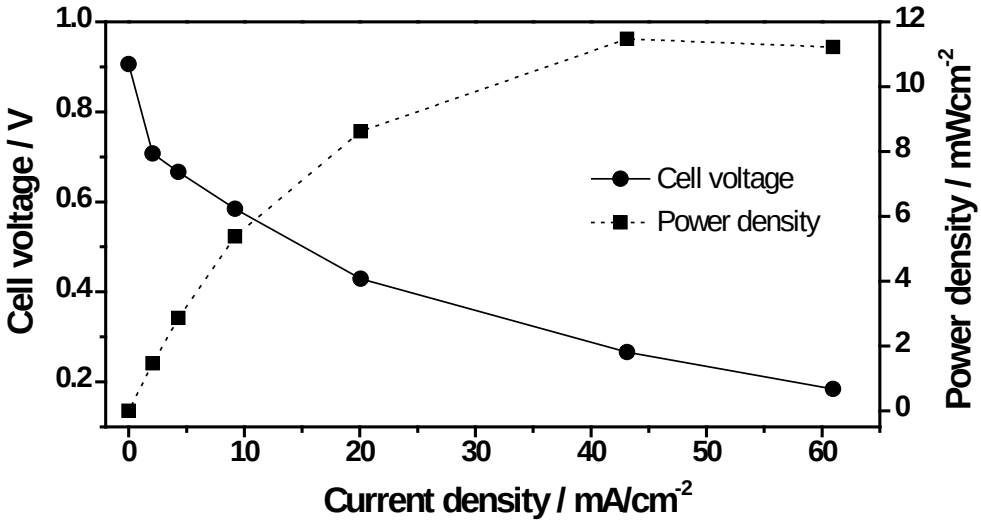

Figure 4.10 Polarization curve for phosphoric acid-doped PODOcoF-C at 100 RH, after 1 h conditioning.

Figure 4.10 shows a typical fuel cell polarization curve for single-cell tests with phosphoric acid doped PODOcoF-C membrane. The highest power densities, obtained at 0.45 Volts and 100% relative humidity, was 0.95 mW cm^{-2}. This performance is too deficient for fuel cell application. Furthermore, the operating cell voltage was not stable after 5 hours, and the open circuit voltage becomes after 16 hours too low even for application of the test load.

The most probable explanation for this poor performance is the leaching of phosphoric acid by water from the humidified reactants flows. This results in a quick reduction of the proton carriers available. Electrochemical impedance measurements at 100% RH on these membranes confirmed a dramatic drop in conductivity after a few hours. The hydrogen crossover values obtained for the cell prepared with phosphoric acid doped PODOcoF-C membrane was 1.9 mA cm^{-2}, which is relatively

low and comparable to commercial membranes. This crossover value rules out membrane degradation as a cause for poor durability.

The ODF-Silica composite membranes prepared with these copolymers had better dimensional properties, as shown in the previous chapter. However, the main reason for the low fuel cell performance for these copolymers is their low conductivity. Thus, the corresponding composite membranes might have better durability, but will still perform too poorly for practical fuel cell application.

4.3 Summary

A series of Nafion composite and random copolymer oxadiazole composite membranes were tested in order to evaluate their suitability to fuel cell application. For Nafion composites, the best fuel cell performance was obtained for membranes loaded with 10 wt. % ODF-functionalized silica for solvent cast membranes, while the optimal loading was 5% for the extruded composites. The composite membranes allowed for operation in high temperature PEM fuel cells. Hydrogen crossover, however, was higher for the composites than for pure Nafion membranes, probably due to the replacement of the dense fluorinated matrix with porous silica phase. Even though the fuel cell performance of the composite membranes decreases with decreasing the relative humidity, good performance values are still obtained at 34% RH and 95°C. In the case of the sulfonated random oxadiazole copolymer membranes studied, while their mechanical properties are improved by the ODF-functionalized silica, the low conductivity of the matrix precludes their use in practical fuel cells.

Conclusion

The objective of this work was to explore the use of silica nanoparticles, functionalized with oxadiazole telechelic oligomers, in the fabrication of composite polymer electrolyte membranes with improved properties relevant to fuel cell application.

The experimental work started with the synthesis of three different oxadiazole-type telechelic oligomers, and their use to prepare functonalized silica nanoparticles, following the protocol developed by Gomes et al [14]. The chemical structure of the compounds and functionalized particles was studied by 1H-NMR, elemental analysis and FTIR techniques, confirming the success of each synthesis step. In addition, the molecular weight of the synthesized telechelics was studied by size exclusion chromatography (SEC). For all three cases, the degree of polymerization obtained was around 10. Thermal analysis allowed the identification of the reactant mixture composition necessary to obtain maximum particle loading. Based on its optimal thermal and chemical properties, a fluorinated oxadiazole telechelic oligomer (ODF) was chosen for the preparation of composites. The resulting ODF-functionalized particles display their first degradation steps above 350°C, well beyond the needed thermal stability for PEM fuel cell application.

For the composite membrane preparation, three polymer matrices were employed: Nafion®, poly(arylene ether 1,3,4-oxadiazole), and fluorinated polyoxadiazole random copolymers. The resulting membranes were extensively characterized to better understand their morphology (SEM) and their electrochemical (ion exchange capacity, conductivity) physicochemical (water uptake, thickness expansion) and thermal properties (TGA, DSC, DMTA).

Nafion®-functionalized silica composite membranes were fabricated both by solvent casting and melt extrusion processes. The membranes were post-sulfonated in order to attach sulfonic groups on the functionalized silica filler particles. It was found that that the inclusion of nanoparticles proved beneficial, mainly due to a reinforcement effect and an improvement in water retention. Moreover, due to their higher affinity for the matrix, the functionalized nanoparticles perform better than the pristine silica particles. For the same filler loading, better nanoparticle dispersion was achieved for solvent-cast membranes, which in turn results in higher proton conductivity. The composite membranes showed excellent thermal stability, allowing for operation in high temperature PEM fuel cells.

For the preparation of aromatic oxadiazole-matrix composite membranes, poly(arylene ether 1,3,4-oxadiazole) was synthesized. The molecular weight of the resulting polymer was around 14000 g mol^{-1}, contributing to the good mechanical properties of its membranes. Its thermal stability up to 300 °C, along with its glass transition temperature around 210 °C allow comfortably for its use in fuel cell operation conditions. Furthermore, a series of fluorinated polyoxadiazole random copolymers were provided, containing a hydrophobic unit, 2-[4,4'-(Hexafluoroisopropylidene)diphenyl]-1,3,4-oxadiazole (FDBA), and a hydrophilic unit, 2-(diphenyl ether)-1,3,4-oxadiazole (ODBA) in increasing ratios (0.5, 1.0, 2.0 and 3.0). The resulting composite membranes were also post-sulfonated in order to attach proton conducting groups both on the filler particles and on the sulfonatable units of the polymer matrix. Regarding the fluorinated polyoxadiazole random copolymer membranes, their dimensional stability was relatively low. The introduction of functionalized silica was shown to improve the mechanical properties of these membranes, without dramatically losing IEC or proton conductivity. Nevertheless, for all polyoxadiazole-matrix composite membranes studied, their proton conductivity values were low when compared to current commercially available polymer electrolyte membranes.

Finally, a series of Nafion® composite and random oxadiazole copolymer composite membranes were tested in order to evaluate their suitability to fuel cell application. The MEAs for Nafion®-based membranes were prepared by hot pressing method,

while the catalyst-coated membrane method was used for oxadiazole copolymer-matrix membranes.

In the case of the sulfonated random oxadiazole copolymer membranes studied, while their mechanical properties are improved by the ODF functionalized silica, the low conductivity of the matrix precludes their use in practical fuel cells.

For Nafion composites, on the other hand, better fuel cell performances were obtained. The best results were found for membranes loaded with 10 wt. % ODF-functionalized silica for solvent cast membranes, while the optimal loading was 5% for the extruded composites. The composite membranes allowed for operation in high temperature PEM fuel cells. Hydrogen crossover, however, was higher for the composites than for pure Nafion membranes, probably due to the replacement of the dense fluorinated matrix with porous silica phase. Even though the fuel cell performance of the composite membranes decreases with decreasing the relative humidity, good performance values are still obtained at 34% RH and 95°C.

Appendix A. Characterization methods

The following sections contain brief descriptions of the instrumental parameters and characterization protocols employed throughout this work.

A.1 Chemical structure and morphology

Elemental Analysis (EA)

A Flash EA1112 (Thermo Finnigan-CE Instruments) was employed to perform CHNS elemental analysis. A small amount of sample (2-3 mg) is burned in an excess of oxygen, and the combustion products (NO_2, CO_2, SO_2, H_2O) are separated in a chromatographic column, and measured with a thermal conductivity detector.

Fourier Transform Infrared Spectroscopy (FTIR)

FTIR spectra were obtained in a Bruker Equinox IFS 55 spectrophotometer, in the range 4000–400 cm^{-1}. The samples were mixed (1 wt.%) with dried KBr, and compressed to obtain a translucent disc. The instrument optics area was kept under nitrogen atmosphere during the measurements.

Nuclear Magnetic Resonance Spectroscopy (NMR)

^{1}H- and ^{13}C-NMR spectroscopy was employed to confirm the chemical structure of synthesized compounds. Samples were dissolved in a suitable deuterated solvent (either deuterated dimehtylsulfoxide (DMSO-d6), deuterated toluene (toluene-d8), or deuterated chloroform ($CDCl_3$)). The spectra were recorded in a 300 MHz Avance Bruker NMR spectrometer, equipped with an UltraShield magnet.

Size Exclusion Chromatography (GPC)

Size exclusion chromatography ("Gel Permeation Chromatography", GPC) was performed on a Polymer Laboratories (PL) chromatograph, equipped with an ERC 7515A refractive index detector, and a PL Mixed-D column. Chloroform was used as eluent solvent, and polystyrene as standard polymer.

Scanning Electron Microscopy (SEM)

The samples were prepared by freeze-fracture method. The micrographs were obtained in a FEI Quanta 650 scanning electron microscope, equipped with an Everhart-Thornley detector (ETD). The accelerating voltage was set to 5.00 kV.

A.2 Thermal properties

Thermogravimetric Analysis (TGA)

Information on the thermal stability of the polymer composite membranes was obtained by thermogravimetric analysis in a Netzsch TG 209 F1 Iris thermo-microbalance. The temperature was scanned in the range 25–800 °C, with a heating rate of 10 °C min^{-1}, under Argon sweep.

Differential Scanning Calorimetry (DSC)

Differential scanning calorimetry (DSC) measurements were carried out in a Netzsch DSC 204 Phoenix® calorimeter. A mass of 8 to 20 mg of sample was introduced in an aluminium pan with a perforated cover, and a preliminary DSC run at 10 °C min^{-1}, from 25 to 150 °C, was employed on all samples to eliminate adsorbed water. The

sample was subsequently cooled down to −150 °C at 30 °C min^{-1}, and finally a dynamic run at 10 °C min^{-1} was performed up to 280 °C. An empty aluminium pan was used as reference.

TGA-coupled Infrared Spectroscopy (FTIR-TGA)

For the analysis of volatile thermal degradation products in inert atmosphere, a Bruker Equinox 55 infrared spectrometer was employed, connected through a Bruker TGA-FTIR interface to a Netzsch TG 209 thermo-microbalance. The thermograms were carried out at 10 °C min^{-1}, and Argon was used as sweep gas to transfer the gaseous products of thermal degradation through a heated PTFE tubing into a heated 8.7 mL cell in the spectrometer interface.

Dynamic Mechanical Thermal Analysis (DMTA)

Dynamic mechanical analysis (DMTA) was performed on films cut into rectangular samples of approximately 1.5 × 5 cm. The measurements were carried out in a Gabo EPLEXOR® 500 N instrument, in tension mode with a target strain of 0.1%. Samples were heated using a dynamic temperature ramp from 30 to 160 °C, at a heating rate of 3 °C min^{-1}.

A.3 Physicochemical properties

Water Uptake Measurement and Thickness Expansion

For water uptake characterization, the films were fully hydrated by immersion during 2 days in deionized (DI) water at room temperature. The water-saturated membrane samples were weighed after quickly wiping the excess water with residue-free tissue paper. The samples were then placed in a vacuum oven at 80 °C overnight to remove the sorpted water. After cooling down to room temperature, the weight of the dry membranes was measured. The mass-based water uptake (*WUm*) was calculated with the equation:

$$WUm_{(\%)} = \frac{m_{wet} - m_{dry}}{m_{dry}} \times 100 ,$$

where m_{dry} and m_{wet} are the masses of dry and wet samples, respectively.

The swelling ratio (Δt) of the membranes was calculated by measuring the thickness of the membranes before and after the water uptake measurement, according to the equation:

$$\Delta t_{(\%)} = \frac{t_{wet} - t_{dry}}{t_{dry}} \times 100$$

where t_{dry} and t_{wet} are the thickness of the dried and wet samples, respectively.

Ion Exchange Capacity (IEC)

In order to determine the ion exchange capacity, the films in H^+ form were first equilibrated for 48 hours in 0.2 M NaCl at room temperature with regular agitation. The equilibration baths were then titrated with NaOH (0.005M) with a Mettler Toledo T50 automatic titrator. The procedure was carried out three times and the results averaged.

Ionic Conductivity

Ionic conductivity was measured by electrochemical impedance spectroscopy (EIS), at room temperature and 100% relative humidity, using an HP4192A impedance analyzer. The frequency scan was scanned from 50 kHz to 5 MHz with an AC perturbing signal amplitude of 0.1 V. Pure polymer membrane samples were measured as a reference before each series of measurements. The resistivity of the membrane was obtained from the high frequency part of the Nyquist plot, corresponding to the bulk resistance of the polymer. The ionic conductivity of the samples was calculated using the equation:

$$\sigma = \frac{1}{R_{bulk}} \times \frac{d}{A}$$

where σ is the conductivity, d is the interelectrode distance, A is the contact area between the electrodes and the polymer film, and R_{bulk} is the bulk resistance obtained from the Nyquist plot of the impedance spectrum.

Appendix B. List of abbreviations

^{13}C NMR	Carbon nuclear magnetic resonance
^{1}H NMR	Proton nuclear magnetic resonance
bp	Boiling point
$CDCl_3$	Deuterated chloroform
CL	Catalyst layer
CO	Carbon monoxide
CO_2	Carbon dioxide
DI water	Deionized water
DMA	Dynamic mechanical analysis
DMAc	Dimethylacetamide
DMFC	Direct methanol fuel cell
DMSO	Dimethyl sulfoxide
DMSO-d6	Deuterated dimethyl sulfoxide
DSC	Differential scanning calorimetry
DTG	Differential thermal analysis
EA	Elemental analysis
EIS	Electrochemical impedance spectroscopy
FDBA	2-[4,4’-(Hexafluoroisopropylidene)diphenyl]-1,3,4-oxadiazole
FTIR	Fourier transform infrared spectroscopy
GDE	Gas diffusion electrode

GDL	Gas diffusion layer
GPC	Gel permeations chromatography
HF	Hydrofluoric acid
HNO_3	Nitric acid
IEC	Ion exchange capacity
IEMFC	Ion exchange membrane fuel cell
K_2CO_3	Potassium carbonate
KBr	Potassium bromide
KOH	Potassium hydroxide
MEA	Membrane electrode assembly
M_n	Number average molecular weight
M_w	Weight average molecular weight
NaCl	Sodium chloride
NMP	N-Methyl-2-pyrrolidone
OCV	Open circuit voltage
ODA	Telechelic oligomer from 4,4′-Isopropylidenediphenol
ODBA	2-(diphenyl ether)-1,3,4-oxadiazole
ODF	Telechelic oligomer from 4,4'-(Hexafluoroisopropylidene)diphenol
ODF-SiO_2	Silica funcitionalized with ODF (ODF-Silica)
ODS	Telechelic oligomer from 4,4′-Sulfonyldiphenol
PDI	Polydispersity index
PEEK	Poly(ether ether ketone)

PEM	Polymer electrolyte membrane
PEMFC	Polymer electrolyte membrane fuel cell
PFSA	Perfluorosulfonic acid
POD	Polyoxadiazole
PODOcoF	Fluorinated polyoxadiazole random co-polymer
PPA	Polyphosphoric acid
PTFE	Polytetrafluoroethylene
RH	Relative humidity
SEC	Size-exclusion chromatography
SEM	Scanning electron microscope
Si	Silicon
SiO_2	Silicon dioxide
Sn	Tin
$–SO_2F$	Sulfonyl fluoride group
$–SO_3H$	Sulfonic acid group
SP(E)MFC	Solid polymer (electrolyte) membrane fuel cell
SPEEK	Sulfonated poly(ether ether ketone)
Tg	Glass transition temperature
TGA	Thermogravimetric analysis
Ti	Titanium
Zr	Zirconium
ZrO_2	Zirconium oxide

List of symbols and constants

% RH	Percent relative humidity
°C	Degree Celsius
µm	Micrometer
A	Contact area between the electrodes and the polymer film
A	Active area (cm^2)
CL^a	Anode catalyst layer
CL^c	Cathode catalyst layer
d	Distance between electrodes
E'	Storage modulus
E"	Loss modulus
F	Faraday constant (~96485 A s mol^{-1})
g mol^{-1}.	gram per mol
GDL^a	Anode gas diffusion layer
GDL^c	Cathode gas diffusion layer
h	Hour
$I_{H_2}^{cross}$	Current produced
$J_{H_2}^{cross}$	Hydrogen crossover rate
kHz	Kilohertz

m	Mass
mA cm^{-2}	Miliampere per squre centimeter
meq g^{-1}	Miliequivalent per gram
MHz	Megahertz
mL	Mililiter
nm	Nanometer
$P^{0}_{H_2O}$	Saturated water vapor pressure
ppm	Parts per million
rad s^{-1}	Radian per second
R_{bulk}	Bulk resistance
rpm	Revolutions per minute
S cm^{-1}	Siemens per centimeter
tan δ	Phase angle
t_{dry}	Thickness of dried membrane
t_{wet}	Thickness of wet membrane
V	Volt
W cm^{-2}	Watt per square centimeter
W^{a}_{CL}	Water in the anodic catalyst layers of the fuel cell
W^{a}_{inlet}	Water flowing into the fuel cell at anode sides
W^{a}_{outlet}	Water drained out of the fuel cell at anode sides
W^{c}_{CL}	Water in the cathodic catalyst layers of the fuel cell

W_{inlet}^{c}	Water flowing into the fuel cell at cathode sides
W_{outlet}^{c}	Water drained out of the fuel cell at cathode sides
$W_{produced}^{c}$	Water produced at the cathodic catalyst layer
$W_{diffusion}$	Water back-diffused from cathode to anode
W_{drag}	Water osmotically dragged from anode to cathode
W_{dry}	Weight of dried membrane
wt.%	Weight percentage
WUm	mass-based water uptake
W_{wet}	Weight of wet membrane
$\Delta\bar{g}_f$	Gibbs free energy
Δt	Swelling ratio
v	stretch
v_{as}	asymmetric stretch
v_s	symmetric stretch
σ	Conductivity (S cm^{-1})

References

1 Peighambardoust, S.J., Rowshanzamir, S. & Amjadi, M. Review of the proton exchange membranes for fuel cell applications. *Int. J. Hydrogen Energy* 35, 9349–9384 (2010).

2 Hamrock, S. J. & Yandrasits, M. A. Proton exchange membranes for fuel cell applications. *J. Macromol. Sci., Polym. Rev.* 46, 219–244 (2006).

3 Kariduraganavar, M. Y., Nagarale, R. K., Kittur, A. A. & Kulkarni, S. S. Ion-exchange membranes: preparative methods for electrodialysis and fuel cell applications. *Desalination* 197, 225–246 (2006).

4 Smitha, B., Sridhar, S. & Khan, A.A. Solid polymer electrolyte membranes for fuel cell applications–a review. *J. Membr. Sci.* 259, 10–26 (2005).

5 Hickner, M. A. *et al.* Alternative polymer systems for proton exchange membranes (PEMs). *Chem. Rev.* 104, 4587–4612 (2004).

6 Kerres, J. A. Development of ionomer membranes for fuel cells. *J. Membr. Sci.* 185, 3–27 (2001).

7 Zhang, J. *et al.* High temperature PEM fuel cells. *J. Power Sources* 160, 872–891 (2006).

8 Dupuis, A. C. Proton exchange membranes for fuel cells operated at medium temperatures: Materials and experimental techniques. *Prog. Mater. Sci.* 56, 289–327 (2011).

9 Peron, J. *et al.* Properties of Nafion® NR-211 membranes for PEMFCs. *J. Membr. Sci.* 356, 44–51 (2010).

10 Shao, Y., Yin, G., Wang, Z. & Gao, Y. Proton exchange membrane fuel cell from low temperature to high temperature: material challenges. *J. Power Sources* 167, 235–242 (2007).

11 Mauritz, K.A. & Moore, R.B. State of understanding of Nafion. *Chem. Rev.* 104, 4535–4586 (2004).

12 Gomes, D. Roeder, J., Ponce, M.L. & Nunes, S.P. Characterization of partially sulfonated polyoxadiazoles and oxadiazole-triazole copolymers. *J. Membr. Sci.* 295, 121–129 (2007).

13 Gomes, D. Roeder, J., Ponce, M.L. & Nunes, S.P. Single-step synthesis of sulfonated polyoxadiazoles and their use as proton conducting membranes. *J. Power Sources* 175, 49–59 (2008).

14 Gomes, D. Buder, I. & Nunes, S.P. Sulfonated silica-based electrolyte nanocomposite membranes. *J. Polym. Sci., Part B: Polym. Phys.* 44, 2278–2298 (2006).

15 Gomes, D., Marschall, R., Nunes, S.P. & Wark, M. Development of polyoxadiazole nanocomposites for high temperature polymer electrolyte membrane fuel cells. *J. Membr. Sci.* 322, 406–415 (2008).

16 Tripathi, B. P. & Shahi, V. K. Organic–inorganic nanocomposite polymer electrolyte membranes for fuel cell applications. *Prog. Polym. Sci.* 36, 945–979 (2011).

17 Laberty-Robert, C., Vallé, K., Pereira, F. & Sanchez, C. Design and properties of functional hybrid organic–inorganic membranes for fuel cells. *Chem. Soc. Rev.* (2011).

18 Nagarale, R. K., Shin, W. & Singh, P. K. Progress in ionic organic-inorganic composite membranes for fuel cell applications. *Polym. Chem.* 1, 388–408 (2010).

19 S.P. Nunes, in: S.M.J. Zaidi, T. Matsuura (Eds.), Polymer Membranes for Fuel Cells, Springer, 2009, pp. 223-234.

20 Jones, D. & Rozière, J. Advances in the development of inorganic–organic membranes for fuel cell applications. *Adv. Polym. Sci.* 219–264 (2008).

21 Herring, A. M. Inorganic–polymer composite membranes for proton exchange membrane fuel cells. *J. Macromol. Sci., Polym. Rev.* 46, 245–296 (2006).

22 Licoccia, S. & Traversa, E. Increasing the operation temperature of polymer electrolyte membranes for fuel cells: From nanocomposites to hybrids. *J. Power Sources* 159, 12–20 (2006).

23 G. Alberti, M. Casciola, in: Peinemann, K. V. & Nunes, S. P. *Membrane Technology: Volume 2: Membranes for Energy Conversion*. 2, (Wiley-VCH: 2008). 97-122.

24 W. Vielstich, A. Lamm, H.A. Gasteiger (Eds.), Handbook of Fuel Cells, FundamentalsTechnology and Applications, vol. 3 Wiley (2003), 447–455.

25 Gosalawit, R., Chirachanchai, S., Shishatskiy, S. & Nunes, S.P. Sulfonated montmorillonite/sulfonated poly (ether ether ketone)(SMMT/SPEEK) nanocomposite membrane for direct methanol fuel cells (DMFCs). *J. Membr. Sci.* 323, 337–346 (2008).

26 Rhee, C. H., Kim, H. K., Chang, H. & Lee, J. S. Nafion/Sulfonated Montmorillonite Composite: A New Concept Electrolyte Membrane for Direct Methanol Fuel Cells. Chem. Mater. 17, 1691–1697 (2005).

27 G. Alberti, M. Casciola, in: K.V. Peinemann, S.P. Nunes (Eds.), Membranes for Energy Conversion, 2008, pp. 97-122.

28 A.S. Aricò, V. Baglio, V. Antonucci, in: Peinemann, K. V. & Nunes, S. P. *Membrane Technology: Volume 2: Membranes for Energy Conversion*. 2, (Wiley-VCH: 2008). 123-167.

29 Sacca, A. *et al.* Nafion–TiO2 hybrid membranes for medium temperature polymer electrolyte fuel cells (PEFCs). *J. Power Sources* 152, 16–21 (2005).

30 Sanchez, C., Ribot, F. & Lebeau, B. Molecular design of hybrid organic-inorganic nanocomposites synthesized via sol-gel chemistry. *J. Mater. Chem.* 9, 35–44 (1999).

31 Di Vona, M. L. *et al.* SPEEK-TiO_2 nanocomposite hybrid proton conductive membranes via in situ mixed sol–gel process. *J. Membr. Sci.* 296, 156–161 (2007).

32 Sahu, A. K., Selvarani, G., Pitchumani, S., Sridhar, P. & Shukla, A. K. A sol-gel modified alternative Nafion-silica composite membrane for polymer electrolyte fuel cells. *J. Electrochem. Soc.* 154, 123–132 (2007).

33 Baradie, B., Dodele, J. P. & Guay, D. Hybrid Nafion®-inorganic membrane with potential applications for polymer electrolyte fuel cells. *J. Electroanal. Chem.* 489, 101–105 (2000).

34 Mauritz, K. A. *et al.* Microstructural evolution of a silicon oxide phase in a perfluorosulfonic acid ionomer by an in situ sol–gel reaction. *J. Appl. Polym. Sci.* 55, 181–190 (1995).

35 Gnana Kumar, G., Kim, A. R., Suk Nahm, K. & Elizabeth, R. Nafion membranes modified with silica sulfuric acid for the elevated temperature and lower humidity operation of PEMFC. *Int. J. Hydrogen Energy* 34, 9788–9794 (2009).

36 Wang, H. *et al.* Nafion-bifunctional silica composite proton conductive membranes. *J. Mater. Chem.* 12, 834–837 (2002).

37 Abbaraju, R. R., Dasgupta, N. & Virkar, A. V. Composite Nafion Membranes Containing Nanosize TiO2/ SnO2 for Proton Exchange Membrane Fuel Cells. *J. Electrochem. Soc.* 155, 1307–1313 (2008).

38 Guan, R., Dai, H., Li, C., Liu, J. & Xu, J. Effect of casting solvent on the morphology and performance of sulfonated polyethersulfone membranes. *J. Membr. Sci.* 277, 148–156 (2006).

39 Gao, Y. *et al.* Comparison of PEM properties of copoly (aryl ether ether nitrile)s containing sulfonic acid bonded to naphthalene in structurally different ways. *Macromolecules* 40, 1512–1520 (2007).

40 Saeki, S., Cowie, J. M. G. & McEwen, I. J. The effect of molecular weight and casting solvent on the miscibility of polystyrene-poly([alpha]-methyl styrene) blends. *Polymer* 24, 60–64 (1983).

41 Mokrini, A., Huneault, M.A., Shi, Z., Xie, Z. & Holdcroft, S. Non-fluorinated proton-exchange membranes based on melt extruded SEBS/HDPE blends. *J. Membr. Sci.* 325, 749–757 (2008).

42 Choi, J., Lee, K. M., Wycisk, R., Pintauro, P. N. & Mather, P. T. Nanofiber network ion-exchange membranes. *Macromolecules* 41, 4569–4572 (2008).

43 Choi, J., Lee, K. M., Wycisk, R., Pintauro, P. N. & Mather, P. T. Sulfonated Polysulfone/POSS Nanofiber Composite Membranes for PEM Fuel Cells. *J. Electrochem. Soc.* 157, 914 (2010).

44 Gomes, D. & Nunes, S.P. Fluorinated polyoxadiazole for high-temperature polymer electrolyte membrane fuel cells. *J. Membr. Sci.* 321, 114–122 (2008).

45 Appleby, A.J. Fuel cell handbook. (1988).

46 Sopian, K. & Wan Daud, W.R. Challenges and future developments in proton exchange membrane fuel cells. *Renewable energy* 31, 719–727 (2006).

47 Li, X., Roberts, E.P.L. & Holmes, S.M. Evaluation of composite membranes for direct methanol fuel cells. *J. Power Sources* 154, 115–123 (2006).

48 Kinoshita, K. Electrochemical uses of carbon. *Electrochemistry Encyclopedia* (2001) at http://electrochem.cwru.edu/encycl/art-c01-carbon.htm.

49 Neef, H.J. International overview of hydrogen and fuel cell research. *Energy* 34, 327–333 (2009).

50 Heitner-Wirguin, C. Recent advances in perfluorinated ionomer membranes: structure, properties and applications. *J. Membr. Sci.* 120, 1–33 (1996).

51 Hsu, W.Y. & Gierke, T.D. Ion transport and clustering in Nafion perfluorinated membranes. *J. Membr. Sci.* 13, 307-326 (1983).

52 Rikukawa, M. & Sanui, K. Proton-conducting polymer electrolyte membranes based on hydrocarbon polymers. *Prog. Polym. Sci.* 25, 1463–1502 (2000).

53 Nunes, S.P., Ruffmann, B., Rikowski, E., Vetter, S. & Richau, K. Inorganic modification of proton conductive polymer membranes for direct methanol fuel cells. *J. Membr. Sci.* 203, 215–225 (2002).

54 Zhai, Y., Zhang, H., Hu, J. & Yi, B. Preparation and characterization of sulfated zirconia (SO42-/ZrO2)/Nafion composite membranes for PEMFC operation at high temperature/low humidity. *J. Membr. Sci.* 280, 148–155 (2006).

55 Chen, C.Y. *et al.* Nafion/polyaniline/silica composite membranes for direct methanol fuel cell application. *J. Power Sources* 166, 324–330 (2007).

56 Easton, E.B. *et al.* Characteristics of polypyrrole/Nafion composite membranes in a direct methanol fuel cell. *J. Electrochem. Soc.* 150, C735 (2003).

57 Hagihara, H., Uchida, H. & Watanabe, M. Preparation of highly dispersed SiO2 and Pt particles in Nafion® 112 for self-humidifying electrolyte membranes in fuel cells. *Electrochim. Acta* 51, 3979–3985 (2006).

58 Huang, R.Y.M. Shao, P. Burns, C.M. & Feng, X. Sulfonation of poly (ether ether ketone)(PEEK): kinetic study and characterization. *J. Appl. Polym. Sci.* 82, 2651–2660 (2001).

59 Xing, P. *et al.* Synthesis and characterization of sulfonated poly(ether ether ketone) for proton exchange membranes 1. *J. Membr. Sci.* 229, 95–106 (2004).

60 Li, X. et al. Preparation and characterization of sulfonated poly(ether ether ketone ketone) proton exchange membranes for fuel cell application. J. Membr. Sci. 255, 149–155 (2005).

61 Li, X. *et al.* Preparation and properties of sulfonated poly(ether ether ketone)s (SPEEK)/polypyrrole composite membranes for direct methanol fuel cells. *J. Power Sources* 162, 1–8 (2006).

62 Şengül, E. *et al.* Effects of sulfonated polyether-etherketone (SPEEK) and composite membranes on the proton exchange membrane fuel cell (PEMFC) performance. *Int. J. Hydrogen Energy* 34, 4645–4652 (2009).

63 Zaidi, S.M.J., Mikhailenko, S.D., Robertson, G.P., Guiver, M.D. & Kaliaguine, S. Proton conducting composite membranes from polyether ether ketone and heteropolyacids for fuel cell applications. *J. Membr. Sci.* 173, 17–34 (2000).

64 Fink, J.K. *High performance polymers*. (William Andrew Pub: 2008).

65 Hensema, E.R., Sena, M.E.R., Mulder, M.H.V. & Smolders, C.A. Gas separation properties of new polyoxadiazole and polytriazole membranes. *Gas Sep. Purif.* 8, 149–160 (1994).

66 Zaidi, S.M.J., Chen, S.F., Mikhailenko, S.D. & Kaliaguine, S. Proton conducting membranes based on polyoxadiazoles. *J. New Mater. Electrochem. Syst.* 3, 27–32 (2000).

67 Larminie, J., Dicks, A. & (Firm), K. Fuel cell systems explained. (2003).

68 Cheng, X. *et al.* Hydrogen crossover in high-temperature PEM fuel cells. *J. Power Sources* 167, 25–31 (2007).

69 Collier, A., Wang, H., Zi Yuan, X., Zhang, J. & Wilkinson, D.P. Degradation of polymer electrolyte membranes. *Int. J. Hydrogen Energy* 31, 1838–1854 (2006).

70 Zhang, J. *et al.* PEM fuel cell relative humidity (RH) and its effect on performance at high temperatures. *Electrochim. Acta* 53, 5315–5321 (2008).

71 Zeus Industrial Products, Inc. Melt extrusion: the basic process. (2006) at www.zeusinc.com/UserFiles/zeusinc/Documents/Zeus_Melt_Extrusion.pdf.

72 Rosato, D. V. Extruding Plastics: A Practical Processing Handbook. (Springer: 1998).

73 Vlachopoulos, J. & Strutt, D. Polymer processing. *Mater. Sci. Technol.* 19, 1161–1169 (2003).

74 Breitenbach, J. Melt extrusion: from process to drug delivery technology. *Eur. J. Pharm. Biopharm.* 54, 107–117 (2002).

75 Gomes, D. & Nunes, S.P. Synthesis and Characterization of Poly(arylene ether oxadiazole) Telechelics. *Macromol. Chem. Phys.* 204, 2130–2141 (2003).

76 Gomes, D., Pinto, J.C. & Borges, C. Determination of hydrazide content in poly(oxadiazole-hydrazide) copolymers by NMR and thermal analysis. *Polymer* 44, 6223-6233 (2003).

77 Tsai, C.J. & Chen, Y. Thermotropic liquid-crystalline poly (oxadiazole) s with poly(methylene) spacers: Preparation and extraordinary odd–even effect. *J. Polym. Sci., Part A: Polym. Chem.* 40, 293–301 (2002).

78 Haworth, B., Gilbert, M. & Myers, D.J.B. Melt-state shear flow and elasticity of a thermoplastic fluorosulphonated—PTFE copolymer. *J. Mater. Sci.* 40, 955-964 (2005).

79 Arkles, B. Silane coupling agents: connecting across boundaries v2. 0. Gelest. *Inc.: Morrisville, PA* 56 (2006).

80 Zapilko, C. *et al.* Advanced surface functionalization of periodic mesoporous silica: Kinetic control by trisilazane reagents. *J. Am. Chem. Soc.* 128, 16266–16276 (2006).

81 Lide, David R. Handbook of Chemistry and Physics, 81st ed.; CRC Press: Boca Raton, FL, 2000–2001.

82 Lin, J., Lee, J. K., Kellner, M., Wycisk, R. & Pintauro, P. N. Nafion-flourinated ethylene-propylene resin membrane blends for direct methanol fuel cells. *J. Electrochem. Soc.* 153, A1325–A1331 (2006).

83 E. I. du Pont de Nemours and Company, Technical information sheet NAE302, 2002.

84 Corti, H.R., Nores-Pondal, F. & Pilar Buera, M. Low temperature thermal properties of Nafion 117 membranes in water and methanol-water mixtures. *J. Power Sources* 161, 799–805 (2006).

85 Tiwari, S.K., Nema, S.K. & Agarwal, Y.K. Thermolytic degradation behavior of inorganic ion-exchanger incorporated Nafion-117. *Thermochimica acta* 317, 175–182 (1998).

86 Surowiec, J. & Bogoczek, R. Studies on the thermal stability of the perfluorinated cation-exchange membrane Nafion-417. *J. Therm. Anal. Calorim.* 33, 1097–1102 (1988).

87 Deng, Q., Moore, R. & Mauritz, K. Nafion®/(SiO2, ORMOSIL, and dimethylsiloxane) hybrids via in situ sol–gel reactions: Characterization of fundamental properties. *J. Appl. Polym. Sci.* 68, 747–763 (1998).

88 Lage, L. G., Delgado, P. G. & Kawano, Y. Thermal stability and decomposition of Nafion® membranes with different cations. *J. Therm. Anal. Calorim.* 75, 521–530 (2004).

89 Frański, R., Schroeder, G., Rybachenko, V. & Szwajka, O. P. Loss of isocyanic acid from the internal oxadiazole ring of protonated molecules of some 2, 5-diaryl-1, 3, 4-oxadiazoles. *Rapid Commun. Mass Spectrom.* 16, 390–395 (2002).

90 Ponce, M. L., Roeder, J., Gomes, D. & Nunes, S. P. Stability of sulfonated polytriazole and polyoxadiazole membranes. *Asia-Pac. J. Chem. Eng.* 5, 235–241 (2009).

91 Wilkie, C. A., Thomsen, J. R. & Mittleman, M. L. Interaction of poly(methyl methacrylate) and Nafions. *J. Appl. Polym. Sci.* 42, 901–909 (1991).

92 Deng, Q., Wilkie, C. A., Moore, R. B. & Mauritz, K. A. TGA–FTir investigation of the thermal degradation of Nafion® and Nafion®/[silicon oxide]-based nanocomposites. *Polymer* 39, 5961–5972 (1998).

93 Mashino, M., Ninomiya, Y., Kawasaki, M., Wallington, T. J. & Hurley, M. D. Atmospheric chemistry of CF3CF= CF2: Kinetics and mechanism of its reactions with OH radicals, Cl atoms, and ozone. *J. Phys. Chem. A* 104, 7255–7260 (2000).

94 Samms, S. R., Wasmus, S. & Savinell, R. F. Thermal stability of Nafion® in simulated fuel cell environments. *J. Electrochem. Soc.* 143, 1498–1504 (1996).

95 Kyu, T., Hashiyama, M. & Eisenberg, A. Dynamic mechanical studies of partially ionized and neutralized Nafion polymers. *Can. J. Chem.* 61, 680–687 (1983).

96 Asaka, K., Fujiwara, N., Oguro, K., Onishi, K. & Sewa, S. State of water and ionic conductivity of solid polymer electrolyte membranes in relation to polymer actuators. *J. Electroanal. Chem.* 505, 24–32 (2001).

97 Gomes Lage, L., Gomes Delgado, P. & Kawano, Y. Vibrational and thermal characterization of Nafion® membranes substituted by alkaline earth cations. *Eur. Polym. J.* 40, 1309–1316 (2004).

98 Vetter, S. & Nunes, S. P. Synthesis and characterization of new sulfonated poly(arylene ether 1,3,4-oxadiazole)s. *React. Funct. Polym.* 61, 171–182 (2004).

99 Bottino, F.A., Di Pasquale, G. & Iannelli, P. Synthesis, characterization, and study of the thermal properties of new poly(arylene ether 1, 3, 4-oxadiazole)s. *Macromolecules* 34, 33–37 (2001).

100 Loos, M. R. & Gomes, D. The effect of sulfonation level and molecular weight on the tensile properties of polyoxadiazoles. *High Perform. Polym.* 21, 697–708 (2009).

101 Zhang, J., Tang, Y., Song, C., Zhang, J. & Wang, H. PEM fuel cell open circuit voltage (OCV) in the temperature range of 23 °C to 120 °C. *J. Power Sources* 163, 532–537 (2006).

102 Sun, L., Ran, R. & Shao, Z. Fabrication and evolution of catalyst-coated membranes by direct spray deposition of catalyst ink onto Nafion membrane at high temperature. *Int. J. Hydrogen Energy* 35, 2921–2925 (2010).

103 Cong, H., Hu, X., Radosz, M. & Shen, Y. Brominated poly(2, 6-diphenyl-1,4-phenylene oxide) and its silica nanocomposite membranes for gas separation. *Ind. Eng. Chem. Res.* 46, 2567–2575 (2007).

104 Tang, H., Wang, S., Jiang, S. P. & Pan, M. A comparative study of CCM and hot-pressed MEAs for PEM fuel cells. *J. Power Sources* 170, 140–144 (2007).

Curriculum Vitae

Personal details

Last name: Treekamol

First name: Yaowapa

Date of birth: 24/03/1984

Place of birth: Khon Kean, Thailand

Education

09/2008–present Institute of Polymers and Composites, Technische Universität Hamburg-Harburg, Hamburg, Germany. *PhD student.*

04/2006–05/2008 The Petroleum and Petrochemical College, Chulalongkorn University, Bangkok, Thailand. *Course: Polymer Science (International program). Degree: Master in Polymer Science*

04/2002–03/2006 Khonkaen University, Khonkaen, Thailand. *Course: Chemistry. Degree: Bachelor in Science*

Work experience

06/2008–present: Scientific assistant: “Composite polymer membranes for fuel cells”, Helmholtz-Zentrum Geesthacht, Centre for Materials and Coastal Research, Geesthacht, Germany.

10/2010–03/2011: Visiting researcher: Institute of Fuel Cell Innovation, National Research Council Canada, Vancouver, BC, Canada.

04/2010–09/2010: Visiting researcher: Industrial Materials Institute, National Research Council Canada, Montreal, QC, Canada.

Publications

05/2013: Poster: Performance improvement in fluorinated-oligomer functionalized-silica / Nafion® composite membranes. Y. Treekamol, M. Schieda, L. Robitaille, S. M. MacKinnon, A.

Mokrini, Z. Shi, S. Holdcroft, K. Schulte, S. P. Nunes. 2nd International Conference on Materials for Energy. Karlsruhe, Germany

01/2013: Paper. *Nafion®/ODF-silica composite membranes for medium temperature proton exchange membrane fuel cells.* Y. Treekamol, M. Schieda, L. Robitaille, S. M. MacKinnon, A. Mokrini, Z. Shi, S. Holdcroft, K. Schulte, S. P. Nunes. J. Power Sources 246 (2014) 950-959.

05/2012: Oral communication: *Nafion® ODF-silica composite membranes for medium temperature proton exchange membrane fuel cells.* Y. Treekamol, M. Schieda, L. Robitaille, S. M. MacKinnon, A. Mokrini, Z. Shi, S. Holdcroft, K. Schulte, S. P. Nunes. The 95th Canadian Chemistry Conference and Exhibition. Calgary, Canada.

06/2009: Poster: *Silica with amphoteric functionalization for proton conductive membranes.* Y. Treekamol, M. Schieda, D. Gomes, K. Schulte, S. P. Nunes. The E-MRS 2009 Spring Meeting. Strasbourg, France.

03/2009: Poster: *Development of membrane-electrode-assemblies based on polyoxadiazole nanocomposites for high temperature fuel cells.* Y. Treekamol, M. Schieda, D. Gomes, K. Schulte, S. P. Nunes. NanoMemCourse. Lillehammer, Norway.

09/2008: Oral communication: *Development of membrane-electrode assemblies for fuel cell operation at high temperature and low humidity conditions.* Y. Treekamol, M. Schieda, D. Gomes, K. Schulte, S. P. Nunes. The 10th Network Young Membrains. Berlin, Germany.

04/2008: Poster: *Development of epoxy bipolar plate for polymer electrolyte membrane fuel cell*. Y. Treekamol, T. Chaisuwan, S. Chirachanchai. PPC Annual Research Presentation 2008. Bangkok, Thailand

03/2008: Poster: *Light weight and high conductive bipolar plate for fuel cells*. Y. Treekamol, T. Chaisuwan, S. Chirachanchai. The 235th ACS National Meeting & Exposition. Louisiana, USA.

03/2006: Oral Communication: *Effect of Oxygen on the Oscillatory Belousov-Zhabotinsky Reaction*. Y. Treekamol, A. Sirimungkala. The Conference on Science and Technology "Science for Younth". Bangkok, Thailand.